ABSTRACT

COPPA, BRIAN JOSEPH. Electrical, Chemical, and Structural Characterization of Au Schottky Contacts on Remote Plasma-Treated n-Type ZnO{0001}. (Under the direction of Professors Robert F. Davis and Robert J. Nemanich)

In situ cleaning procedures for $ZnO(000\bar{1})$[1] and ZnO(0001) surfaces have been developed and their efficacy evaluated in terms of the removal of residual hydrocarbons and hydroxide and the crystallography, microstructure, and electronic structure of these surfaces. Annealing $ZnO(000\bar{1})$ in pure oxygen at (600-650°C)±20°C and 0.100±0.001 Torr for 30 min. reduced but did not eliminate all detectable hydrocarbon contamination. However, annealing under similar conditions at 700°C±20°C for 15 min. caused desorption of both the hydrocarbons and the hydroxide constituents to concentrations below the detection limits of X-ray photoelectron spectroscopy. However, thermal decomposition degraded the surface microstructure. Exposure of the $ZnO(000\bar{1})$ surface to a remote plasma containing an optimized 20% O_2/80% He mixture for the optimized time, temperature, and pressure of 30 min, 525 °C, and 0.050 Torr resulted in smooth, highly-ordered, atomically-stepped and stoichiometric surfaces with a nearly flat electronic band structure. A 0.5 eV change in band bending was attributed to the significant reduction of the accumulation layer associated with surface contamination. The hydrocarbons were undetectable and only ~0.4±0.1 ML of hydroxide remained. The latter appeared to be more tightly bound to the ZnO(0001) surface due to unfilled dangling bonds associated with the polarity of this surface. This effect increased the optimal time and temperature of the plasma cleaning process to 60 min. and 550 °C,

---

[1] (0001) and $(000\bar{1})$ are used in this Dissertation to designate the polar zinc- and oxygen-terminated surfaces, respectively.

respectively, at 0.050 Torr. Approximately 0.4±0.1 ML of hydroxide also remained on this surface.

Current-voltage results of Au contacts deposited on as-received, n-type ZnO(0001) surfaces showed an ~0.01 A/cm^2 leakage current density to 4.6 V reverse bias and ideality factors (n) >2 before sharp, permanent breakdown. This behavior was due primarily to the presence of hydroxide on this surface, which typically increases the surface conductivity and forms an accumulation layer. Cooling in the plasma ambient caused the chemisorption of oxygen and the formation of a depletion layer of lower surface conductivity. These process steps produced smooth, highly-ordered, stoichiometric ZnO(0001) surfaces that possessed 0.3 eV of upward band bending. Sequentially deposited, unpatterned Au and the most rectifying gold contacts initially grew on these surfaces via the formation of islands that subsequently coalesced. The latter displayed a barrier height of 0.71±0.05 eV, a saturation current density of 4.04 μA/cm^2, a value of n = 1.17±0.05, a significantly lower leakage current density of ~0.1 mA/cm^2 to 8.5 V reverse bias, and a sharp, permanent breakdown at ~ –8.75 V. All measured barrier heights were lower than the predicted Schottky-Mott value of 1.0 eV, indicating that the interface structure and the associated interface states affect the Schottky barrier. However, the constancy in the FWHM of the core levels for Zn 2p (1.9±0.1 eV) and O 1s (1.5±0.1 eV), before and after sequential *in situ* Au depositions indicated an abrupt, unreacted Au/ZnO(0001) interface.

Similar results were obtained for Schottky contacts deposited on remote plasma treated ZnO($000\bar{1}$) surfaces, which possessed a step and terrace microstructure. Analysis

of transmission electron microscopy results revealed the growth of epitaxial, single crystal Au forming an abrupt, unreacted interface.

ELECTRICAL, CHEMICAL, and STRUCTURAL CHARACTERIZATION of Au SCHOTTKY CONTACTS on REMOTE PLASMA-TREATED n-TYPE ZnO{0001}

By

BRIAN JOSEPH COPPA

A dissertation submitted to the Graduate Faculty of North Carolina State University in partial fulfillment of the requirements for the degree of Doctor of Philosophy

DEPARTMENT OF MATERIALS SCIENCE AND ENGINEERING

Raleigh, NC

2003

APPROVED BY:

R.F. Davis, Chair of Advisory Committee	R.J. Nemanich, Co-chair
N.A. El-Masry	R.M. Kolbas

DEDICATION

To God and His Church

BIOGRAPHY

Brian Joseph Coppa was born to Frank and Eleanor Coppa in Cumberland, Maryland on September 22, 1977. He is the youngest of three children and attended West Side Elementary and Braddock Middle Schools in Cumberland. Brian was encouraged by his mother to enter the science fair in the 6th grade, and he continued to participate for the next six years until qualifying for the International Science and Engineering Fair in the Physics Division as a senior in high school. His project was conducted at the Metals and Ceramics Division of Oak Ridge National Laboratory, as an extension of a two-week summer research program funded by the Appalachian Regional Commission (affiliated with the DOE). Consequently, this program inspired him to eventually pursue a Ph.D. in materials science and engineering.

After graduating from Allegany High School in 1995, Brian entered the University of Arizona to study physics. Brian received his first paid internship position in the field during the summer after his freshmen year at the National Science Foundation-funded Tandem Accelerator Mass Spectrometry facility, dedicated to radiocarbon dating, under the direction of Dr. Douglass Donahue. This facility possessed an ~50 foot Van de Graaff accelerator, foreshadowing the 47 foot ultra-high vacuum transfer line lab where he would complete his Ph.D. dissertation. He continued experimental research throughout his undergraduate career and graduated in May 1999 with a B.S. in physics and a minor in economics.

Coppa joined the research groups of Professors Robert F. Davis and Robert J. Nemanich in the Materials Science and Engineering Department at North Carolina State University on June 21, 1999. He completed a Master's in this field in Fall 2001 before

completing his Ph.D. dissertation during the summer of 2003. His Ph.D. minor is in interdisciplinary studies with an emphasis on high-technology entrepreneurship.

ACKNOWLEDGMENTS

The completion of my degree would not have been possible without the love and support of my parents. I am deeply thankful for their emotional and financial assistance enabling me to pursue this major goal in life. Also, my heart is filled with gratitude for the blessings of the Holy Family of Jesus, Mary and Joseph, the intercession of the communion of saints and my guardian angel, while in graduate school. It is clear that the guidance of the Holy Spirit illuminated the dark path followed in these explorations with ZnO. The reception of daily Eucharist at various Catholic parishes including Our Lady of Lourdes, St. Raphael the Archangel, St. Francis of Assisi, and Sacred Heart Cathedral sustained me through the daily grind of graduate studies.

Professors Robert Davis and Robert Nemanich were instrumental for technical and financial support for this project, primarily through the Kenan Institute and the Office of Naval Research. Ms. Edna Deas was extremely helpful as an academic advisor with her abundant knowledge of the details of the degree and other related issues. Mrs. Cecilia Upchurch, Ms. C. J. Hathorne, and Mrs. Janet Jackson provided constant and courteous administrative support. The Physical and Mathematical Science machine shop staff at N.C. State assisted in this project by providing urgent repairs to equipment for experiments, while also processing numerous material components for this research.

Several former and current members of the Surface Science Lab were key personnel in enabling this project to be completed. Dr. Kieran Tracy was my first mentor and trained me regarding the orientation of the lab, operation of the transfer line and several pieces of equipment, while Dr. Philip Hartlieb provided key technical advice and training concerning my initial studies. Direct assistance in experiments was received by

Charlie Fulton, Brian Rodriguez, Sharon Kiesel, Brendan Shields, Chethan Pandarinath, James Burnette, Dr. Ted Cook Jr., and Jacob Garguilo. In addition, the students and affiliated members of both the research groups of Professors Davis and Nemanich were helpful for direct and indirect general support as colleagues and friends.

Finally, I would like to acknowledge the guidance and direction of other Ph.D. committee members including Prof. Nadia El-Masry, Prof. Robert Kolbas, and Prof. Jerome Cuomo (sitting in for Prof. El-Masry). Professor Salah Bedair assisted in the initial phase of this research by serving as a Master's committee member.

TABLE OF CONTENTS

LIST OF TABLES……………………………………………………………......x

LIST OF FIGURES…………………………………………………………….xii

1. INTRODUCTION ……………………………………………………………….1

1.1 Introduction………………………………………………………………1

1.2 References……………………………………………………………..6

2. SCHOTTKY BARRIER MEASUREMENT TECHNIQUES………………...8

2.1 Introduction………………………………………………………………8

2.2 Current-Voltage………………………………………………………..8

2.3 Capacitance-Voltage…………………………………………………….10

2.4 Photoemission Spectroscopy……………………………………………11

2.5 Internal Photoemission………………………………………………….12

2.6 Summary……………………………………………………………...13

2.7 References…………………………………………………………… 14

3. *IN SITU* CLEANING AND CHARACTERIZATION OF OXYGEN AND ZINC-TERMINATED n-TYPE ZnO{0001} SURFACES…..………..………….15

3.1 Abstract………………………………………………………………….15

3.2 Introduction……………………………………………………………...16

3.3 Experimental Procedures……………………………………………..19

3.4 Results and Discussion………………………………………………….23

3.4.1 Oxygen Annealing of ZnO($000\bar{1}$)……………………………….23

3.4.2 Remote Plasma Cleaning of the ZnO($000\bar{1}$) surface…………….. 25

3.4.3 Post-plasma Oxygen Annealing of the ZnO($000\bar{1}$) surface……….31

3.4.4 Remote Plasma Cleaning of the ZnO(0001) surface……………...32

3.5 Summary……………………………………………………………...34

3.6 Acknowledgments……………………………………………………….35

3.7 References……………………………………………………………….36

4. GROWTH MODE AND SUBSEQUENT SCHOTTKY BARRIER FORMATION OF AU ON REMOTE PLASMA-TREATED n-TYPE ZnO$(000\bar{1})$……………………………………………………………...49

4.1 Abstract……………………………………………………………..50

4.2 Introduction……………………………………………………………51

4.3 Experimental Procedures………………………………………………...53

4.4 Results and Discussion……………………………………………..54

4.4.1 Analyses of remote plasma-cleaned ZnO$(000\bar{1})$ cooled in vacuum……………………………………………54

4.4.2 AFM analyses remote plasma-cleaned ZnO$(000\bar{1})$ cooled in vacuum…………………………………………… 56

4.4.3 Analyses of remote plasma-cleaned/O_2 adsorbed ZnO$(000\bar{1})$...56

4.4.4 Growth mode and characterization of the Au/ZnO$(000\bar{1})$ interface…………………….…..…………58

4.4.5 I-V Characterization of Au/ZnO$(000\bar{1})$/Ti…………………….64

4.5 Summary………………………………………………………… …66

4.6 Acknowledgments……………………………………………………….68

4.7 References……………………………………………………………….68

5. STRUCTURAL, MICROSTRUCTURAL, CHEMICAL, AND ELECTRIAL PROPERTIES OF GOLD SCHOTTKY CONTACTS ON REMOTE PLASMA-CLEANED, n-TYPE ZnO(0001)………..…83

5.1 Abstract………………………………………………………………….84

5.2 Introduction………………………………………………………… 85

5.3 Experimental Procedures…………………………………………......89

5.4 Results and Discussion…………………………………………….....91

5.4.1 Analyses of remote plasma-cleaned ZnO(0001) cooled in vacuum………………………………...…………91

5.4.2 Analyses remote plasma-cleaned ZnO(0001) cooled in plasma ambient……………………………...……93

5.4.3 AFM analyses of remote plasma-cleaned ZnO(0001) cooled in vacuum.…………………………………..……...94

5.4.4 Growth mode and characterization of the Au/ZnO ZnO(0001) interface……………….…………...95

5.4.5 I-V-T Characterization of Au/ZnO(0001)/Ti…………………100
5.5 Summary…………………………………………………………..103
5.6 Acknowledgments…………………………………………….....…104
5.7 References……………………………………………...………… 105

6. SUMMARY …………………………………………………………...…..120

7. RECOMMENDATIONS FOR FUTURE WORK …………………………..124

APPENDIX …………………………………………………………...……..126

A. Gold Schottky contacts on oxygen plasma-treated, n-type ZnO($000\bar{1}$)..126

LIST OF TABLES

Table 3.1. Sets of temperature, total pressure and time investigated to determine the efficacy of annealing ZnO(000$\bar{1}$) in pure O_2 for the removal of surface contaminants……………………………………………………………….38

Table 3.2. Sets of sample and remote 20-W plasma parameters, O_2/He ratios as well as parameters used in the optional annealing step in pure O_2 for the removal of surface contaminants from the ZnO(000$\bar{1}$) surface. The change in band bending associated with the process is indicated by $\Delta(q\Psi_S)$, and the optimum cleaning procedure and associated results are in bold print. …………………………………………………………………………..39

Table 3.3. Sets of remote 20-W, 20% O_2/80% He remote plasma parameters investigated for the removal of surface contaminants from the ZnO(0001) surface. The change in band bending associated with the process is indicated by $\Delta(q\Psi_S)$, and the optimum cleaning procedure and related results are in bold print………………………………………………………......40

Table 4.1. Evolution of Zn $2p_{3/2}$ core level as a function of Au overlayer thickness on 20%O_2/80% He remote plasma-cleaned ZnO(000$\bar{1}$) following oxygen adsorption. The evolution of the Schottky barrier was monitored up to 0.2 nm, as highlighted in bold print…………………………………………...71

Table 4.2. Evolution of O 1s core level as a function of Au overlayer thickness on 20% O_2/80% He remote plasma-cleaned ZnO(000$\bar{1}$) following oxygen adsorption. The evolution of the Schottky barrier was monitored up to 0.2 nm, as highlighted in bold print…………………………………………...72

Table 4.3. Evolution of Au $4f_{7/2}$ core level as a function of Au overlayer thickness on 20% O_2/80% He remote plasma-cleaned ZnO(000$\bar{1}$) following oxygen adsorption……………………………………………………………………73

Table 5.1. Zn $2p_{3/2}$ core level spectra acquired from the as-received, cleaned in a 20%O_2/80% He remote plasma and cooled in the plasma ambient to ~RT (O_2 adsorption) as a function of Au overlayer thickness. The evolution of the Schottky barrier was monitored up to a thickness of 0.2 nm of Au…………………………………………………………………..108

Table 5.2. O 1s core level acquired from the ZnO(0001) surface in the as-received state, after cleaning in a 20% O_2/80% He remote plasma and cooling in either a vacuum or in the plasma ambient (O_2 adsorption) and as a function of the thickness of a Au overlayer deposited on the surface exposed to the last environment. The evolution of the Schottky barrier was monitored up to a thickness of 0.4 nm of Au………………………………………...…109

Table 5.3. Au $4f_{7/2}$ core level as a function of Au overlayer thickness on 20%O_2/80% He remote plasma-cleaned ZnO(0001) surface cooled in the plasma ambient to ~RT……………………………………………………………………110

FIGURE LIST

Figure 3.1. AES spectra of the ZnO($000\bar{1}$) surface acquired from (i) as-received and (ii) samples annealed in 0.100 Torr of pure O_2 at 700 °C for 15 min……..….41

Figure 3.2. XPS O 1*s* core level spectra of the ZnO($000\bar{1}$) surface acquired from (i) as-received samples and (ii) samples annealed in 0.100 Torr of pure O_2 at 700 °C for 15 min……………………………………………………………………...42

Figure 3.3. XPS C 1*s* core level spectra of ZnO($000\bar{1}$) surfaces acquired from (i) as-received samples and (ii) samples cleaned by exposure to a room-temperature, 20-W, 2% O_2/98% He remote plasma for 0.5 min. at 0.050 Torr……………………………………………………………………..…43

Figure 3.4. XPS O 1*s* core level spectra of ZnO($000\bar{1}$) surfaces acquired from (i) as-received samples and samples exposed to a 20-W remote O_2/He plasma for 0.5-30 min at 0.050 Torr separately at (ii) 20 °C (iii) 350 °C, (iv) 450 °C, (v) 475 °C, (vi) 500 °C and (vii) 525 °C. The amount of hydroxide varied for each as-received sample investigated…………………………………44

Figure 3.5. UPS spectra of ZnO($000\bar{1}$) surfaces acquired from (i) as-received samples and (ii) cleaned at 525 °C in a 20-W remote 20% O_2/80% He plasma for 30 min. at 0.050 Torr. The inset shows that the valence band turn-on for an (i-i) as-received sample is sharpened for a (ii-ii) plasma-cleaned surface….45

Figure 3.6. (5 µm x 5 µm) AFM images of the ZnO($000\bar{1}$) surface of (a) as-received samples and (b) samples cleaned at 525 °C via 30 min. exposure to a remote 20-W, 20% O_2/80% He plasma at 0.050 Torr……………………………46

Figure 3.7. XPS spectra of the Zn 2p core level of (i) as-received samples and samples separately heated to (ii) 525 °C for 30 min., (iii) 525 °C for 60 min., (iv) 550 °C for 60 min. and cleaned for these times in a remote 20-W, 20% O_2/80% He plasma at 0.050 Torr………………………………………47

Figure 3.8. (5 µm x 5 µm) AFM images of the ZnO(0001) surface of (a) as-received samples and (b) samples cleaned at 550 °C via 60 min. exposure to a remote 20-W, 20% O_2/80% He plasma at 0.050 Torr……………………………48

Figure 4.1. Electronic band structure derived from UPS spectra for ZnO($000\bar{1}$) surfaces (a) in the as-received state, (b) after exposure to a 20-W 20% O_2/ 80% He remote plasma for 30 min. at 525 °C and 0.050 Torr, and (c) after cooling under same conditions to ~RT (O_2 adsorption)…………………………...74

Figure 4.2. UPS valence band spectra from the (i) as-received ZnO($000\bar{1}$) surface, (ii) following remote plasma cleaning and O_2 adsorption, and sequential Au deposition generating thicknesses of (iii) 0.2 nm, (iv) 0.4 nm, (v) 5.0 nm, and (vi) 100 nm. The Au-induced band bending is indicated by the movement of the Zn 3d and O 2p bulk features located at 10.4 eV and 4.0 eV, respectively. All spectra were acquired using the He I photon line (hν = 21.2 eV). The binding energy is measured with respect to the Fermi level (E_F = 0 eV)……………………………………………………………75

Figure 4.3. LEED images, and corresponding insets, taken of ZnO($000\bar{1}$) surface at primary beam energies of (i) 100 eV for samples in the as-received state (ii) 42 eV after remote plasma cleaning, (iii) 42 eV following oxygen adsorption and (iv) at 80 eV after 100 nm Au metallization, in succession. ……………………………………………………………………………76

Figure 4.4. XPS Zn $2p_{3/2}$ core level spectra from the as-received ZnO($000\bar{1}$) surface and following remote plasma cleaning, O_2 adsorption, and sequential Au metallization. All spectra were acquired using Mg Kα (hν = 1253.6 eV) radiation………………………………………………………………… 77

Figure 4.5. Attenuation of the Zn 2p core level photoelectron peak as a function of the overlying Au thickness. The experimental data is indicated by solid diamonds for comparison to Volmer-Weber (VW), Stranski-Krastanov (SK), and Frank van der Merwe (FM) growth modes…………………...78

Figure 4.6. AFM image of ZnO($000\bar{1}$) surface (a) remote plasma cleaned (5 x 5 μm scan size) showing an atomic step and terrace microstructure and (b) TEM image of Au islands in the coalescence phase after oxygen adsorption and 100 nm Au metallization ………………………………………………...79

Figure 4.7. XPS Au $4f_{7/2}$ core level curve-fitted spectra as a function of Au deposition following remote plasma cleaning and O_2 adsorption. Shifts of 0.5 eV and 1.0 eV are depicted for the peak position and FWHM, respectively, over the course of sequential Au metallization. All spectra were acquired using Mg Kα (hν = 1253.6 eV) radiation………………………………………...80

Figure 4.8. XRD 2θ plots for 100 nm Au contacts on a cleaned-and-oxygen adsorbed ZnO($000\bar{1}$) surface (a) as-deposited at room-temperature and (b) after post-deposition annealing in air at 175 °C for 15 min. The spectrum was acquired using Cu *Kα* (λ = 0.1542 Å) radiation…………………….…..81

Figure 4.9. (a) Moderate and (b) high resolution TEM images of the cleaned-and-oxygen adsorbed (100nm)Au/ZnO($000\bar{1}$) interface, (c) and (d) fast-fourier transform (FFT) of the twin boundary region of Au, (e) FFT of ZnO, and (f) diffraction pattern of ZnO and Au. …………………………………..…82

Figure 5.1. Electronic band structure derived from UPS spectra for ZnO(0001) surfaces (a) in the as-received state, (b) after exposure to a 20-W 20% O_2/ 80% He remote plasma for 60 min. at 550 °C and 0.050 Torr and cooling in vacuum from 425°C, and (c) after cooling under the same conditions to ~RT in the unignited plasma ambient to ~RT (O2 adsorption)……………………111

Figure 5.2. UPS valence band spectra from the as-received ZnO(0001) surface, after exposure to a 20-W 20% O_2/ 80% He remote plasma for 60 min. at 550 °C and 0.050 Torr and cooling in the unignited plasma ambient (O_2 adsorption), and after several sequential Au depositions of increasing thickness. Au-induced band bending is indicated by the movement of the Zn 3d and O 2p bulk features located at 10.4 eV and 4 eV, respectively. All spectra were acquired using the He I photon line (hν = 21.2 eV). The binding energy is measured with respect to the Fermi level (E_F = 0 eV)……………………………………………………………..112

Figure 5.3. XPS O 1s core level spectra from the as-received ZnO(0001) surface, after remote plasma cleaning and cooling from 425°C in the plasma ambient to ~RT (O_2 adsorption), and sequential Au metallization. All spectra were acquired using Mg Kα (hν = 1253.6 eV) radiation………………………113

Figure 5.4. XPS Zn 2p core level spectra from the as-received ZnO(0001) surface after remote plasma cleaning and cooling from 425°C in the plasma ambient to ~RT (O_2 adsorption), and sequential Au metallization. All spectra were acquired using Mg Kα (hν = 1253.6 eV) radiation………………………114

Figure 5.5. Attenuation of the O1s core level photoelectron peak as a function of the overlying Au thickness. The experimental data is indicated by solid diamonds for comparison with theoretical curves for Volmer-Weber (VW), Stranski-Krastanov (SK), and Frank-Van der Merwe (FM) growth modes……………………………………………………………….115

Figure 5.6. XPS Au $4f_{7/2}$ core level curve-fitted spectra as a function of Au deposition following remote plasma cleaning and O_2 adsorption. A shift of 1.1 eV and 1.0 eV is depicted for the peak position and FWHM, respectively, over the course of sequential Au metallization. All spectra were acquired using Mg Kα (hν = 1253.6 eV) radiation…………………………………………...116

Figure 5.7. Curve-fitted XRD 2θ plots for 75 nm thick Au contacts deposited on a cleaned ZnO(0001) surface cooled in the plasma ambient. (a) as-deposited and (b) after post-deposition annealing in air at 175 °C for 15 min. The spectrum was acquired using Cu *Kα* (λ = 0.1542 nm) radiation…………117

Figure 5.8. *J-V* characteristics for the best performing ~100-μm-diameter Au contact deposited on an as-received ZnO(0001) surface…………………………118

Figure 5.9. *J-V* characteristics for the best performing ~100-μm-diameter Au contact deposited on cleaned-and-oxygen adsorbed ZnO(0001) surface in (i) forward and (ii) reverse bias; at 80 °C in (iii) forward and (iv) reverse bias; at 150 °C in (v) forward and (vi) reverse bias……………………………119

.

1. INTRODUCTION

1.1 INTRODUCTION

Zinc oxide normally occurs in the hexagonal wurtzite crystal structure wherein both the Zn and the O are tetrahedrally coordinated. This material has a direct band-gap energy[1] of 3.4 eV and lattice parameters[2] of a_0 = 0.325 nm and c_0 = 0.5207 nm at room-temperature (RT); these three values are similar to those in hexagonal GaN. ZnO is significantly softer than GaN, and it is more sensitive to chemical reaction, which makes *ex situ* cleaning a significant challenge.

Classical applications for bulk polycrystalline and powdered ZnO include surface acoustic wave devices, gas sensors, varistors, phosphors, pigments in paints, and piezoelectric transducers.[3] The latter device utilizes the spontaneous polarization of ZnO along the <0001> directions.

From an applications perspective, within the context of the subjects of this dissertation, several important devices can be fabricated using ZnO Schottky barrier diodes (SBDs). For example, Schottky-type, ZnO ultraviolet photodetectors have technical advantages in speed and lower noise than their photoconductive counterpart.[4] The former are expected to be particularly useful in space applications, as this material is extremely resistant to MeV proton irradiation relative to other semiconductors.[5] These types of diodes are also essential for probing defects in semiconductors by junction spectroscopic characterization techniques such as deep-level transient spectroscopy (DLTS)[6] and admittance spectroscopy.[7] For example, Auret *et al.*,[5] using Au as the rectifying contact on the ZnO($000\bar{1}$) surface, have reported a 1 nA leakage current to an applied bias of –1 V and an ideality factor of 1.19 in their ZnO SBDs fabricated for DLTS studies. Metal-

semiconductor-field-effect-transistors also rely on SBD structures. However, the device capability of ZnO is expected to be limited to low power applications, since contacts on this material have a low breakdown voltage, as shown later, while ZnO has a low decomposition temperature.[10] It is important that these diodes possess a low leakage current and a low ideality factor at moderate voltages. A recent emphasis in the field has concerned the p-type doping of ZnO and related solid solutions for the future development of homoepitaxial, p-n junction light-emitting devices. As a first step in the achievement of this goal, two-inch ZnO boules have recently been grown via seeded chemical vapor transport.[11] Polished, transparent ZnO wafers sliced from these boules were available commercially and used in the research of this dissertation.

High purity crystals of ZnO are typically n-type. This characteristic has traditionally been attributed to native defects such as oxygen vacancies and zinc interstitials.[12] However, recent theoretical calculations by Kohan *et al*.[8] have shown that none of the native defects exhibit characteristics consistent with a high-concentration of shallow donors. Van de Walle[9] has noted that only vacancies have sufficiently low energies to form during growth of ZnO; however, Zn and O vacancies act as deep acceptors and deep donors, respectively. First-principles calculations by the last author have provided strong evidence that H behaves as a shallow donor in ZnO and can be incorporated in high concentrations in this oxide (and in the hydroxide that invariably forms of the surface of this oxide—see below) via the formation of O-H bonds.

Surface cleaning processes are fundamental to semiconductor device fabrication.[13] Previous studies[14-16] have shown that the removal of contaminants from the surfaces of silicon- and gallium arsenide-based substrates decreases both the concentration of growth-

related zero- and one-dimensional defects in the subsequently deposited epitaxial films. Also, surface cleaning typically enhances device functionality such as the lowering of reverse bias leakage currents in rectifying contacts.[13] Similar gains in the microstructure and electrical properties should be realized in homoepitaxial films of ZnO grown on clean ZnO substrates; however, only a few reports of research concerned with contaminant removal from ZnO surfaces have been published.[17-20]

Device-quality Schottky contacts typically require intimate metal-semiconductor interfaces free of surface contamination. A major deterrent to the development of low leakage Schottky contacts on ZnO with low ideality parameters, is the ~3 monolayer (ML) thick native contamination layer, which includes ~1 ML of adventitious carbon and ~2 ML of hydroxide.[10,22] In the formation of the hydroxide, H atoms donate ~0.5 e^- to each surface oxygen ion on both the (0001) and $(000\bar{1})$ surfaces of ZnO. This strong interaction, comparable to O-metal bonding in the bulk oxide lattice, results in the formation of a shallow electron donor state through the proposed reaction: ($H + O^{2-} \rightarrow OH^- + e^-$), which increases the carrier concentration in the space charge layer at the surface by several orders of magnitude.[23] As such, several groups[24-26] have reported that the formation of a surface hydroxide produces an electron accumulation layer that results in a high surface conductivity on both polar faces of ZnO. This is very likely the reason for the reported low leakage currents only up to –1 V[3-5,26-28] and the relatively high ideality factors (>2)[4,10] for high work function metals (Au) deposited on these surfaces. As noted above, Van de Walle,[7] has indicated from theoretical considerations that the incorporation of H into the bulk (and the presence of the hydroxide) may be the reasons for the n-type behavior of this wide band-gap material.

The sensitivity of the surface conductivity of ZnO to hydrogen and oxygen has been utilized in sensor devices.[26] In contrast with H, adsorbed oxygen species on ZnO act as electron acceptors that generate a depletion layer, which lowers the surface conductivity by several orders of magnitude[26,29-30] and is expected to be advantageous for Schottky barrier formation. It has been proposed[31] that chemisorption of oxygen occurs preferentially at surface defect sites as O^{2-} or O^{-}.

This thesis is composed of seven chapters, primarily dealing with the development of a suitable cleaning process for the characterization and fabrication of low leakage, low ideality parameter Schottky contacts to ZnO. Chapter 2 is focused on common principles and measurement techniques of Schottky barriers. The development of an *in situ* cleaning procedure for n-type ZnO{0001} surfaces is discussed in Chapter 3. The structural, microstructural, chemical, and electrical properties of Au Schottky contacts on remote plasma treated n-type ZnO($000\bar{1}$) and ZnO(0001) is presented in Chapters 4 and 5, respectively. The improvement of the properties of rectifying contact is discussed and is based on the adsorption of oxygen on the ZnO surface during cooling in the O_2/He plasma ambient to ~RT. This step takes advantage of the sensitivity of the ZnO surface conductivity to the presence of oxygen. This several investigations undertaken for this dissertation are summarized in Chapter 6. Suggestions for future research in the general areas of study reported herein are presented in Chapter 7.

More specifically, Chapter 3 describes the *in situ* cleaning procedures involving annealing in either oxygen or a remote O_2/He plasma that were investigated for the removal of adventitious hydrocarbons and hydroxide from the polished {0001} faces of

ZnO wafers. The efficacy of these procedures was determined using several *in situ* spectroscopies and *ex situ* microstructural and structural characterization techniques.

Chapter 4 discusses an *in situ* remote plasma cleaning procedure and a subsequent oxygen adsorption step, which were developed in conjunction with investigations of the deposition and the current-voltage (I-V) properties of Au Schottky contacts on polished ZnO($000\bar{1}$) surfaces. The rectifying characteristics for the Au contacts were determined on as-received, plasma-cleaned, and cleaned-and-oxygen adsorbed ZnO($000\bar{1}$) samples to evaluate the efficacy of the cleaning process steps for improving these characteristics. Photoemission of the electronic structure and the growth mode of Au on the ZnO($000\bar{1}$) interface were also studied via ultraviolet photoelectron spectroscopy (UPS) and X-ray photoelectron spectroscopy (XPS). The structural and microstructural characteristics of all the materials used in this program were investigated using X-ray diffraction (XRD), low-energy electron diffraction (LEED), transmission electron diffraction (TEM), and atomic force microscopy (AFM).

In the study presented in Chapter 5, an *in situ* remote plasma cleaning procedure and a subsequent oxidation step were developed in conjunction with investigations of the deposition and the temperature-dependent current-voltage (I-V-T) properties of Au Schottky contacts on polished ZnO(0001) surfaces. Analyses similar to those noted above for Chapter 4 were performed with comparable results.

1.2 REFERENCES

1. D. C. Look, Mater. Sci. Eng. B 80, 383 (2001).
2. V. E. Henrich and P. A. Cox, *The Surface Science of Metal Oxides* (Cambridge Univ., Cambridge, 1994) p. 55.
3. F. D. Auret, S. A. Goodman, M. Hayes, M. J. Legodi, H. A. van Laarhoven, and D. C. Look, J. Phys.: Condens. Matter 13, 1 (2001).
4. Fabricius, T. Skettrup, and Paul Bisgaard, Applied Optics 25, 2764 (1986).
5. F. D. Auret, S. A. Goodman, M. Hayes, M. J. Legodi, H. A. van Laarhoven, and D. C. Look, Appl. Phys. Lett. 79, 3074 (2001).
6. F. D. Auret, S. A. Goodman, M. Hayes, M. J. Legodi, W. E. Meyer, and D. C. Look, Appl. Phys. Lett. 80, 1340 (2002).
7. Y. Kanai, Jpn. J. Appl. Phys. 29, 1426 (1990).
8. A. F. Kohan, G. Ceder, D. Morgan and C. G. Van de Walle, Phys. Rev. B 61, 15019 (2000).
9. G. Van de Walle, Phys. Rev. Lett. 85, 1012 (2000).
10. B. J. Coppa, R. F. Davis, and R. J. Nemanich, Appl. Phys. Lett. 82, 400 (2003).
11. D. C. Look, D. C. Reynolds, J. R. Sizelove, R. L. Jones, C. W. Litton, G. Cantwell, and W. C. Harsch, Solid State Commun. 105, 399 (1998).
12. W. Göpel, L. J. Brillson, and C. F. Brucker, J. Vac. Sci. Technol. 17, 894 (1980).
13. S.W. King, J. P. Barnak, M.D. Bremser, K. M. Tracy, C. Ronning, R. F. Davis, and R. J. Nemanich, J. Appl. Phys. 84, 9 (1998).
14. R. P. Vasquez. B. F. Lewis, and F. J. Grunthaner, Appl. Phys. Lett. 42, 293 (1983).
15. M. Yamada and Y. Ide, Jpn. J. Appl. Phys. Part 2 33, L671 (1994).

16. C. M. Rouleau and R. M. Park, J. Appl. Phys. 73, 4610 (1993).

17. L. Fiermans, E. Arijs, J. Vennik, and Vorst, Surf. Sci. 39, 357 (1973).

18. H. Jacobs, W. Mokwa, D. Kohl, and G. Heiland, Surf. Sci. 160, 217 (1985).

19. M. Mintas and G.W. Filby, Zeitschrift fur Naturforschung 36a, 140 (1981).

20. S. Roberts and R. J. Gorte, J. Chem. Phys. 93, 5337 (1990).

21. V. E. Henrich and P. A. Cox, *The Surface Science of Metal Oxides* (Cambridge Univ., Cambridge, 1994) p. 297.

22. B. J. Coppa, C. C. Fulton, P. J. Hartlieb, R. F. Davis, B. J. Rodriguez, B. J. Shields and R. J. Nemanich, submitted to the J. Appl. Phys.

23. H. Moormann, D. Kohl, and G. Heiland, Surf. Sci 100, 302 (1980).

24. G. Heiland and P. Kunstmann, Surf. Sci. 13, 72 (1969).

25. M. Nakagawa and H. Mitsudo, Surf. Sci. 175, 157 (1986).

26. R. A. Rabadanov, M. K. Guseikhanov, I. Sh. Aliev, and S. A. Semiletov, Fizika 6, 72 (1981).

27. Y. Liu, C. R. Gorla, S. Liang, N. Emanetoglu, Y. Lu, H. Shen, and M. Wraback, Journal of Electronic Materials 29, 69 (2000).

28. H. Sheng, S. Muthukumar, N. W. Emanetoglu, and Y. Lu, Appl. Phys. Lett. 80, 2132 (2002).

29. E. Arijs, F. Cardon, and W. Maenhout-Van Der Vorst, Surf. Sci. 17, 387 (1969).

30. L. Lagowski, E. S. Sproles, Jr., and H. C. Gatos, J. Appl. Phys. 48, 3566 (1977).

31. V. E. Henrich and P. A. Cox, *The Surface Science of Metal Oxides* (Cambridge Univ., Cambridge, 1994) p. 288.

2. SCHOTTKY BARRIER CHARACTERIZATION TECHNIQUES

2.1 INTRODUCTION

An array of techniques may be applied towards the measurement and characterization of Schottky barriers. Electrical characterization involves the measurement of the current or capacitance as a function of the applied voltage. The metal contacts may be damaged by the sharp probe tips during the electrical characterization procedure and result in marked changes in the electrical characteristics of these contacts. The use of wire-bonded probes may prevent this damage. However, the use of photoemission spectroscopy to determine the Schottky barrier height (SBH) is completely non-destructive. In addition, internal photoemission (photoresponse) is one of the most accurate and direct methods of measuring the SBH. The purpose of this chapter is to introduce these various techniques.

2.2 CURRENT-VOLTAGE (I-V)

When a voltage is applied to the metal contact, current flows through a uniform metal-semiconductor interface. The movement of majority carriers across the interface such as electrons in n-type material or holes in p-type material generates a flow of current. Four main current processes can occur, namely, 1) thermionic emission over the barrier; 2) tunneling through the barrier; 3) recombination in the depletion region; 4) recombination in the neutral region.[1] Thermionic emission is dominant for most moderately doped semiconductors, whereas tunneling can dominate transport in heavily doped semiconductors.

The current-voltage technique involves the application of a range of biases, both positive and negative, to the metal-semiconductor system and the measurement of the resulting current.[2] The energy levels of an n-type semiconductor are raised with respect to the metal Fermi level, when a positive or forward DC bias is applied to the semiconductor, which flattens the previously bent bands. In this scenario, the barrier for electrons to traverse from the metal to the semiconductor remains essentially the same, but the barrier for electrons to traverse from the semiconductor to the metal is reduced. Thus, equilibrium conditions in the current flow are altered, and the flow of current from the metal to the n-type semiconductor is greater than the opposing current. Reverse or negative biasing of the semiconductor with respect to the metal, results in the Fermi level of the semiconductor being lowered compared to the metal.[2] The barrier for electrons in the semiconductor is increased as a result of the increased band bending, associated with the lowering of the Fermi level. In this case, the electron flow from the semiconductor to the metal is decreased; thus, the net current flow passes from the semiconductor to the metal.

Device-quality rectifying contacts possess a forward bias current many orders of magnitude greater than the reverse bias current.[2] The resistance of the material causes a linear increase of the current for large forward biases. Most Schottky contacts are fabricated on moderately doped semiconductors; thus, thermionic emission over the barrier is generally assumed. Sze has discussed the derivations of the equations by Bethe for this theory.[1] The application of this theory in the determination of the SBH is presented in Chapters 4 and 5. A major index of the rectification of Schottky contacts is the ideality factor, n, which is derived from thermionic emission theory.[2] Deviation of n from the ideal range $1.01 < n < 1.1$ may be generated by a thick interface layer or substantial

recombination in the depletion region. A non-uniform interface will also produce an increase in n from 1.01.

2.3 CAPACITANCE-VOLTAGE (C-V)

The determination of the SBH by the Capacitance-Voltage (C-V) method is based upon the voltage dependence of the charge in the depletion region of the diode. The C-V method measures the electrostatic properties of the Schottky barrier and is not affected by transport processes such as tunneling and image force lowering.[3] In contrast to the I-V method, C-V measurements employ reverse biasing of the contact to determine the barrier height. A DC reverse bias is applied to the contact with a small AC signal superimposed onto the DC signal. Charges of opposite sign are induced on the semiconductor and metal surfaces, after applying the signal, which generates a junction capacitance. The assumption of a parallel plate capacitor may be used to model the depletion region that acts as a separation between the electrodes. Measuring the resulting capacitances upon applying a range a reverse biases, forms the basis of this technique.[2] The derivation of the SBH from C-V analysis is discussed by Rhoderick and Williams[4] and Sze.[1] Technically, C-V measures the flat-band barrier height versus the zero-bias barrier height found by I-V.

This technique is not universally applicable. If the semiconductor acts as a large series resistor, this will introduce measurement error, since the junction in this case resembles back-to-back Schottky diodes. For an inhomogeneous interface, the C-V method averages over the whole sample area and measures the mean barrier height. High densities of impurities or defects with deep energy levels in the band gap complicate the measurement of the SBH by C-V, since these defects alter the space-charge region and

hence the intercept voltage. These deep level defects typically cause the SBH(C-V) to be greater than the SBH(I-V).

2.4 PHOTOEMISSION SPECTROSCOPY

Photoelectron spectroscopy is based on the photoelectric effect and measures the energy distribution of the excited electrons, which are emitted from a solid. The closely related techniques of X-ray photoelectron spectroscopy (XPS) and ultraviolet photoelectron spectroscopy (UPS) may be utilized. In photoemission, some of the photoelectrons within ~1 nm of the semiconductor surface can escape without loss of energy.[3] The electrons with the maximal energy in the spectrum of the semiconductor are those emitted from the valence band maximum at the surface. In order to measure the position of the Fermi level at the semiconductor surface, a metal in intimate contact with the semiconductor is analyzed.

In the UPS method, the SBH, Φ_B, for an n-type semiconductor is defined as $\Phi_B = E_g - (E_F - E^m_{VBM})$, where E_g is the RT band gap and $(E_F - E^m_{VBM})$ is the difference between the VBM of the thinly metal-coated semiconductor surface and the Fermi level position. By analogy, in the XPS method Φ_B is defined for an n-type semiconductor as $\Phi_B = E_g - E^m_{core} + (E^i_{core} - E^c_{VBM})$, where E^m_{core} is the final position of the semiconductor core level after sequential metal depositions, E^i_{core} is the position of the core level before metal deposition, and E^c_{VBM} is the Fermi level position relative the VBM for the clean semiconductor surface. In a manner similar to the I-V method, the zero-bias barrier height is measured with photoemission, and the values for the two techniques usually agree well.

Photoemission spectroscopy also measures the energy of photoelectrons from the core levels of atoms near the semiconductor surface. Core level electrons generate sharp, well-defined peaks for each element in the photoemission spectra.[3] The binding energy of these peaks may be used to measure changes in the Fermi level position and band bending as a result of metallization of semiconductor surfaces. To observe both the metal and semiconductor states, thin metal overlayers of a few angstroms are sequentially deposited *in situ* onto a clean semiconductor surface.[4] This method gives the p-type SBH accurately, but it is necessary to know the band gap to deduce the n-type barrier. Moreover, chemical shifts due to interface reactions can complicate the determination of the band bending and Fermi level position, which limits an accurate measurement of the SBH.[4] Intermixing usually results in a metallic layer or an intermediate insulating layer, which changes the electronic structure in the interface region. Another pitfall to this technique is when the metal grows by a Volmer-Weber growth mode leaving regions of the semiconductor surface uncovered. In this case, the true, bulk barrier height cannot be measured.

2.5 INTERNAL PHOTOEMISSION (PHOTORESPONSE)

In this technique, monochromatic light is directed to the metal/semiconductor contact, which excites charge carriers at the Fermi level of the metal. If the quantum energy, $h\nu$, of the photons is greater than the threshold $h\nu_0 = \Phi_B - \Delta\Phi_{if}$ (image-force lowering term), then some of these excited carriers form a photocurrent, I_p, in the external circuit. Fowler discovered that this photocurrent is proportional to $\sim (h\nu - h\nu_0)^2$, when $h(\nu - \nu_0) > 5kT$.[3] The SBH may be extrapolated from a plot of $I_p^{1/2}$ versus $h\nu$, which typically

shows a direct proportional relationship with the x-intercept at $hv_0 = \Phi_B - \Delta\Phi_{if,}$ where the latter term denotes barrier-lowering. This method has a major advantage in that it can be used at an arbitrary but fixed bias without the need for extrapolation to zero bias or the flat band voltage.[3] Therefore, internal photoemission may be utilized to measure the SBH voltage dependence directly. The limitations of this technique include (1) the need for a thin metal contact without breakthrough and (2) the interference associated with optical excitations in the semiconductor or back contact. Furthermore, the photocurrent due to a large SBH may be obscured due to band-to-band excitations. In some cases, wave-vector effects may also influence the results.

2.6 SUMMARY

Schottky barriers may be characterized either by I-V, C-V, photoemission spectroscopy and/or internal photoemission. The choice of a particular method depends on the advantages and disadvantages of each technique, the nature of the metal-semiconductor interface, and laboratory resources. Ideally, multiple techniques should be applied to confirm the value of the SBH.

2.7 REFERENCES

1. S. M. Sze, *Physics of Semiconductor Devices*, Second ed. (John Wiley & Sons, NY, 1981).
2. K. M. Tracy, Ph. D. dissertation, N. C. State University, Raleigh, NC (2000).
3. J. F. Luy and P. Russer, *Silicon-Based Millimeter-Wave Devices* (Springer-Verlag, Berlin, 1994).
4. E. H. Rhoderick and R. H. Williams, *Metal-Semiconductor Contacts*, Vol. 19, Second ed. (Oxford Science Publications, Oxford, 1988).

3. *IN SITU* CLEANING AND CHARACTERIZATION OF OXYGEN- AND ZINC-TERMINATED, n-TYPE ZnO{0001} SURFACES[1]

Submitted for consideration for publication

to

The Journal of Applied Physics

By

B. J. Coppa, C. C. Fulton, P. J. Hartlieb, and R. F. Davis[a]
Department of Materials Science and Engineering
North Carolina State University
Box 7907
Raleigh, NC 27695

and

B. J. Rodriguez, B. J. Shields and R. J. Nemanich
Department of Physics
North Carolina State University
Box 8202
Raleigh, NC 27695

[1] (0001) and $(000\bar{1})$ are used in this paper to designate the polar zinc- and oxygen-terminated surfaces, respectively.

[a] Corresponding author.
Email address: robert_davis@ncsu.edu
Tele: 919-515-3272; FAX: 919-515-7724

3.1 ABSTRACT

In situ cleaning procedures for ZnO($000\bar{1}$) and ZnO(0001) surfaces have been developed and their efficacy evaluated in terms of residual hydrocarbons and hydroxide, crystallography, microstructure, and electronic structure. Annealing ZnO($000\bar{1}$) in pure oxygen at 600-650±20 °C reduced but did not eliminate all hydrocarbon contamination. Hydrocarbon and hydroxide constituents were desorbed to concentrations below the detection limits of X-ray photoelectron spectroscopy by annealing for 15 min. in pure O_2 at 700 °C and 0.1 Torr. However, thermal decomposition degraded the surface microstructure. Exposure of the ZnO($000\bar{1}$) surface to a remote plasma having an optimized 20% O_2/80% He mixture for the optimized time, temperature, and pressure of 30 min, 525 °C, and 0.050 Torr showed smooth, highly-ordered, atomically-stepped and stoichiometric surfaces with nearly flat bands. A 0.5 eV change in band bending was attributed to the significant reduction of the accumulation layer associated with surface contamination, and only ~0.4 ML of hydroxide remained. The hydroxide appeared to be more tightly bound to the ZnO(0001) surface, which was attributed to the presence of unfilled dangling bonds associated with the polarity of the material. This effect resulted in an increase in the optimal time and temperature for the plasma cleaning process to 60 min. and 550 °C at 0.050 Torr, respectively.

3.2 INTRODUCTION

Zinc oxide normally occurs in the hexagonal wurtzite crystal structure and, as such, has the direct band-gap energy of 3.4 eV at room temperature.[1] This material is typically n-type due primarily to oxygen vacancies and/or zinc interstitials.[2] Applications for bulk

polycrystalline and powdered ZnO include surface acoustic wave devices, gas sensors, piezoelectric transducers, varistors, transparent conducting films for the photovoltaic industry, phosphors and pigments in paints.[3] Large-area (2 inch) substrates have been commercially produced for growth of ZnO-based films. A review of the recent advances in ZnO materials and devices has recently been published.[1]

Surface cleaning processes are fundamental to semiconductor device fabrication.[4] Previous studies[5-7] have shown that the removal of contaminants from the surfaces of silicon- and gallium arsenide-based substrates decreases both the concentration of growth-related zero- and one-dimensional defects in the subsequently deposited epitaxial films and the reverse bias leakage current in rectifying contacts, and enhances device functionality.[4] Similar gains in the microstructure and electrical properties should be realized in homoepitaxial films of ZnO grown on clean ZnO substrates; however, only a few reports of research concerned with the contaminant removal from ZnO surfaces have been published.[8-11]

Initial cleaning studies of ZnO single-crystals were performed by Fiermans et al.[8] using chemical etching and annealing at an unspecified ambient and pressure. The results of X-ray photoelectron spectroscopy (XPS) and Auger electron spectroscopy (AES) for ZnO($000\bar{1}$) revealed faint traces of S and Cl remaining on the surface from the chemical treatments in H_2SO_4 and HCl, respectively. AES spectra indicated that annealing at 700°C for 10 min. resulted in significant oxygen desorption and the removal of all detectable carbon. Out-diffused Ca impurities were detected, as well. Low-energy electron diffraction (LEED) revealed the formation of a (1x1) hexagonal pattern with spots of peculiar symmetry, which were related to the thermal etching process. After applying this

same cleaning procedure to the ZnO(0001) face, relatively large Cl, S, and Ca XPS and AES signals were measured, while the resulting (1x1) hexagonal LEED pattern was weaker than the one observed for the ZnO($000\bar{1}$) face. Thus, these processes are neither suitable for wafer cleaning nor compatible with standard device processing procedures.

Jacobs and co-workers[9] determined from AES spectra that annealing ZnO($000\bar{1}$) at 597 °C in 3 x 10^{-3} Torr of O_2 for 30 min. reduced the carbon concentration on the surface. A more defined (1x1) hexagonal LEED pattern was also obtained. However, removal and/or characterization of the surface hydroxide was not reported.

Several groups have utilized Ar^+ ion gun bombardment followed by annealing for the removal of surface contamination from ZnO. XPS results acquired by Mintas and Filby[10] from the surface of as-received, sintered ZnO tablets revealed the hydroxide component of the O 1*s* core level located 1.5-2 eV higher in binding energy than the lattice oxygen and a significant concentration of carbon, as determined from analysis of the C 1*s* core level. Exposure to 6-kV Ar^+ ions in a beam current of 40 µA for 20 min. removed all detectable concentrations of these contaminants.[10] After exposure to these ions and subsequent annealing in vacuum at 527 °C for 30 min. and at 427 °C for 30 min. in O_2 at 1 x 10^{-8} Torr, AES spectra obtained by Roberts and Gorte[11] revealed the removal of C and Ar impurities on the {0001} surfaces of ZnO single crystals. Hydroxide removal was not discussed in this report, since only AES was used as a characterization tool, where the oxidation states of the oxygen are not readily distinguished. In general, ion bombardment typically results in physical and chemical alteration of the surface and the underlying layers through mixing, roughening, formation of craters, and/or a change in oxidation state.[10]

In the study reported herein, *in situ* cleaning procedures involving annealing in either oxygen or a remote O_2/He plasma were investigated for the removal of adventitious hydrocarbons and hydroxide from the polished {0001} faces of ZnO wafers. The efficacy of these procedures was determined using several *in situ* spectroscopy, microstructural, and structural characterization techniques, as described in the following sections.

3.3 EXPERIMENTAL PROCEDURES

Two millimeter-thick, single-crystal ZnO($000\bar{1}$) and ZnO(0001) two-inch wafers, diced from boules produced by seeded chemical vapor transport by Eagle-Picher Technologies, Incorporated,[12] and chemo-mechanically polished on both sides, were employed in the present research. Hall and C-V measurements, the latter at 1 x 10^4 Hz, taken from the ($000\bar{1}$) surface of the as-received wafer showed a bulk carrier concentration of 1±5 x $10^{17}/cm^3$ and a nominal effective donor concentration, (N_D-N_A), of 5±5 x $10^{16}/cm^3$, respectively, for the as-received samples. The wafers were cleaved into smaller sections, rinsed in methanol for 5 sec and dried in flowing nitrogen. *Ex situ* exposure of the $2.5cm^2$ samples to a UV/ozone environment for 15 min. reduced the carbon concentration below the detection limit of AES. However, this method was not further employed due to the persistent photoconductivity of ZnO when exposed to UV light, as reported peviously.[13-14] Samples were stored in a dessicator under ~1 Torr vacuum with packets of humidity sponges that were replaced monthly. The use of the dessicator minimized further reaction with water vapor and the continued formation of the hydroxide.

All *in situ* cleaning and surface characterization experiments were conducted within a unique ultrahigh vacuum (UHV) configuration, which integrates several independent

cleaning, thin-film growth and analysis systems via a transfer line[15] having a base pressure of 1 x 10^{-9} Torr. Each ZnO sample was mounted with Ta wires on an inconel® holder that was transferred to larger inconel® holder located 40 cm below the center of the rf coil in a remote plasma chamber, having a base pressure of 5 x 10^{-9} Torr. Two different investigations were conducted to remove the hydrocarbon and hydroxide contaminants from the ZnO surfaces: (1) annealing ZnO($000\bar{1}$) in flowing oxygen and (2) exposure of both ZnO($000\bar{1}$) and ZnO(0001) to a remote oxygen plasma at elevated temperatures. In the former study, each sample was heated at a rate of a ~20 °C/min to 300 °C. Pure oxygen was subsequently flowed through the system at 300 °C to produce a constant pressure of 0.100 Torr, which was regulated using a turbomolecular pump. The selected sample was then heated at 30 °C/min to a single annealing temperature of 600 °C, 625 °C, 650 °C, or 700 °C; held for the time associated with that temperature, as shown in Table 3.1, and cooled at 30 °C/min to 300 °C. The system was then evacuated, and the sample was cooled to room temperature.

Heating of the sample was achieved with a stage consisting of a wound 70% platinum-30% rhodium heating filament mounted on a boron nitride disk that was supported by three alumina tubes. Heating profiles were controlled with a 20 A semiconductor current rectifier power supply. A chromel-alumnel (K-type) thermocouple with an inconel sheath located in close proximity to the sample was used to measure the temperature. An optical pyrometer with a spectral response of 0.96-1.05 μm was used to calibrate the heater for the extrapolation of temperatures above 600 °C. An emissivity of 0.64 was programmed for the 40-nm-thick titanium, which was deposited by electron beam evaporation on the entire (0001) face of each ZnO piece. This film served to absorb

radiation from the underlying Pt-Rh heater and conduct heat into the wafer during the cleaning of the $(000\bar{1})$ face. The reverse scenario was used in the case of cleaning Zn-terminated surfaces; the uncertainties in temperature were ±20 °C.

The remote plasma was achieved by exciting mixtures of research grade helium and oxygen containing mainly 20%, by volume, of the latter gas by virtue of flowing 15 sccm of O_2 and 60 sccm of He through a quartz tube mounted at the top of the chamber. The tube was surrounded by a copper coil connected to a tuned 20-W power supply operated at 13.56 MHz. The ZnO samples were processed at ~20 °C, 350 °C, 450 °C, 475 °C, 500 °C, 525 °C, 575 °C, or 600 °C, and the heating rate was ~ 20 °C/min. The gas mixture was introduced into the system when the sample temperature reached 425 °C (except for the 20 °C and 350 °C exposures where the gases were introduced at those temperatures) before striking the plasma. It was found that heating ZnO in vacuum up to 425 °C did not generate surface degradation, so this temperature was chosen thereafter for entry of helium and oxygen gas into the chamber. Plasma exposure times ranged from 0.5-60 min. In some experiments, the samples were subsequently annealed in pure, unexcited oxygen at the temperature of the plasma exposure in an attempt to further reduce the hydroxide, before cooling and subsequent evacuation at 425 °C.

A 3-kV beam voltage and 1-mA beam was used in the AES analyses. Spectra were collected in the undifferentiated mode and numerically differentiated. A constant 2-mA beam current was used to obtain the LEED patterns; however, it was necessary to vary the beam voltages between 20-100 eV because of the varying amounts of surface contamination.

All XPS spectra were acquired, typically over a period of one hour, using a

Mg K-a source (h ? = 1253.6 eV) operated at 13-kV and 20-mA emission current in tandem with a hemispherical electron energy analyzer with a mean radius of 100 mm (VG CLAM II). Periodic scans of the Au 4 $f_{7/2}$ peak of a gold standard made by e-beam evaporation on a Si(100) wafer allowed calibration corrections to be made for discrepancies from the known value of 84.0 eV.[16] The data were most accurately represented by a mixed Gaussian-Lorentzian peak shape with a linear background, which was systematically subtracted from the initial spectra.

An Omicron HIS 13 VUV discharge lamp powered by a NG HIS power supply and emitting He I 21.2 eV radiation was used in conjunction with an angle-resolved ultraviolet photoelectron spectrometer (ARUPS) with a base pressure of 5 x 10^{-10} Torr to to obtain spectral information regarding the electronic structure of the ZnO surface. A 500V potential, 50mA discharge current and 4V sample bias were used in these studies. Helium leaked into the ARUPS from the lamp inlet raised the pressure of the chamber to ~1 x 10^{-8} Torr during operation; however, this inert environment did not produce surface contamination. A VSW HA50 50-mm-radius hemispherical electron energy analyzer having a 4-element lens was used to collect the UPS results.

Before and after the cleaning experiment, atomic force microscopy (AFM) of the surface microstructure, was performed primarily in the contact mode to determine if the cleaning procedures introduced surface damage from thermal decomposition and chemical and/or mechanical interactions with the plasma species. A commercially available PSI M5 system and silicon and/or silicon nitride tips were used for this study.

3.4 RESULTS AND DISCUSSION

3.4.1 *Oxygen Annealing of ZnO($000\bar{1}$)*

Numerous AES and XPS scans confirmed carbon and hydroxyls as the only measurable surface contaminants on as-received ZnO($000\bar{1}$). As-received samples in this study are denoted as ones that were rinsed 5 sec in methanol and dried in flowing nitrogen before loading into UHV. A LEED pattern was not observed with an incident beam energy = 100 eV, which was attributed to a relatively thick, amorphous hydroxide layer. The combined LEED, AES and XPS results indicated that the contamination layer on each face of the as-received ZnO contained at least 1.0±0.1 ML of carbon and 1.6±0.1 ML of hydroxide; this is in agreement with other reports.[9,17] The report by Jacobs mentioned earlier provided the initial conditions for the annealing experiments in the present research.

The removal of carbon was not measurable after comparing the C *KLL* AES peaks acquired from the ZnO($000\bar{1}$) surface of the as-received sample with that acquired from the same sample annealed at 600 ºC. Annealing at 625 °C resulted in a 20% reduction in intensity of the C *KLL* AES peak. Increasing the annealing temperature to 650°C allowed a well-defined (1x1) hexagonal LEED pattern to be obtained using a primary beam potential of 20 eV. This was apparently due to desorption of some of the hydroxide, as the intensity of the C *KLL* AES peak was unchanged from that observed after the anneal at 625°C. Moreover, carbon has been reported to only lessen the clarity of a LEED pattern for ZnO($000\bar{1}$), indicating that it may be more ordered and/or less thick than the OH layer.[8]

Annealing at 700 ºC for 15 min. resulted in a similar LEED pattern at 20 eV and increases in the intensities of the O *KLL* and Zn *LMM* Auger peaks by 100% and 67%, respectively. The carbon signal was not detectable, as shown in Fig. 3.1. Companion XPS

spectra in Fig. 3.2 (a) of the O 1*s* core level of the as-received ZnO($000\bar{1}$) surface revealed a doublet, associated with a hydroxylated ZnO surface. The higher binding energy peak at 532.9 eV is indicative of ~2 ML of OH^-.[8] XPS core level spectra in these studies have an uncertainty of ±0.1 eV, and 1 atomic % hydroxide corresponded to ~0.1 ML. Oxygen bonded to zinc in the lattice is identified at 531.3 eV, which is the lower binding energy peak in Fig. 3.2 (a). The hydroxide signal is not observed after the cleaning process, as shown in Fig. 3.2 (b), which means that less than ~0.3 at.% of hydroxyls remain on the surface, as this value represents the detection limit of our XPS system. The lattice oxygen peak is also shifted 0.2 eV to a lower binding energy of 531.1 eV. The intensity of the C 1*s* core level peak of the as-loaded surface, observed at 285.6 eV, decreased to below the noise level as a result of the annealing process; this confirms the carbon removal indicated by AES spectra in Fig. 3.1. Furthermore, the Zn $2p_{1/2}$ core level peak at 1045.2 eV and Zn $2p_{3/2}$ peak at 1022.1 eV were reduced in binding energy by 0.4 eV. The average value of 0.3±0.1 eV for the Zn 2*p* and O 1*s* core level shifts are ascribed to a change in band bending associated with the cleaning process.

Extending the annealing time to 30 min. caused surface decomposition by the associated formation of needles separated by ~1 μm and oriented in three crystallographic directions over the entire surface. As a result, the RMS surface roughness increased from 5.7±0.2 nm measured on the as-received material to 15.8±0.2 nm for the oxygen-annealed material. Similar observations were found in decomposition studies by Leonard and Searcy.[18,19] Further evidence of the decomposition of ZnO was deduced from the LEED pattern, where the 1x1 hexagonal pattern was replaced by a diffuse background. XPS studies revealed an increase in the Zn/O atomic ratio from 0.7±0.1 for the as-received

surface to 1.2±0.1 for the decomposed surface, which may indicate the diffusion of interstitial Zn to the surface and/or the loss of lattice oxygen. Decomposition of the ZnO($000\bar{1}$) surface has been investigated by quadrupole mass spectrometer measurements under UHV conditions by D. Kohl *et al.*[20] This group reported that measurable sublimation in the form of atomic Zn and O from a UHV-cleaved surface begins at 600 °C.[20] L. Fiermans *et al.*[8] reported that annealing ZnO($000\bar{1}$) at 700 °C and 1 x 10^{-10} Torr for periods greater than 10 min. caused thermal etching, as indicated by the formation of (1x1) hexagonal maverick LEED spots with peculiar symmetries. In addition, Nowok[21] has reported that prolonged exposure of the ZnO($000\bar{1}$) surface to a several-hundred-volt electron beam generated a hexagonal-to-cubic phase transformation measured by X-ray diffraction and the formation of dendrites observed in scanning electron microscopy.

3.4.2 *Remote plasma cleaning of the ZnO(*$000\bar{1}$*) surface*

Remote O_2/He plasma exposures, creating free radicals of oxygen atoms and molecules, at 20-W were employed to achieve a clean, well-ordered, stoichiometric and undamaged ZnO surface. Table 3.2 summarizes the various plasma cleaning experiments and XPS results, in ascending order based on temperature, which is not the exact chronological order of the studies. Carbon was removed below the detection limit of XPS, by every remote plasma exposure listed in Table 3.2, beginning with the shortest exposure time of 0.5 min at room-temperature, as shown in Fig. 3.3. Thus, remote O_2/He plasma cleaning of ZnO is much more effective in desorbing carbon constituents compared to oxygen annealing, which required a high temperature and lengthy annealing time, ie. 700 °C and 15 min. After the plasma exposures numbered 1-3 in Table 3.2, LEED diffraction

spots were not observed, indicating that significant hydroxide coverage of ~1.7 ML remained on this nonstoichiometric surface with Zn/O = 0.4. Representative XPS O1 s core level spectra for experiment #3 in Table 3.2 are shown in Fig. 3.4 (ii). In these studies, desorption of OH from ZnO is related to an increase in the Zn/O ratio and the band bending, as listed in Table 3.2 and described in the electron accumulation layer model discussed previously.

To enhance the removal of the hydroxide we considered either increasing the energy of the plasma and risk surface damage or increasing the temperature of the ZnO substrate and risk the evaporation that occurs in high-temperature annealing experiments. The latter approach was selected to determine if a combination of plasma exposure time and elevated temperature existed whereby significant removal of the hydroxide could be achieved without measurably affecting the microstructure of the substrate surface. Subsequent oxygen annealing steps listed in Table 3.2 did not indicate additional OH desorption.

Remote plasma exposures were carried out at elevated temperatures beginning at 350 °C (exp. #4, Table 3.2). The volume percent of O_2 was increased to 12% in an attempt to suppress desorption of lattice oxygen from the ZnO surface during heating of the substrate. Heating ZnO to 350 °C before exposing the sample for 0.5 min. to a 20-W 12% O_2/88% He remote plasma at 0.050 Torr reduced the hydroxide thickness by ~0.5 ML and increased Zn/O from 0.4 to 0.5, as compared to the as-received surface. The Zn $2p_{1/2}$ and Zn $2p_{3/2}$ XPS core level peaks were shifted from 1044.9 eV and 1021.9 eV for the as-received surface to 1044.6 eV and 1021.7 eV for the plasma-cleaned surface. Similarly, the O 1*s* lattice XPS peak showed this same 0.3 eV change in band bending through the

core level shift from 530.6 eV for the as-received surface to 530.3 eV after cleaning, as seen in Fig. 3.4 (iii). A diffuse (1x1) hexagonal LEED pattern emerged at 57 eV after cleaning, while only an amorphous background was observed for the as-received surface.

A similar plasma exposure at 450 °C (exp. #5, Table 3.2) resulted in a 58% reduction in the concentration of hydroxyls or ~0.9 ML. The Zn $2p_{1/2}$ and Zn $2p_{3/2}$ XPS core level peaks were shifted from 1044.9 eV and 1021.9 eV for the as-received surface to 1044.3 eV and 1021.2 eV for the plasma-cleaned surface; this change in band bending was confirmed by UPS spectral analysis. As seen in Fig. 3.4 (iv), the O 1*s* lattice XPS peak showed a 0.5 eV change in band bending through the core level shift from 530.6 eV for the as-received surface to 530.2 eV after cleaning. The average change in band bending between these two core levels of 0.5 eV was confirmed by UPS analysis. The OH peak at 532.3 eV in Fig. 3.4(iv) is representative of ~1.7 ML of residual OH remaining on the surface. Further analysis showed an increase in Zn/O from 0.1 to 0.4, for the as-received and plasma-cleaned surfaces, respectively. Since the sample surface was not polished, a LEED pattern was not observed.

Increasing the temperature to 475 °C for the remote plasma exposure (exp. #6, Table 3.2) resulted in a reduction of the residual hydroxide by ~0.8 ML without generating AFM evidence of thermal decomposition of ZnO. Temperature was deemed a critical parameter, based on the effectiveness in removing OH at 350 °C and 450 °C. The volume ratio of O_2/He was adjusted to 20%/80% at 475 °C, which was found to be a sufficient mixture to suppress any possible desorption of lattice oxygen, while providing enough free oxygen radicals to chemically interact with the surface for the removal of surface contaminants. This oxygen-helium mixture was left unchanged for subsequent

experiments and was not deemed the critical factor in minimizing residual hydroxide. The XPS spectra showed a 0.7 eV core level shift in binding energy based on the as-received Zn 2*p* multiplet moving from 1022.1 eV and 1045.2 eV for the as-received surface to 1021.4 eV and 1044.5 eV, after cleaning. For the as-received surface, the O 1*s* lattice peak was located at 530.9 eV, while the hydroxide signal was detected at 532.8 eV. A 0.5 eV shift in the O 1*s* lattice peak to 530.4 eV was measured; as depicted in Fig. 3.4(v), the suppressed hydroxide component was found at 532.1 eV. An average core level shift between Zn 2*p* and O 1*s* indicated a 0.6 eV change in band bending associated with the removal of surface contaminants, which correlated to an increase in the Zn/O ratio of 0.4 for the as-received surface to 0.8 after the cleaning process. A (1x1) hexagonal LEED pattern with sharp spots and minimal background was observed at 50 eV.

UPS spectra of the as-received ZnO(000$\bar{1}$) surface showed that the 3*d* bulk feature is located at 11.2 eV below the Fermi level.[20] The Fermi level was located 0.1 eV above the conduction band minimum (CBM), giving rise to 0.4 eV of downward band bending at the surface due to the accumulation layer. This behavior and associated charge transfer process has been reported in previous work for ZnO contaminated by the chemisorption of water.[22] In comparison, the flat band condition for n-type ZnO places the Fermi level at 0.3 eV below the CBM.[20,22]

The 475 °C remote plasma cleaning resulted in a sharper valence band turn-on and more distinct bulk features in the spectra for ZnO. An electron affinity[20,22] of 4.4±0.2 eV was deduced from the width of the spectrum. Extrapolation of the VBM from the leading edge of the spectra resulted in a value of 2.7 eV below the Fermi level. The O 2*p* peak emerged at 4.1 eV below the Fermi level, while the Zn 3*d* feature shifted 0.7 eV to 10.5 eV

below the Fermi level. Also, the surface Fermi level shifted down to 0.7 eV below the CBM, indicating upward band bending of 0.4 eV. The Fermi level for bulk ZnO is located at 0.3 eV below the CBM. Overall, these results indicate a 0.8±0.1 eV shift upwards in band bending, which agree with the XPS result of 0.6±0.1 eV.

Significant amounts of the hydroxide were removed from the ZnO(000$\bar{1}$) surface at 500 °C, 525 °C, 575 °C and 600 °C, as described in Table 3.2. The surfaces heated at or above 575 °C possessed needles associated with thermal decomposition, which were similar in microstructure to the surfaces of samples annealed in oxygen at 700 °C. Thus, the plasma cleaning temperature was set at 525 °C, the O_2/He ratio, plasma pressure and plasma power maintained at 20/80, 0.050 Torr and 20 W, respectively, and the time of exposure to the plasma increased to determine the optimum value.

The optimal plasma exposure time was determined to be 30 min., as processing for 45 min. at 525 °C did not generate any decrease in the measurable hydroxide concentration. After the optimized plasma-clean at 525 °C, a shift was measured in the lattice O core level peak from 530.7 eV to a final position of 530.3 eV, as shown in Fig. 3.4(vii), and a reduction in the OH concentration was also observed. This change in band bending is expected to lead to a reduction in surface conductivity. Approximately 0.4 ML of the OH remained, as derived from the peak at 532.4 eV in Fig. 3.4(vii). A related core level shift of 0.6 eV for Zn 2*p* was observed with the Zn multiplet moving from 1021.9 eV and 1044.9 eV to 1021.3 eV and 1044.4 eV, respectively. This significant removal of ~1.2 ML of the OH was critical for eliminating the proposed accumulation layer[22-23] and for generating a Zn/O stoichiometric ratio of 1.0±0.1.

The UPS results shown in Fig. 3.5 also show a 0.5 eV change in band bending, which are in agreement with the XPS results noted above. It is shown in curve (i) in Fig. 3.5 that for the as-received surface the Zn *3d* bulk feature is located at 11.3 eV below the Fermi level, while the O *2p* bulk feature was not discernible.[20] Thus, the Fermi level was located 0.2 eV above the CBM, giving rise to 0.6 eV of downward band bending at the surface. In comparison, the Fermi level for bulk ZnO is located at 0.3 eV below the CBM. Curve (ii) in Fig. 3.5 shows that after cleaning, the O *2p* bulk feature emerged at 4.0 eV, and the Fermi level shifted down to 0.1 eV below the CBM, conveying 0.1 eV of downward band bending. An electron affinity of 4.1±0.2 eV was calculated for the clean surface, after extrapolating the VBM from the leading edge of the spectra to 3.3 eV below the Fermi level, as shown in curve (ii-ii) in the inset in Fig. 3.5. Furthermore, the 0.6 eV shift of the Zn 3*d* bulk feature to 10.7 eV matched the corresponding change in band bending found in the XPS spectra. The large peak in the high binding energy region of curves (i) and (ii) in Fig. 3.5 is due to secondary electrons.[24]

Extensive AFM analysis revealed a smooth surface microstructure, as shown in Fig. 3.6(a) and (b), and a RMS surface roughness of 0.2±0.2 nm before and 0.6±0.2 nm after the optimum cleaning process. These results confirmed the absence of observable microstructural change associated with the plasma exposure at 525°C. As shown in Fig 3.6(b), the cleaning process also revealed ordered atomic steps with a unit cell step height of 0.53±0.01 nm and step width of ~0.2 µm. The slight double diffraction of LEED spots in the (1x1) hexagonal pattern obtained at 42 eV was likely due to these atomic steps. The propensity of step formation on this surface may explain similar LEED results reported by Nakagawa and Mitsudo.[25] At energies > 42 eV, i.e., 60 eV, only discrete spots were

observed, as the incident beam probed deeper into the ZnO. Very low leakage Schottky contacts with low ideality factors were also deposited on this optimally cleaned surface by the present authors, as reported elsewhere.[26]

3.4.3 *Post-plasma oxygen annealing of the ZnO(*$000\bar{1}$*) surface*

While in a transition phase of experiments between strictly oxygen annealing and strictly remote plasma cleaning of ZnO($000\bar{1}$), a secondary step was added comprised of a hybrid of these two techniques. Remote O_2/He plasma cleaning of ZnO is a new way of cleaning this material, since the majority of previously reported related work dealt simply with oxygen annealing.[9,11] Partial OH removal at 350 °C (exp. #4, Table 3.2) was indicated by XPS and LEED results. However, it was shown that oxygen annealing ZnO($000\bar{1}$) at 650 °C and 0.100 Torr for 30 min. (exp. #3, Table 3.1) gave rise to a diffuse (1x1) hexagonal LEED pattern associated with the reduction of the OH layer. It was believed that OH could be removed at a lower temperature, but while requiring a higher pressure of O_2, to prevent decomposition of lattice O, which occurs at or above 575 °C. Thus, a post-plasma oxygen annealing step for 5 min. at 5 Torr of pure O_2 was added in exp. #5 in Table 3.2 at 450 °C. The XPS and UPS spectra showed no enhancement in OH removal or adsorption of oxygen, as a result of the oxygen annealing step. In addition, another post-plasma annealing step (exp. #8, Table 3.2) was attempted at 525 °C and 0.500 Torr of pure O_2 for 10 min. with the same consequences. Thus, pure O_2, in the case of oxygen annealing, appears less reactive than atomic oxygen, in the case of a remote He/O_2 plasma, at elevated temperatures in desorbing hydroxide from ZnO. The lack of measurable adsorbed oxygen on this surface after the annealing step is consistent with the

reported chemisorption temperature range 20-377 °C,[26] which is well below the post-plasma annealing temperatures in Table 3.2.

3.4.4 *Remote plasma cleaning of the ZnO(0001) surface*

Low-energy electron diffraction of the as-received ZnO(0001) surface showed only a bright background, indicative of a disordered contamination layer. Deconvolution of the O 1*s* core level peak obtained via XPS studies revealed that this surface contained ~2.0 ML of OH, as determined by a peak at 532.9 eV, and a nonstoichiometric ratio of Zn/O = 0.3 was calculated. The development of an effective cleaning procedure for this surface employed the optimal cleaning procedure developed for the $(000\bar{1})$ surface as the starting point for this study, as noted in Table 3.3. A summary of XPS results corresponding to these cleaning experiments is listed in this table. The XPS spectra acquired after plasma exposures for 30 and 60 min. at 525 °C (exp. # 1-2, Table 3.3) are shown in Fig. 3.7. Approximately 1.6 ML of OH remained on the surface, the ratio of Zn/O = 0.5 and diffuse (1x1) hexagonal LEED patterns were obtained. The hydroxide was more tightly bound to this surface, and this effect was attributed to the presence of unfilled dangling bonds associated with the polarity of ZnO.[27] The temperature of the plasma exposure was increased only slightly in order to avoid evaporation.

The optimal cleaning procedure employed a 20% O_2/80% He remote plasma at 550 °C and 0.050 Torr for 60 min., followed by evacuation at and cooling from 425 °C. The XPS spectra of the plasma-cleaned surface revealed a shift in the lattice O core level peak from 530.9 (FWHM= 1.6 eV) to 530.4 eV (FWHM= 1.4 eV) indicating a change in band bending. These results also showed ~0.4 ML of OH remaining as the sole contaminant

with a peak at 532.7 eV. Figure 3.7 (i) and (iv) show the corresponding core level shift of 0.6 eV with the Zn $2p_{1/2}$ and Zn $2p_{3/2}$ peaks moving from 1022.0 eV and 1045.1 eV (both FWHM= 2.3 eV) to 1021.4 eV and 1044.5 eV (both FWHM= 2.1 eV), respectively. Figure 3.7 also indicates the increased intensity of the Zn $2p$ core level after the successive plasma exposures in comparison to the as-received state. Satellite peaks were commonly observed at approximately 1013.2 eV and 1036.2 eV.

This significant removal of ~1.6 ML of the OH was critical for eliminating the proposed accumulation layer[23-24] and for generating a surface with a Zn/O stoichiometric ratio of 1.0. The 0.6 eV change in band bending was confirmed by UPS investigations. The UPS spectra of the clean ZnO(0001) surface directly matched the ZnO(000$\bar{1}$) surface, indicating the lack of polarity effects in modifying the electronic structure. Distinct surface states were not observed after conducting the optimum cleaning procedure for either surface.

Prior and post-cleaning AFM analyses of the (0001) surface confirmed the absence of any observable damage associated with the annealing and/or plasma exposure. A smooth ZnO(0001) microstructure was observed with average RMS surface roughness values of 1.2±0.2 nm before and 1.7±0.2 nm after the cleaning process, respectively, as shown in Fig. 3.8. Sharp LEED spots in the (1x1) hexagonal pattern were obtained at 50 eV. Low leakage Schottky contacts with low-ideality parameters were also produced on these cleaned surfaces.[29]

The use of the remote O_2/He plasma allowed the operation of both the Langmuir-Hinshelwood (LH) and Eley-Rideal (ER) mechanisms.[30] Oxygen atoms and molecules produced in the plasma extracted both the hydrocarbons and the hydroxide from the

surfaces without being measurably, thermally accommodated at these surfaces after cleaning, possibly due to their high excess potential energy. The LH mechanism was apparently dominant, since the level of adsorbed oxygen on either face was determined to be below the detection limit of XPS. Futhermore, the time-dependent nature of the hydroxide removal from ZnO may be indicative of a LH mechanism, where an intrinsic surface process is associated with the surface residence time of oxygen species interacting with the ZnO surface.

3.5 SUMMARY

It was confirmed that annealing ZnO(000$\bar{1}$) in pure oxygen is effective for desorbing surface contaminants, primarily adventitious carbon and hydroxide. Hydrocarbon and hydroxide constituents were desorbed to concentrations below the detection limits of XPS by annealing for 15 min. in pure O_2 at 700 °C and 0.1 Torr. However, thermal decomposition degraded the surface microstructure. Thus, an alternative, non-destructive cleaning process was developed.

Smooth, highly-ordered, atomically-stepped and stoichiometric ZnO(000$\bar{1}$) surfaces with nearly flat bands were developed by exposure to a 20-W remote plasma of 20% O_2/80% He for the optimized time, temperature, and pressure of 30 min, 525 °C, and 0.050 Torr, as confirmed by AFM, LEED, XPS, and UPS, respectively. Only ~0.4 ML of hydroxide remained, as the sole contaminant, after this cleaning process that generated a 0.5 eV change in band bending and a significant reduction in the electron accumulation layer, which has been associated primarily with the presence of hydroxide on the surface.

It was found that the hydroxide was more tightly bound to the ZnO(0001) surface, which has been attributed to the presence of unfilled dangling bonds associated with the polarity of ZnO. This effect increased the temperature and time of the plasma cleaning process to obtain nearly identical results relative to the ZnO($000\bar{1}$) surface. The optimum cleaning procedure entailed a 60 min. 20% O_2/80% He remote plasma at 550 °C and 0.050 Torr, which was applied in another study for the development of very low leakage and low ideality parameter Schottky contacts.

3.6 ACKNOWLEDGMENTS

This research was partially funded by both the Kenan Institute for Technology, Engineering, and Science at NCSU and by the Office of Naval Research under contract N00014-98-1-0654 (H. Dietrich, monitor). The authors express their appreciation to Gene Cantwell, David Eason of Eagle-Picher, Inc. and Aloysius Gonzaga for helpful discussions. Robert Davis was partially supported by a Kobe Steel Ltd. Professorship.

3.7 REFERENCES

1. D. C. Look, Mater. Sci. Eng. B 80, 383 (2001).
2. W. Göpel, L. J. Brillson, and C. F. Brucker, J. Vac. Sci. Technol. 17, 894 (1980).
3. F. D. Auret, S. A. Goodman, M. Hayes, M. J. Legodi, H. A. van Laarhoven, and D. C. Look, J. Phys.: Condens. Matter 13, 1 (2001).
4. S.W. King, J. P. Barnak, M.D. Bremser, K. M. Tracy, C. Ronning, R. F. Davis, and R. J. Nemanich, J. Appl. Phys. 84, 9 (1998).
5. R. P. Vasquez. B. F. Lewis, and F. J. Grunthaner, Appl. Phys. Lett. 42, 293 (1983).
6. M. Yamada and Y. Ide, Jpn. J. Appl. Phys. Part 2 33, L671 (1994).
7. C. M. Rouleau and R. M. Park, J. Appl. Phys. 73, 4610 (1993).
8. L. Fiermans, E. Arijs, J. Vennik, and Vorst, Surf. Sci. 39, 357 (1973).
9. H. Jacobs, W. Mokwa, D. Kohl, and G. Heiland, Surf. Sci. 160, 217 (1985).
10. M. Mintas and G.W. Filby, Zeitschrift fur Naturforschung 36a, 140 (1981).
11. S. Roberts and R. J. Gorte, J. Chem. Phys. 93, 5337 (1990).
12. D. C. Look, D. C. Reynolds, J. R. Sizelove, R. L. Jones, C. W. Litton, G. Cantwell, and W. C. Harsch, Solid State Commun. 105, 399 (1998).
13. T. L. Tansley and D. F. Neely, Thin Solid Films 121, 95 (1984).
14. R. J. Collins and D. G. Thomas, Physical Review 112, 388 (1958).
15. J. van der Weide, Ph.D. dissertation, N. C. State University, Raleigh, NC, 1994.
16. D. Briggs and M. P. Seah, *Practical Surface Analysis*, 2nd edition, Appendices (Wiley, New York, 1990).
17. I. R. Lauks and M. Green, Surf. Sci. 71, 735 (1978).
18. R. Leonard and A. Searcy, J. Chem. Phys. 50, 5419 (1969).

19. R. Leonard and A. Searcy, J. App. Phys. 42, 4047 (1971).

20. D. Kohl, M. Henzler, and G. Heiland, Surf. Sci. 41, 403 (1974).

21. J. Nowok, Kristall and Technik 11, 947 (1976).

22. K. Jacobi, G. Zwicker, and A. Gutmann, Surf. Sci. 141, 109 (1984).

23. H. Moormann, D. Kohl, and G. Heiland, Surf. Sci 100, 302 (1980).

24. G. Heiland and P. Kunstmann, Surf. Sci. 13, 72 (1969).

25. M. Nakagawa and H. Mitsudo, Surf. Sci. 175, 157 (1986).

26. B. J. Coppa, R. F. Davis, and R. J. Nemanich, Appl. Phys. Lett. 82, 400 (2003).

27. V. E. Henrich and P. A. Cox, *The Surface Science of Metal Oxides* (Cambridge Univ., Cambridge, 1994) p. 298.

28. R. Leysen, G. van Orshaegen, H. van Hove, and A. Neyens, Phys. Stat. Sol. (a) 18, 613 (1973).

29. B. J. Coppa, C. C. Fulton, R. F. Davis, C. Pandarinath, J. E. Burnette, and R. J. Nemanich, submitted to J. Appl. Phys.

30. A. Zangwill, *Physics at Surfaces* (Cambridge Univ., Cambridge, 1988) p. 401-18.

Experiment Number	**Sample Temperature (±20°C)**	**Process Pressure (±0.001 Torr)**	**Process Time (min)**
1	600	0.100	30
2	625	0.100	30
3	650	0.100	30
4	700	0.100	15
5	700	0.100	30

Table 3.1. Sets of temperature, total pressure and time investigated to determine the efficacy of annealing ZnO($000\bar{1}$) in pure O_2 for the removal of surface contaminants.

Exp. #	Samp. Temp. (±20°C for T>RT)	O_2/He Vol.% Ratio	Plasma Pressure (±0.001 Torr)	Plasma Exposure Time (min)	Anneal Temp. (±20°C)	Anneal Pressure (±0.001 Torr)	Anneal Time (min)	Zn/O Ratio (±0.1)	OH Reduction (±0.1 ML)	Change in band bending (±0.1 eV)
1	~20	2/98	5.0	0.5	--	--	--	0.4	0.0	0.1
2	~20	2/98	0.050	0.5	--	--	--	0.4	0.0	0.1
3	~20	2/98	0.050	1.0	--	--	--	0.4	0.0	0.1
4	350	12/88	0.050	0.5	--	--	--	0.5	0.5	0.3
5	450	12/88	0.050	0.5	450	5.000	5	0.4	0.9	0.5
6	475	20/80	0.050	0.5	--	--	--	0.8	0.8	0.6
7	500	20/80	0.050	2.0	--	--	--	0.5	0.7	0.6
8	525	20/80	0.050	0.5	525	0.500	10	0.4	0.7	0.5
9	525	20/80	0.050	15	--	--	--	0.9	0.7	0.4
10	**525**	**20/80**	**0.050**	**30**	**--**	**--**	**--**	**1.0**	**1.2**	**0.5**
11	525	20/80	0.050	45	--	--	--	1.0	1.2	0.5
12	575	20/80	0.050	0.5	575	0.500	15	0.9	0.9	0.4
13	600	20/80	0.050	1	600	0.050	15	0.7	1.3	0.6
14	600	20/80	0.050	15	600	0.050	30	0.7	0.7	0.3

Table 3.2. Sets of sample and remote 20-W plasma parameters, O_2/He ratios as well as parameters used in the optional annealing step in pure O_2 for the removal of surface contaminants from the ZnO(000$\bar{1}$) surface. The optimum cleaning procedure and associated results are in bold print.

Experiment Number	**Sample Temperature (±20°C)**	**Plasma Process Pressure (±0.001 Torr)**	**Plasma Exposure Time (min)**	**Zn/O Ratio (±0.1)**	**OH reduction (±0.1 ML)**	**Change in band bending (±0.1 eV)**
1	525	0.050	30	0.5	1.2	0.5
2	525	0.050	60	0.5	1.3	0.6
3	**550**	**0.050**	**60**	**1.0**	**1.0**	**0.6**

Table 3.3. Sets of remote 20-W, 20% O_2/80% He remote plasma parameters investigated for the removal of surface contaminants from the ZnO(0001) surface. The optimum cleaning procedure and related results are in bold print.

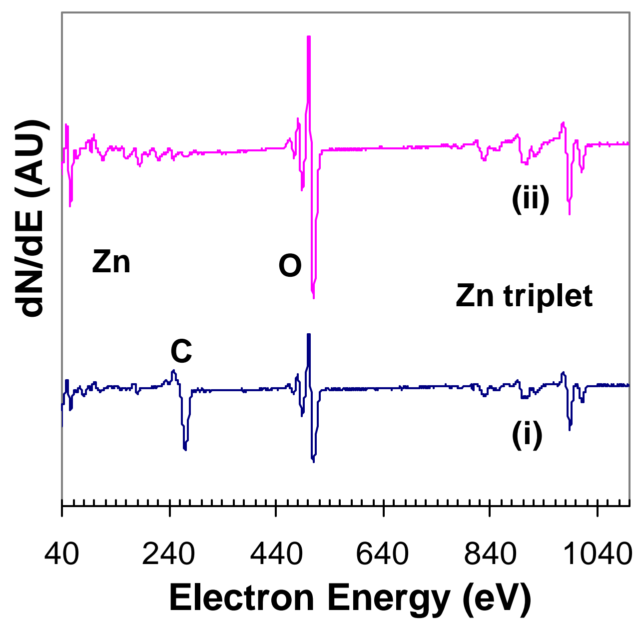

Figure 3.1. AES spectra of the ZnO(000$\bar{1}$) surface acquired from (i) as-received and (ii) samples annealed in 0.100 Torr of pure O_2 at 700 °C for 15 min.

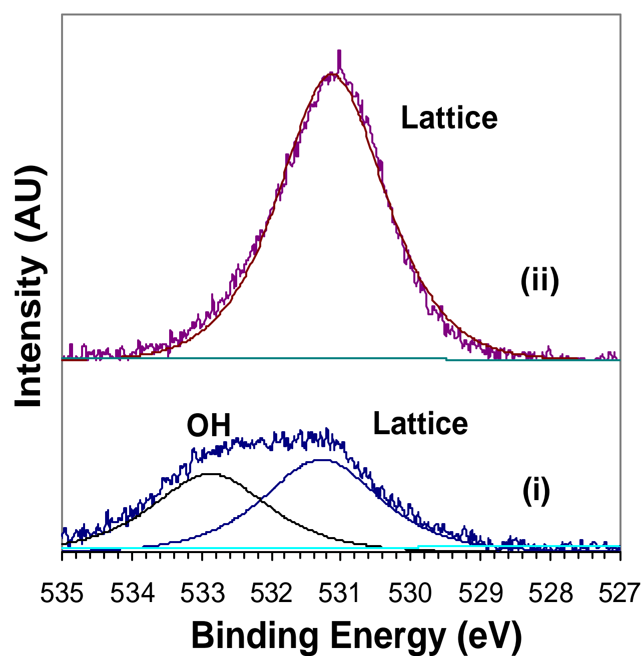

Figure 3.2. XPS O 1*s* core level spectra of the ZnO(000$\bar{1}$) surface acquired from (i) as-received samples and (ii) samples annealed in 0.100 Torr of pure O_2 at 700 °C for 15 min.

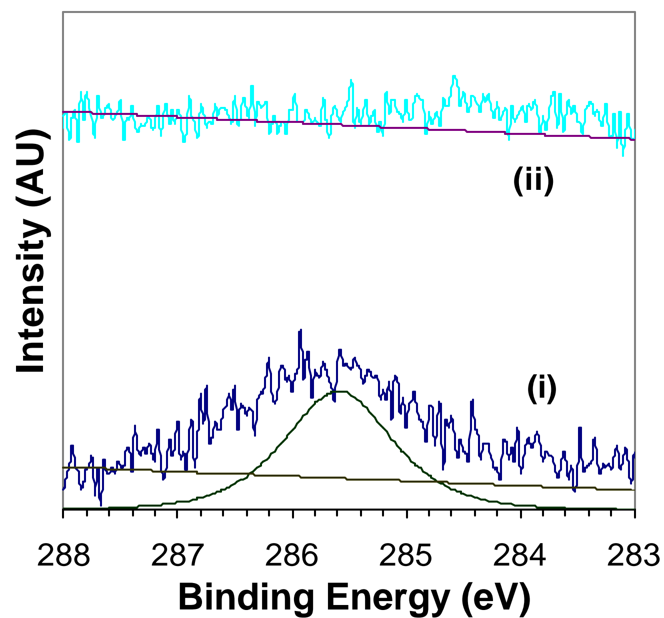

Figure 3.3. XPS C 1*s* core level spectra of ZnO(000$\bar{1}$) surfaces acquired from (i) as-received samples and (ii) samples cleaned by exposure to a room-temperature, 20-W, 2% O_2/98% He remote plasma for 0.5 min. at 0.050 Torr.

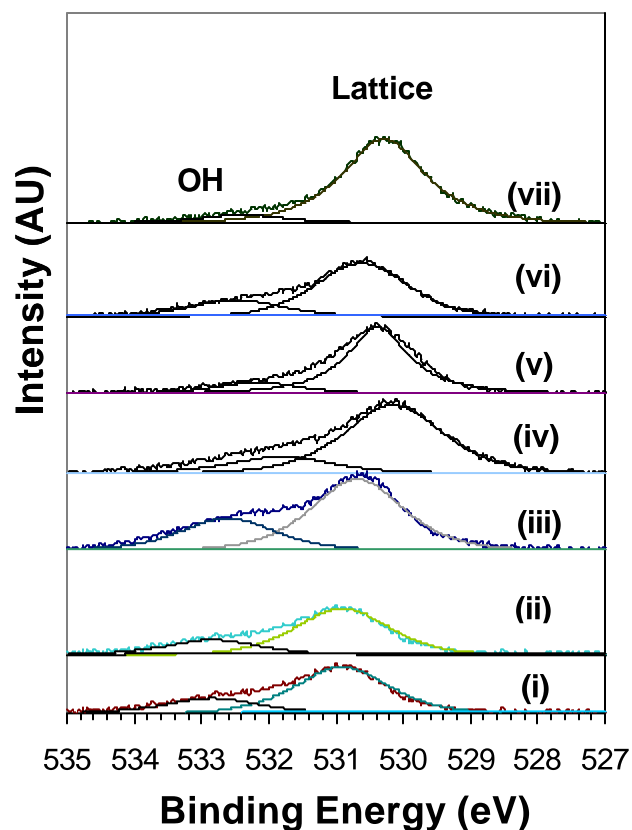

Figure 3.4. XPS O 1*s* core level spectra of ZnO(000$\bar{1}$) surfaces acquired from (i) as-received samples and samples exposed to a 20-W remote O_2/He plasma for 0.5-30 min at 0.050 Torr separately at (ii) 20 °C (iii) 350 °C, (iv) 450 °C, (v) 475 °C, (vi) 500 °C and (vii) 525 °C. The amount of hydroxide varied for each as-received sample investigated.

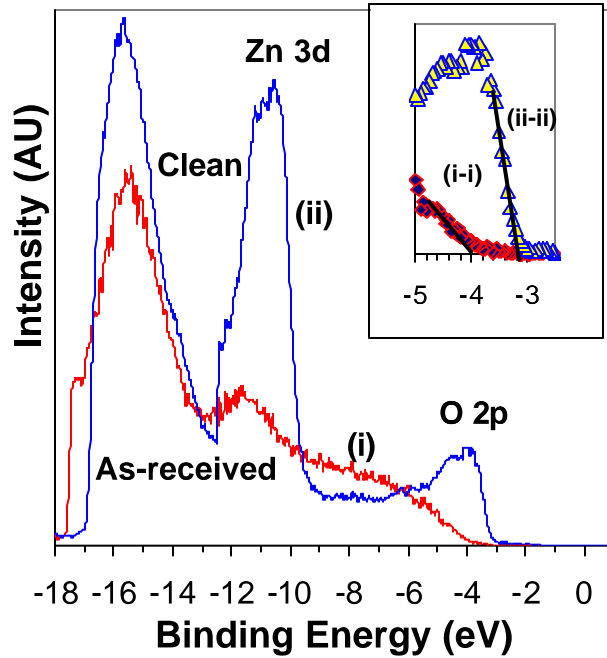

Figure 3.5. UPS spectra of ZnO(000$\bar{1}$) surfaces acquired from (i) as-received samples and (ii) cleaned at 525 °C in a 20-W remote 20% O_2/80% He plasma for 30 min. at 0.050 Torr. The inset shows that the valence band turn-on for an (i-i) as-received sample is sharpened for a (ii-ii) plasma-cleaned surface.

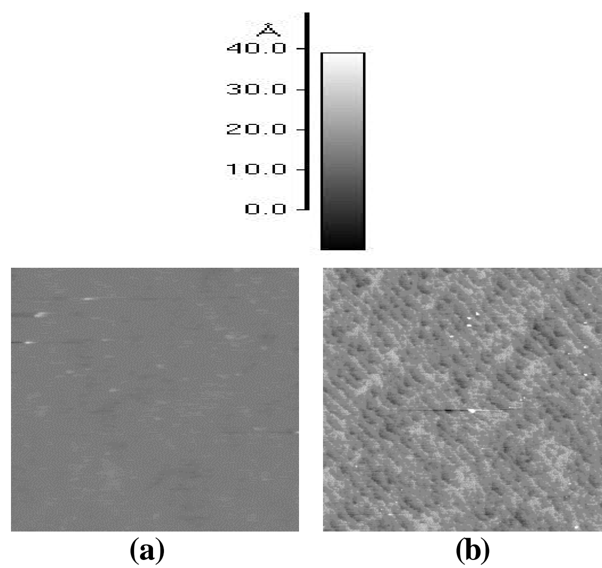

Figure 3.6. (5 µm x 5 µm) AFM images of the ZnO(000$\bar{1}$) surface of (a) as-received samples and (b) samples cleaned at 525 °C via 30 min. exposure to a remote 20-W, 20% O_2/80% He plasma at 0.050 Torr.

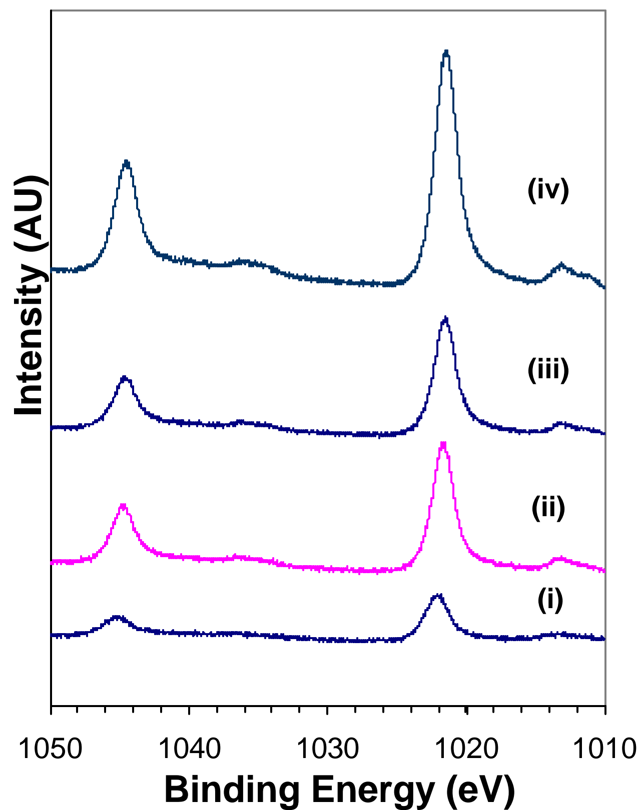

Figure 3.7. XPS spectra of the Zn 2p core level of (i) as-received samples and samples separately heated to (ii) 525 °C for 30 min., (iii) 525 °C for 60 min., (iv) 550 °C for 60 min. and cleaned for these times in a remote 20-W, 20% O_2/80% He plasma at 0.050 Torr.

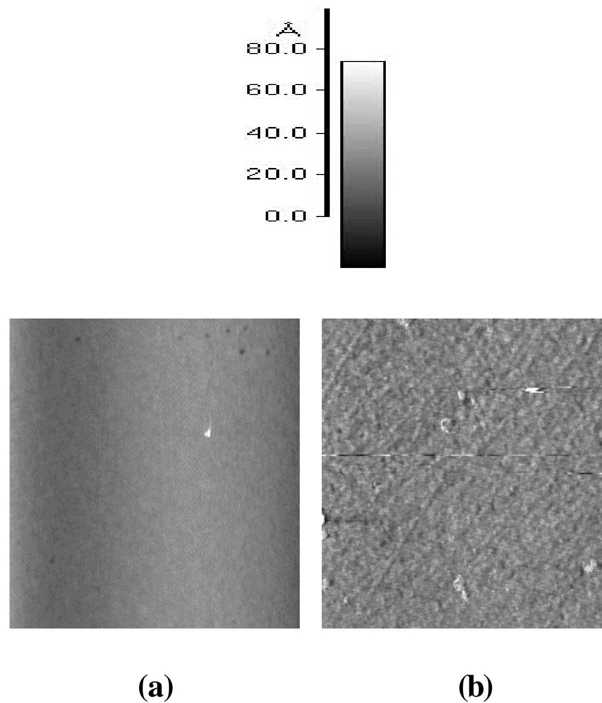

Figure 3.8. (5 µm x 5 µm) AFM images of the ZnO(0001) surface of (a) as-received samples and (b) samples cleaned at 550 °C via 60 min. exposure to a remote 20-W, 20% O_2/80% He plasma at 0.050 Torr.

4. GROWTH MODE AND SUBSEQUENT SCHOTTKY BARRIER FORMATION OF Au ON REMOTE PLASMA-TREATED, n-TYPE ZnO($000\bar{1}$)[1]

Submitted for consideration for publication

to

The Journal of Applied Physics

by

B. J. Coppa, C. C. Fulton, S. M. Kiesel and R. F. Davis*
Department of Materials Science and Engineering
North Carolina State University
Box 7907
Raleigh, NC 27695

and

J. E. Burnette and R. J. Nemanich
Department of Physics
North Carolina State University
Box 8202
Raleigh, NC 27695

[1] (0001) and ($000\bar{1}$) are used in this paper to designate the polar zinc- and oxygen-terminated surfaces, respectively.

*Corresponding Author:
Tele: 919-515-3272
FAX: 919-515-7724
robert_davis@ncsu.edu

4.1 ABSTRACT

Current-voltage measurements of Au contacts deposited on as-received, n-type ZnO($000\bar{1}$) surfaces showed an ~0.02 A/cm^2 leakage current density to 4 V reverse bias and ideality factors >2, before soft breakdown, attributed to the presence of ~1.6±0.1 ML of hydroxide, which typically increases the surface conductivity and forms an accumulation layer. Remote plasma cleaning reduced the hydroxide layer to ~0.4±0.1 ML, and subsequent cooling in the plasma ambient resulted in adsorbed oxygen on the surface. These species on the ZnO surface lead to the formation of a depletion layer of lower surface conductivity, which is advantageous for the creation of a Schottky barrier diode. The cleaning and subsequent O_2 adsorption produced smooth, highly-ordered, and stoichiometric ZnO($000\bar{1}$) surfaces containing a step and terrace microstructure that displayed 0.3 eV of upward band bending for the latter process. The most rectifying contacts were obtained from the deposition of Au on cleaned-and-oxygen adsorbed surfaces. A Volmer-Weber island growth mode was observed, the resultant junction possessed a barrier height of 0.60±0.05 eV, a saturation current density of 2.0±0.5 x 10^{-4} A/cm^2, a lower value of n = 1.03±0.05, a significantly lower leakage current density of ~91 nA/cm^2 to 7 V reverse bias, and a soft breakdown at this voltage. The measured barrier heights differ from the predicted Schottky-Mott value of 1.0 eV, indicating that the interface structure significantly affect the Schottky barrier. However, the constancy in the FWHM of core levels for Zn 2*p* (1.9±0.1 eV) and O 1*s* (1.6±0.1 eV), before and after sequential *in situ* Au depositions indicated an abrupt, unreacted Au/ZnO(0001) interface. Transmission electron microscopy results confirm the abruptness of the interface, while also showing the growth of epitaxial, single-crystal gold.

4.2 INTRODUCTION

Zinc oxide (ZnO) occurs most commonly in the hexagonal wurtzite crystal structure that possesses a direct band-gap of ~3.4 eV at room temperature and exhibits spontaneous polarization along the {0001} directions.[1] 'Single-crystal' boules and wafers of this material have recently been produced commercially.[2] High purity crystals of ZnO are typically n-type; this characteristic has traditionally been attributed to native defects such as oxygen vacancies and zinc interstitials.[3] However, recent theoretical calculations by Kohan *et al*.[4] have shown that none of the native defects exhibit characteristics consistent with a high-concentration shallow donor. Van de Walle[5] has noted that only vacancies have sufficiently low energies to form during growth of ZnO; first-principals calculations by the last author have provided strong evidence that H behaves as a shallow donor in ZnO, which may be related with the effect of adsorbed hydroxide on ZnO from water vapor.

Device-quality Schottky contacts typically require intimate metal-semiconductor interfaces free of surface contamination. A major deterrent to the development of low leakage Schottky contacts on ZnO with low ideality parameters, is the ~3 monolayer (ML) thick native contamination layer, including ~1 ML of adventitious carbon and ~2 ML of hydroxide that forms in ambient conditions.[6] The effects of this hydroxide in the formation of an accumulation layer of high surface conductivity[7-10] are very likely the reason for the reported high leakage currents above –1 V[11-15] and relatively high ideality factors (>2)[16-17] for high work function metals deposited on these contaminated surfaces. Alternatively, adsorbed oxygen species on clean ZnO may act as electron acceptors that

generate a depletion layer, which lowers the surface conductivity by several orders of magnitude[18-19] and is advantageous for Schottky barrier formation.

The Schottky-Mott model[20] predicts that metals with high work functions are prime candidates for rectifying contacts on n-type semiconductors. This model defines the Schottky barrier height (SBH) as the difference between the workfunction of the metal and the electron affinity of the semiconductor. In the case of ZnO, it has been shown[13] that these metals should also possess a low oxygen affinity; thus, the most ideal candidate materials are essentially limited to gold, palladium, and platinum. Silver and copper are potential candidates but are significantly prone to oxidation, which typically degrades rectifying characteristics. Rabadanov, *et al.*[13] measured a constant barrier height of 0.65±0.05 eV for Au, Pt, Pd, and Ag contacts deposited in vacuum at room-temperature on ZnO monocrystals of an unspecified orientation and cleaved in vacuum. However, neither the ideality parameters nor the breakdown voltages were reported.

In this study, an *in situ* remote plasma cleaning procedure and a subsequent oxygen adsorption step were developed in conjunction with investigations of the deposition and the current-voltage (*I-V*) properties of Au Schottky contacts on polished ZnO($000\bar{1}$) surfaces. The electronic structure and the growth mode of Au on the ZnO($000\bar{1}$) interface were also studied via X-ray photoelectron spectroscopy (XPS) and ultraviolet photoelectron spectroscopy (UPS). The structural and microstructural characteristics of all the materials used in this program were investigated using X-ray diffraction (XRD), low-energy electron diffraction (LEED), transmission electron microscopy (TEM), and atomic force microscopy (AFM).

4.3 EXPERIMENTAL PROCEDURES

Two millimeter-thick, {0001}-oriented single-crystal ZnO two-inch wafers, diced from boules produced by seeded chemical vapor transport by Eagle-Picher Technologies, Inc.[2] and chemo-mechanically polished on both sides, were employed in the present research. Each wafer contained highly textured domains with very low angle boundaries and with a collective range of full width half maxima in their rocking curves acquired about the [0001] direction. Thus, the term "single crystal" is used with this caveat. Grade I samples, essentially free of internal microvoids, were utilized for *I-V* studies, while Grade II wafers (high density of microvoids) were used in all other experiments. Hall and *C-V* measurements, the latter at 1 x 10^4 Hz, taken from the $(000\bar{1})$ surface of the as-received wafer showed a bulk carrier concentration of 1±5 x $10^{17}/cm^3$ and a nominal effective donor concentration, $(N_D\text{-}N_A)$, equal to 5±5 x $10^{16}/cm^3$, respectively. The wafers were then cleaved into smaller sections (> 1 cm^2), rinsed in methanol for 5 sec and dried in flowing nitrogen. These wafers are denoted by the term "as-received." A 40 nm-thick Ti film was subsequently deposited by e-beam evaporation on the entire (0001) face of each ZnO section. This film served (1) to absorb radiation from the underlying Pt-Rh heater and conduct heat into the wafer during the *in situ* cleaning of the $(000\bar{1})$ face, and (2) as an ohmic contact. The *in situ* cleaning process was optimized for ZnO$(000\bar{1})$[6] to fabricate low-leakage, low-ideality factor Schottky contacts.[17] ZnO$(000\bar{1})$ surfaces and ZnO$(000\bar{1})$/Au interfaces, free of detectable hydrocarbons and containing ~0.4 ML of hydroxide, were achieved via exposure of the former to a 20-W, 20% O_2/80% He (by volume) remote plasma at 525±20 °C and 0.050±0.001 Torr for 30 min. Gold contacts were deposited on surfaces (1) as-received, (2) remote plasma cleaned and cooled in

vacuum from 425 °C, (3) remote plasma cleaned and cooled in the O_2/He plasma ambient to ~25 °C for the chemisorption of oxygen.

All *in situ* processing and surface characterization experiments were conducted within a unique ultrahigh vacuum (UHV) configuration, which integrates several independent cleaning, thin-film growth and analysis systems via a transfer line[21] having a base pressure of < 1 x 10^{-9} Torr. A detailed description of this processing and the associated structural, microstructural and photo-optical investigations have already been reported.[6, 22]

In addition, a transmission electron microscope (JEM 4000) was used to characterize the Au/ZnO($000\bar{1}$) interface. ZnO cross-sectional specimens were created using sapphire supports. Due to the brittle nature of the material, the samples were initially dimpled to approximately 30 μm on a Gatan dimpler and then polished with 3 μm diamond paste. The samples were then flattened on the edges and inverted. Using 9, 6, 3, and 1 μm grit paper, the samples were then polished to < 30 μm. A copper ring was then glued to the polished side of each sample. Ion milling was conducted at 4 keV with a 17 º tilt angle, as the samples were cooled by a liquid nitrogen stage.

4.4 RESULTS AND DISCUSSION

4.4.1 *Analyses of remote plasma-cleaned ZnO*($000\bar{1}$) *cooled in vacuum*

Low-energy electron diffraction of the as-received ZnO($000\bar{1}$) surface showed only a bright background, indicative of the disordered contamination layer. Deconvolution of the O 1*s* core level peak obtained via XPS studies revealed that this surface contained 16±1 atomic percent (~1.6±0.1 ML) of OH, as determined by a peak at 532.8±0.1 eV. In

addition, ~1 ML of adventitious carbon was detected by XPS analysis; thus, the native contamination layer was typically found to be ~2.6 ML. The Zn/O ratio was 0.6±0.1. One atomic percent of hydroxide is equivalent to ~0.1 ML, in lieu of our operation conditions. The remote plasma cleaning process reduced all carbon species on the surface to below the detection limit of 0.3 atomic percent. Examination of the XPS spectra of the plasma-cleaned $(000\bar{1})$ surface revealed a shift in the lattice O 1*s* peak from 530.9 (FWHM = 1.6±0.1 eV) to 530.2 eV (FWHM = 1.4±0.1 eV), which is attributed to a 0.7 eV change in band bending, as depicted in Figs. 4.1(a) and (b). The electronic structure schematic in Fig. 4.1 was derived from UPS spectra, as shown in Fig. 4.2 and explained later. The XPS results showed a peak at 531.9 eV, which indicates ~0.4 ML of OH remaining on the surface. A corresponding core level shift of 0.7 eV was measured by the change of the Zn $2p_{3/2}$ and Zn $2p_{1/2}$ peak positions for the as-received samples from 1022.0 eV and 1045.1 eV (both FWHM = 2.0 eV) to 1021.3 eV and 1044.4 eV (both FWHM = 1.9 eV) after plasma-cleaning, respectively. In addition, a sharp (1x1) hexagonal LEED pattern was observed at 42 eV from the clean $(000\bar{1})$ surface, indicating a high degree of structural order.

The removal of the ~1.2 ML of OH was critical for eliminating the proposed electron accumulation layer of high surface conductivity and for generating a Zn/O stoichiometric ratio of 1.0. The 0.6 eV change in band bending due to the cleaning process was confirmed by UPS within the ±0.1 eV uncertainty. Figures 4.1(a) and (b) show that the surface Fermi level shifted from 0.6 eV above the conduction band minimum (CBM) for the as-received ZnO$(000\bar{1})$ to 0.1 eV below the CBM after the plasma-clean. The bulk Fermi level of ZnO has been determined to be 0.3 eV below the CBM.[22] In addition, it is

shown that the downward band bending is reduced from 0.9 eV to 0.2 eV for the as-received and plasma-cleaned surfaces, respectively, as the surface conductivity is presumably is reduced. The electron affinity of 4.0±0.2 eV, derived from UPS results, remained essentially constant after cleaning.

4.4.2 *AFM analyses of remote plasma-cleaned ZnO*$(000\bar{1})$ *cooled in vacuum*

Prior and post-cleaning AFM analyses of the surface microstructure indicated the absence of any observable damage associated with the annealing and/or plasma exposure. A smooth ZnO$(000\bar{1})$ microstructure was observed with RMS surface roughness values of 0.2±0.2 nm and 0.6±0.2 nm before and after the cleaning process, respectively. Highly-ordered atomic steps with a unit cell step height of 0.53±0.01 nm and step width of ~0.2 μm were observed, which may have caused minor splitting of the sharp LEED spots in the (1x1) hexagonal pattern obtained at 42 eV and depicted in Fig. 4.3 (ii).

4.4.3 *Analyses of remote plasma-cleaned and* O_2 *adsorbed ZnO*$(000\bar{1})$

Cooling the cleaned ZnO in the unignited plasma gas from 525 °C to approximately room temperature was employed based on our prior studies,[17] which showed that exposure of the ZnO surface to an O_2-containing ambient improved the behavior of subsequently deposited contacts. Thus, efforts were made to study the chemistry and electronic structure of the surface. The reported[23] submonolayer amount of chemisorbed oxygen on the UHV-cleaved polished and annealed ZnO$(000\bar{1})$ face was greater than the ZnO(0001) face, which may be associated with the preferential adsorption of oxygen to an atomically-stepped ZnO surface. A peak attributed to this chemisorbed oxygen on the ZnO$(000\bar{1})$

face was detected at 527.7 eV, and the integrated area corresponded to ~0.1 ML. The Zn and O core level positions measured by XPS conveyed a 0.1 eV change in band bending; however, the uncertainty was ±0.1 eV. In addition, the stoichiometic Zn/O ratio of 1.0 for the clean surface was retained after oxygen adsorption. Examination of the XPS spectra revealed a shift in the lattice O 1*s* peak from 530.2 (FWHM = 1.4 eV) for the plasma-cleaned surface to 530.3 eV (FWHM = 1.6 eV) after oxygen adsorption, which corresponded to the change in the Zn 2*p* multiplet peak positions for this same sample from 1021.3 eV and 1044.4 eV to 1021.4 eV and 1044.5 eV (all FWHM = 1.9 eV). However, UPS is more surface-sensitive than XPS, and a significant variation in the spectra of the former was observed, which subsequently matched the depletion layer model,[18,19,22] as shown in Figs. 4.1 and 4.2 and described below.

The UPS results provided evidence for a change in band bending, associated with O_2 adsorption. Figure 4.1(b) and (c) show a 0.5 eV change in band bending due to the exposure of the cleaned surface to the O_2-containing plasma gas on cooling. This corresponds to the shift of the Zn 3*d* core level from 10.9 eV to 10.4 eV for the plasma-cleaned and O_2/He cooled surfaces, respectively. Moreover, it is shown that the 0.2 eV of downward band bending for the clean surface is changed to 0.3 eV of upward band bending, after the exposure to the O_2/He ambient during cooling. Figures 4.1(b) and (c) show that the surface Fermi level shifted from 0.1 eV below the CBM for clean ZnO$(000\bar{1})$ to 0.6 eV below the CBM after cleaning. The shifting of the surface Fermi level away from the CBM corresponds to a reduction in n-type surface conductivity, which we attributed to adsorbed oxygen species that act as electron acceptors for ZnO.[18-19] The electron affinity varied from 4.1 to 4.3±0.2 eV between the two processing steps. Distinct

surface states were neither observed after cooling nor plasma-cleaning, matching previous work. A shoulder was observed, after the O_2 adsorption, in the O 2*p* core level at ~5.2 eV, as shown in Fig. 4.2 (ii). Separation of the spots in the sharp (1x1) hexagonal LEED pattern in Fig. 4.3 (iii) was observed at 42 eV from the surface after the latter process, which is likely associated with the adsorption of oxygen to preferential sites such as step edges.

It has been found via atomic modeling and AFM by E. Chen[23] that of the two types of step edges in ZnO, steps edges oriented in the $[\bar{1}010]$ direction, having two dangling bonds, are more energetically favorable for adatoms than the $[\bar{1}100]$ oriented step edges with only one dangling bond.[24] Thus, it is proposed that surface contaminants from ambient conditions, adsorbed oxygen, and/or Au atoms in the case discussed below, would preferentially bond to the $[\bar{1}010]$ step edge.[24]

4.4.4 *Growth mode and characterization of Au/ZnO*$(000\bar{1})$ *interface*

The growth mode of Au on the cleaned surface exposed to the plasma ambient on cooling was determined from the results of the attenuation of the Zn $2p_{3/2}$ core level in Fig. 4.4 in a fashion similar to Wolter *et al.*[25] and Sitar *et al.*[26] The three growth modes considered in this study were (i) Frank-van der Merwe (two-dimensional, layer-by-layer growth), (ii) Volmer-Weber (three-dimensional growth of discrete islands), and (iii) Stranski-Krastanov (a combination of the two previous models wherein the initial film growth occurs via a layer-by-layer mechanism and is subsequently followed by the initiation of island growth). The substrate, film and interfacial surface energies, and strain determine the prevailing growth mode.

In XPS analysis, Frank-van der Merwe (FM) growth is expressed as

$$I_s/I_o = \exp(-t/\lambda_o), \quad (1)$$

where I_s is the core level intensity for a given overlayer thickness (t), I_o is the baseline core level intensity (*ie*. from the ZnO surface following the cleaning and subsequent O_2 exposure), and λ_o is the attenuation length of the particular core level electron. The Volmer-Weber (VW) mode of deposition is described by the equation

$$I_s/I_o = (1-\theta) + \theta * \exp(-t/\lambda_o), \quad (2)$$

where θ is the surface coverage of the islands (value between 0 and 1). Stranski-Krastanov (SK) growth is represented by the expression

$$I_s/I_o = (1-\theta) * \exp(-q/\lambda_o) + \theta * \exp(-t/\lambda_o), \quad (3)$$

where q is the deposited thickness before three-dimensional island growth or nucleation. The value of I_s/I_o shown in Fig. 4.5 for the Zn 2*p* core level decreased according to equation (2) from 1.00 before Au deposition to 0.76±0.03 at a thickness of 5.0 nm of Au. Similarly, I_s/I_o for O 1*s* followed the same trend as Fig. 4.5. While there is significant scatter in the data, the closest match is to the VW mechanism. These results corresponded well with those obtained from a prior experiment conducted for Au on ZnO(0001).[22]

TEM results confirmed the growth of Au islands on the clean, atomically-stepped surface, after removing the sample from vacuum. Figure 4.6 (a) shows the steps and terraces observed with AFM on the plasma-cleaned surface with a RMS surface roughness value of 0.6±0.2 nm. TEM results in Fig. 4.6 (b) shows the coalescence of islands at this interface after depositing 100 nm of Au. In comparison, Pt and Pd have been reported[27] to grow on ZnO(0001) and $(000\bar{1})$ by a Frank-van de Merwe mechanism.

The Schottky barrier height was determined from XPS and UPS to compare the SBH resulting from these photoemission techniques with that found by *I-V* measurements. Figure 4.4 shows the evolution of the Zn 2*p* core level spectra as a function of the thickness of the Au overlayer on a cleaned-and-oxygen adsorbed ZnO($000\bar{1}$) surface. The shifts in the Zn 2*p* and O 1*s* core level positions and their FWHM for the cleaning, oxygen adsorption, and sequential Au depositions are listed in Tables 4.1 and 4.2. The spectra were acquired *in situ* over an ~30 hour period. Upon deposition of 0.2 nm of Au, the O 1*s* lattice peak shifted by 0.5 eV from 530.3 eV to 530.8 eV, while the Zn 2*p* multiplet shifted by 0.3 eV from 1021.4 eV and 1044.5 eV to 1021.8 and 1044.9 eV. Both core level positions remained essentially fixed after subsequent deposition steps, suggesting that additional metallization does not affect band bending. Thus, the agreement in shifts of O 1*s* and Zn 2*p* core levels provides evidence for the interpretation of the observed shifts as changes in band bending rather than chemically-induced shifts. The lack of a discernible change in the FWHM of 1.6±0.1 eV and 1.9±0.1 eV for the O 1*s* and Zn 2*p* core levels, before and after Au deposition, is indicative of an abrupt, unreacted interface. In comparison, UPS spectra acquired by Göpel *et al.*[28] indicated that the Schottky barrier formation occurred over the first 1 nm of Au coverage on ZnO($10\bar{1}0$) without an interface reaction.

The evolution of the Au $4f_{7/2}$ core level peak depicted in Fig. 4.7 provided further results in regards to the formation of the Au Schottky barrier. Curve-fitted data is presented to isolate this peak from the Zn $3p_{1/2}$ and Zn $3p_{3/2}$ core level peaks at 91 eV and 89 eV, respectively. The results presented in Table 4.3 show a large-scale shift associated with the Au $4f_{7/2}$ peak as a function of metal thickness. Gold island formation generates an

uncertainty in the exact thickness on the ZnO after each deposition. The binding energy of this peak decreases from an initial value of 84.8 eV at 0.2 nm to 84.0 eV for 100 nm of Au (Δ = 0.8 eV), while the FWHM decreases from 2.5 eV to 1.2 eV (Δ = 1.3 eV). Table 4.3 shows that the integrated area of the Au 4*f* core level is increased as a function of Au thickness. The shifting in Au $4f_{7/2}$ parameters is most likely due to islanding associated with the VM growth mode of Au. However, deposition of Au into varying depths of the wafer through microvoids, constituting at least 20% of the surface, is another possible mechanism. Ideally, the metal overlayer core level position and FWHM should remain constant at each step in order to discriminate a chemical shift or related phenomena from an electronic shift associated with the formation of the Schottky barrier. The following equation[29] was used to calculate the value of Φ_B from these results

$$\Phi_B = E_g - E^m{}_{core} + (E^i{}_{core} - E^{c,ox.}{}_{VBM}), \qquad (4)$$

where E_g is the RT band-gap of ZnO (3.4 eV), $E^m{}_{core}$ is the final position of the Zn (or O) core level after sequential Au depositions, $E^i{}_{core}$ is the position of the Zn (or O) core level before metal deposition, and $E^{c,ox.}{}_{VBM}$ is the Fermi level position relative the VBM for the clean-and-oxygen adsorbed surface. The value of $E^{c,ox.}{}_{VBM}$ was determined from UPS measurements to be 2.8 eV. The calculated values of Φ_B = 0.2±0.1 eV and 0.1±0.1 eV for both the Zn $2p_{3/2}$ and the O 1*s* core levels is lower than the 0.60±0.05 eV value determined from analyses of the *I-V* measurements.

UPS provided an additional method for measuring Φ_B and other detailed electronic structure of the Au/ZnO($000\bar{1}$) interface. Fig. 4.2 shows the UPS spectra for surfaces as-received, clean-and-oxygen adsorbed, and coated with: 0.2 nm, 0.4 nm, 5.0 nm, and 100 nm of Au. The results presented in Fig. 4.2 show that the binding energy of the O 2*p* core

level shifted from 4.0 eV for the cleaned-and-oxygen adsorbed surface to 4.5 eV, after the deposition of 0.2 nm of Au. A corresponding shift occurred in the Zn 3*d* peak from 10.4 eV to 10.8 eV, while the Au 5*d* core level began to emerge at 6.2 eV. The position of these peaks remained unchanged following successive Au depositions, which confirms the XPS result that the Schottky barrier is completely formed at ~0.2 nm. Also, the correlation of the shifts of these bulk features with those measured by XPS, indicates that the observed shifts are changes in band bending rather than chemical shifts or charging effects. The intensity of the Zn 3*d* and O 2*p* peaks is slightly decreased, while the Au 5*d* is intensified, as a function of Au thickness. No apparent surface states and/or Fermi level pinning were observed,[28] but complex interactions between metal-induced gap states may still be possible. The following equation[29] was used to calculate the value of Φ_B from these results

$$\Phi_B = E_g - (E_F - E^m{}_{VBM}), \tag{5}$$

where E_g is the RT band gap of ZnO (3.4 eV), $(E_F - E^m{}_{VBM})$ (3.3 eV) is the difference between the VBM of ZnO for a 0.2 nm-Au-coated surface and the Fermi level position. The use of equation (5) generated a value of $\Phi_B = 0.1\pm0.1$ eV, which agrees with the XPS values but is much lower than the 0.60±0.05 eV value determined by *I-V* analysis.

The *I-V* value determined in this study for Au/ZnO($000\bar{1}$) corresponds well with literature values of ranging from 0.65-0.71±0.05 eV for Au/ZnO,[13,17,30] which helps to clarify a deviation in the photoemission values. We suggest that the photoemission results up to 0.2 nm, where Fermi level scattering occurred, reflect the evolution of the Schottky barrier, but thereafter, the data appears to compromised due to Au island formation. Thus,

incomplete Au coverage of the $ZnO(000\bar{1})$ surface indicated a Φ_B value less than the expected bulk value.

Additional research involved the deposition of bulk (100 nm) Au contacts on clean $ZnO(000\bar{1})$ wafers exposed to the plasma ambient on cooling in tandem with *ex situ* and *in situ* characterization using XRD and LEED, respectively. The curve-fitted XRD spectra of the Au peak at 38.2±0.1º (FWHM = 0.2±0.1º (600”)) shown in Fig. 4.7 indicates that the bulk (100 nm) Au(111) contacts are crystallographically-matched to (1) clean ZnO(0001) wafers exposed to the plasma ambient on cooling, as in Fig. 4.7 (a), and (2) similarly treated wafers that were also heated *ex situ* in air at 175 °C for 15 min., which were unchanged during this post-deposition annealing procedure, as shown in Fig. 4.7 (b). The d-spacing of 0.0235±0.0001 nm was found for samples (1) and (2), which is equivalent to that of single crystal Au. Moreover, the ZnO (0002) and (0004) reflections (not shown) were measured for the lattice at 34.4±0.1º and 72.5±0.1º, respectively, for samples (1) and (2).

TEM results in Fig. 4.8 confirm the growth of epitaxial, single-crystal Au that was inferred by XRD. The large spots in the diffraction pattern shown in Fig. 4.8(f) represent single-crystal ZnO, whereas the smaller spots characterize single-crystal Au. The doublets of Au spots were attributed to twinning, which presumably relaxed the strained Au, having an 11% lattice mismatch to ZnO. Fast-fourier transform (FFT) analysis of the twin boundary region of Au in Fig. 4.8(c) and (d) in conjunction with FFT analysis of ZnO in Fig. 4.8(e) was used to determine this effect. Epitaxial Au forming an abrupt, unreacted $Au/ZnO(000\bar{1})$ interface, important for device-quality Schottky contacts, is depicted in Fig. 4.8(b).

These results support the previous TEM investigations by Wassermann and Polacek[31] that indicated epitaxial growth of Au(111) on the polar surfaces of vacuum-cleaved ZnO. A high degree of structural order was conveyed by well-defined (1x1) hexagonal LEED patterns with a dark background acquired, using an incident energy of 80 eV, from Au(100nm)/ZnO($000\bar{1}$) in Fig. 4.3 (iv) and Au(0.22nm)/ZnO($000\bar{1}$) samples. A sharper pattern was obtained for the thinner Au coverage. In addition, the slight amount of spot splitting in the pattern was attributed to the atomically-stepped ZnO($000\bar{1}$) surface. The existence of the Au(111) XRD 2θ peak corresponds well to an abrupt, well-ordered interface found by XPS, TEM, and LEED, respectively. Consequently, this evidence supports TEM studies by Yoshino *et al.*, whom showed the epitaxial growth of ZnO{0001} films on Au, forming an abrupt, unreacted interface.[32]

4.4.5 *I-V characterization of Au/ZnO*($000\bar{1}$)*/Ti*

The *I-V* data obtained from the Au contacts deposited on Grade I wafers were analyzed using the following methodology. For thermionic emission and V greater than 3 kT/q, the general diode equation in forward bias is

$$J = J_o \exp\left(\frac{qV - IR}{nkT}\right), \qquad (6)$$

where J is the current density, q is the charge of an electron, V is the voltage, I is the current, R is the series resistance, k is Boltzman's constant, and T is the absolute temperature. The saturation current density J_0 is given by $J_0 = A^*T^2 \exp(-\Phi_B/kT)$ where A* is the Richardson constant. The theoretical value of $A^* = 32$ A cm^{-2} K^{-2} was used in this study,[32] since the experimental value has not been determined. The ideality factors

were obtained by fitting the forward bias ln(J)-V curve between 0.1 and 0.2 V over several decades of current and correcting for the substrate series resistance measured directly by *C-V*. Barrier height measurements could not be obtained using *C-V* measurements due to the high series resistance of the unintentionally doped, 2-mm-thick wafers. It was confirmed previously that top-side and bottom-side Ti contacts on ZnO wafers produced good ohmic behavior through the bulk. Soft breakdown was observed for all contacts studied, as evidenced by non-repeatable low leakage current behavior after biasing to the breakdown voltage. The best results presented herein are discussed for all sample types.[17]

Room-temperature (~293 K) *I-V* measurements of the Au contacts on as-received ZnO($000\bar{1}$) wafers revealed reverse bias leakage current densities below ~0.02 A/cm^2 (2.40 x 10^{-4} cm^2 contact area) to 4 V reverse bias, and the ideality factors were >2. These effects were ascribed to the presence of the hydroxide, which increases the surface conductivity and forms an accumulation layer through its shallow surface donor characteristic. Soft breakdown occurred at -4.0 V. Significant improvements in the *I-V* characteristics were obtained for the Au contacts on a plasma-cleaned ZnO($000\bar{1}$) surface, corresponding to the change in electronic band structure in Figs. 4.1(a) and (b). A barrier height of 0.67±0.05 eV was calculated based on J_0 = 6±5 x 10^{-5} A/cm^2. An ~1.6 x 10^{-4} A/cm^2 leakage current density was measured to 4 V reverse bias with soft breakdown at -4.5 V. The value of the ideality factor was 1.86±0.05. Thus, the reduction in the hydroxide layer and adventitious carbon generated a 0.7 eV shift in band bending and the surface Fermi level position, which paralleled the enhancement of rectifying contact properties.

Cooling the cleaned surface in the unignited plasma gas to ~RT for oxygen adsorption prior to *in situ* Au deposition resulted in a barrier height of 0.60±0.05 eV,

saturation current density of 2.0±0.5 x 10^{-4} A/cm^2, lower value of n = 1.03±0.05, leakage current of ~91 nA/cm^2 to 7 V reverse bias and soft breakdown at this voltage. Thirty-three percent of these contacts exhibited leakage currents in the 10 nA range compared to 11% of the contacts that were cooled in vacuum from 425°C. Thus, cooling in the plasma ambient generated a 0.5 eV shift in band bending and the surface Fermi level position, as shown in Figs. 4.1(b) and (c), which enhanced the rectifying contact properties in comparison to cooling in vacuum from 425 °C after cleaning. Presumably, the atomically-stepped ZnO($000\bar{1}$) surface is causing the typical amount of 0.2 eV Schottky barrier lowering.[34] Slightly lower breakdown voltages compared to ~ -9 V for the Au/ZnO(0001)/Ti structure may be associated with a lower barrier height for contacts on the ($000\bar{1}$) face relative to the (0001) face. The measured barrier heights differ from the predicted Schottky-Mott value of 1.0 eV, even after accounting for potential Schottky barrier lowering, indicating that the interface structure also significantly affects the Schottky barrier. However, a lack of significant polarity effects on the rectifying properties was found between the ZnO(0001)[22] and ZnO($000\bar{1}$) surfaces.

4.5 SUMMARY

Gold contacts were deposited *in situ* on n-type ZnO($000\bar{1}$) wafers that were either (1) in the as-received state (2) cleaned via a 20% O_2/80% He remote plasma at 525 °C for 30 min and cooled in vacuum beginning at 425 °C, and (3) cleaned via method (2) but cooled in the plasma ambient to ~RT for the chemisorption of oxygen. The surfaces of the wafers treated via the processes (2) and (3) were smooth, highly-ordered, stoichiometric and contained a step and terrace microstructure. *J-V* results of the contacts on the as-

received surfaces showed reverse bias current densities of ~0.02 A/cm^2 to 4 V and ideality factors >2, before soft breakdown at -4.5 V occurred. The presence of ~1.6 ML of hydroxide, which increases the surface conductivity, is attributed to this poor rectifying behavior.

Plasma cleaning reduced the amount of the hydroxide layer to ~0.4 ML, corresponding to a 0.7 eV reduction in downward band bending and lowering of the surface Fermi level. Subsequent exposure to the plasma ambient generated a 0.5 eV change in band bending, resulting in 0.3 eV of upward band bending, which is indicative of a depletion layer and lower surface conductivity. The most rectifying gold contacts were measured on these surfaces and possessed a barrier height of 0.60±0.05 eV, a saturation current density of 2.0±0.5 x 10^{-4} A/cm^2, a lower value of n = 1.03±0.05, a lower leakage current density of ~91 nA/cm^2 to 7 V reverse bias and a soft breakdown at this voltage. These values are consistent with results obtained for similarly processed Au contacts on the ZnO(0001) face, which indicates a lack of polarity effects, since minor differences can be attributed to surface polishing. The measured barrier height differs from the predicted Schottky-Mott value of 1.0 eV, indicating that the interface structure significantly affects the Schottky barrier. However, the lack of a discernible change in the FWHM of core levels for Zn 2*p* (1.9 eV) and O 1*s* (1.6 eV), before and after sequential Au depositions conducted *in situ* indicates an abrupt, unreacted Au/ZnO($000\bar{1}$) interface. Futhermore, TEM results confirmed the abruptness of the interface, while also conveying the growth of epitaxial, single-crystal Au on the cleaned-and-oxygen adsorbed surface. These Au(111) oriented contacts were grown via the Volmer-Weber (island) mode and exhibited crystallographic stability to 175 °C.

4.6 ACKNOWLEDGMENTS

This research was partially funded by both the Kenan Institute for Technology, Engineering and Science at North Carolina State University and by the Office of Naval Research under contract N00014-98-1-0654 (H. Dietrich, monitor). R. F. Davis was partially supported by a Kobe Steel Ltd. Professorship. The authors their appreciation to Professor Gerry Lucovsky of NCSU for the use of *C-V* equipment

4.7 REFERENCES

1. D. C. Look, Materials Science and Engineering B80, 383 (2001).
2. D. C. Look, D. C. Reynolds, J. R. Sizelove, R. L. Jones, C. W. Litton, G. Cantwell, and W. C. Harsch, Solid State Commun. 105, 399 (1998).
3. P. Bonasewicz, W. Hirschwald, and G. Neumann, Appl. Surf. Sci. 28, 135 (1987).
4. A. F. Kohan, G. Ceder, D. Morgan and C. G. Van de Walle, Phys. Rev. B 61, 15019 (2000).
5. C. G. Van de Walle, Phys. Rev. Lett. 85, 1012 (2000).
6. B. J. Coppa, C. C. Fulton, P. J. Hartlieb, R. F. Davis, B. J. Rodriguez, B. J. Shields and R. J. Nemanich, submitted to the J. Appl. Phys.
7. V. E. Henrich and P. A. Cox, *The Surface Science of Metal Oxides* (Cambridge Univ., Cambridge, 1994) p. 297.
8. H. Moormann, D. Kohl, and G. Heiland, Surf. Sci 100, 302 (1980).
9. G. Heiland and P. Kunstmann, Surf. Sci. 13, 72 (1969).
10. M. Nakagawa and H. Mitsudo, Surf. Sci. 175, 157 (1986).

11. F. D. Auret, S. A. Goodman, M. Hayes, M. J. Legodi, H. A. van Laarhoven, and D. C. Look, Appl. Phys. Lett. 79, 3074 (2001).

12. F. D. Auret, S. A. Goodman, M. Hayes, M. J. Legodi, W. E. Meyer, and D. C. Look, Appl. Phys. Lett. 80, 1340 (2002).

13. R. A. Rabadanov, M. K. Guseikhanov, I. Sh. Aliev, and S. A. Semiletov, Fizika 6, 72 (1981).

14. Y. Liu, C. R. Gorla, S. Liang, N. Emanetoglu, Y. Lu, H. Shen, and M. Wraback, Journal of Electronic Materials 29, 69 (2000).

15. H. Sheng, S. Muthukumar, N. W. Emanetoglu, and Y. Lu, Appl. Phys. Lett. 80, 2132 (2002).

16. H. Fabricius, T. Skettrup, and Paul Bisgaard, Applied Optics 25, 2764 (1986).

17. B. J. Coppa, R. F. Davis, and R. J. Nemanich, Appl. Phys. Lett. 82, 400 (2003).

18. E. Arijs, F. Cardon, and W. Maenhout-Van Der Vorst, Surf. Sci. 17, 387 (1969).

19. L. Lagowski, E. S. Sproles, Jr., and H. C. Gatos, J. Appl. Phys. 48, 3566 (1977).

20. N. F. Mott, Proc. Cambr. Phil. Soc. 34, 568 (1938).

21. J. van der Weide, Ph.D. dissertation, N. C. State University, Raleigh, NC, 1994.

22. B. J. Coppa, C. C. Fulton, R. F. Davis, C. Pandarinath, J. E. Burnette, and R. J. Nemanich, submitted to J. Appl. Phys.

23. V. E. Henrich and P. A. Cox, *The Surface Science of Metal Oxides* (Cambridge Univ., Cambridge, 1994) p. 298-99.

24. E. Y. Chen (private communications).

25. S. D. Wolter, J. M. Delucca, S. E. Mohney, R. S. Kern, and C. P. Kuo, Thin Solid Films 371, 153 (2000).

26. Z. Sitar, L. L. Smith, and R. F. Davis, Journal of Crystal Growth 141, 11 (1994).

27. V. E. Henrich and P. A. Cox, *The Surface Science of Metal Oxides* (Cambridge Univ., Cambridge, 1994) p. 396-97.

28. W. Göpel, L. J. Brillson, and C. F. Brucker, J. Vac. Sci. Technol. 17, 894 (1980).

29. K. M. Tracy, Ph.D. dissertation, N. C. State University, Raleigh, NC (2000).

30. R. C. Neville and C. A. Mead, J. Appl. Phys. 41, 3795 (1970).

31. E. F. Wassermann and K. Polacek, Appl. Phys. Lett. 16, 259 (1970).

32. Y. Yoshino, K. Inoue, M. Takeuchi, T. Makino, Y. Katayama, and T. Hata, Vacuum 59, 403 (2000).

33. S. M. Sze, Physics of Semiconductors Devices (Wiley, New York, 1981) p. 849.

34. J. F. Luy and P. Russer, *Silicon-Based Millimeter-Wave Devices* (Springer-Verlag, Berlin, 1994) p. 120.

Zn $2p_{3/2}$ core level parameters (±0.1 eV)				
Experiment Step	**Center (eV)**	**Shift (eV)**	**FWHM (eV)**	**Shift (eV)**
As-received	1022.0	--	2.0	--
Cleaning	1021.3	0.7	1.9	0.1
O_2 adsorption	1021.4	0.1	1.9	0.0
0.2 nm Au	**1021.8**	**0.4**	**1.9**	**0.0**
0.4 nm Au	1021.8	0.0	2.0	0.1
0.6 nm Au	1021.8	0.0	1.9	0.1
1.1 nm Au	1021.8	0.0	1.9	0.0
1.3 nm Au	1021.8	0.0	1.9	0.0
1.7 nm Au	1021.8	0.0	1.9	0.0
2.2 nm Au	1021.8	0.0	1.9	0.0
5.0 nm Au	1021.8	0.0	2.2	0.3
Net Shift (eV)	**--**	0.2	--	0.2

Table 4.1. Evolution of Zn $2p_{3/2}$ core level as a function of Au overlayer thickness on 20%O_2/80% He remote plasma-cleaned ZnO($000\bar{1}$) following oxygen adsorption. The evolution of the Schottky barrier was monitored up to 0.2 nm, as highlighted in bold print.

O 1s (lattice) core level parameters (±0.1 eV)				
Experiment Step	**Center (eV)**	**Shift (eV)**	**FWHM (eV)**	**Shift (eV)**
As-received	530.9	--	1.6	--
Cleaning	530.3	0.6	1.4	0.2
O_2 adsorption	530.3	0.0	1.6	0.2
0.2 nm Au	**530.8**	**0.5**	**1.4**	**0.2**
0.4 nm Au	530.8	0.0	1.4	0.0
0.6 nm Au	530.8	0.0	1.4	0.0
1.1 nm Au	530.8	0.0	1.3	0.1
1.3 nm Au	530.8	0.0	1.3	0.0
1.7 nm Au	530.8	0.0	1.4	0.1
2.2 nm Au	530.8	0.0	1.4	0.0
5.0 nm Au	530.8	0.0	1.4	0.0
Net Shift (eV)	**--**	0.1	--	0.2

Table 4.2. Evolution of O 1s core level as a function of Au overlayer thickness on 20% O_2/80% He remote plasma-cleaned ZnO($000\bar{1}$) following oxygen adsorption. The evolution of the Schottky barrier was monitored up to 0.2 nm, as highlighted in bold print.

Gold $4f_{7/2}$ XPS Core Level Parameters (±0.1 eV)			
Experiment Step	**Integ. Area**	**Center (eV)**	**FWHM (eV)**
Clean/O_2 adsorbed ZnO($000\bar{1}$)	--	--	--
0.2 nmAu	602	84.8	2.5
0.4 nm Au	730	84.8	2.5
0.6 nm Au	744	84.8	2.5
1.1 nm Au	863	84.8	2.5
1.3 nm Au	898	84.7	2.2
1.7 nm Au	972	84.3	2.2
2.2 nm Au	1035	84.8	2.5
5.0 nm Au	3230	84.3	1.5
100 nm Au (bulk)	--	84.0	1.2
Net Shift (eV)	**--**	**0.8**	**1.3**

Table 4.3. Evolution of Au $4f_{7/2}$ core level as a function of Au overlayer thickness on 20% O_2/80% He remote plasma-cleaned ZnO($000\bar{1}$) following oxygen adsorption.

As-received (a) Clean (b) O_2 adsorbed (c)

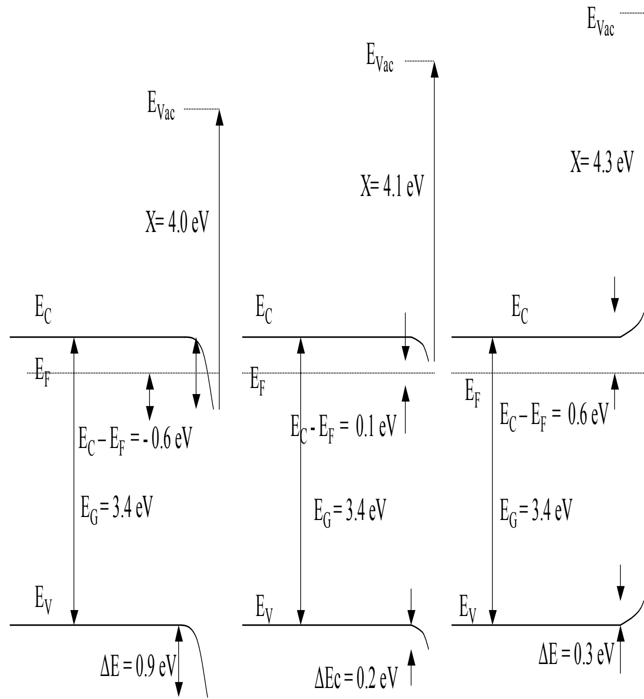

Figure 4.1. Electronic band structure derived from UPS spectra for ZnO($000\bar{1}$) surfaces (a) in the as-received state, (b) after exposure to a 20-W 20% O_2/ 80% He remote plasma for 30 min. at 525 °C and 0.050 Torr, and (c) after cooling under the same conditions to ~RT (O_2 adsorption).

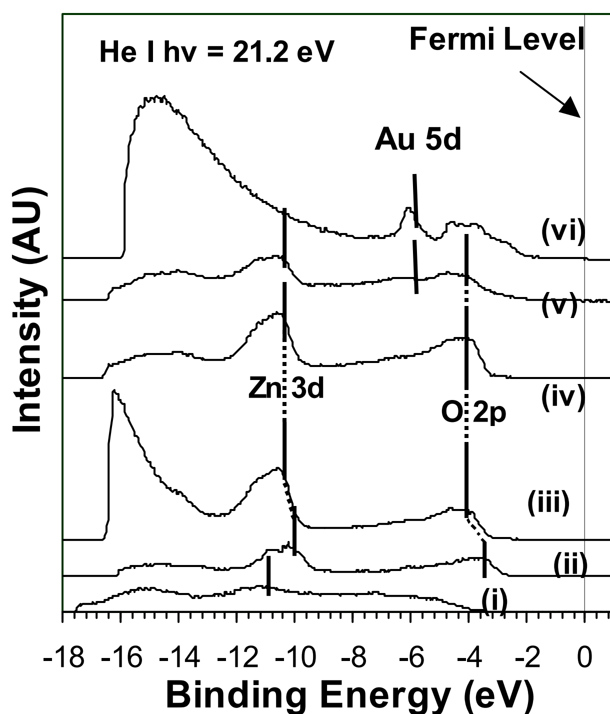

Figure 4.2. UPS valence band spectra from the (i) as-received ZnO($000\bar{1}$) surface, (ii) following remote plasma cleaning and O_2 adsorption, and sequential Au deposition generating thicknesses of (iii) 0.2 nm, (iv) 0.4 nm, (v) 5.0 nm, and (vi) 100 nm. The Au-induced band bending is indicated by the movement of the Zn 3d and O 2p bulk features located at 10.4 eV and 4.0 eV, respectively. All spectra were acquired using the He I photon line (hν = 21.2 eV). The binding energy is measured with respect to the Fermi level (E_F = 0 eV).

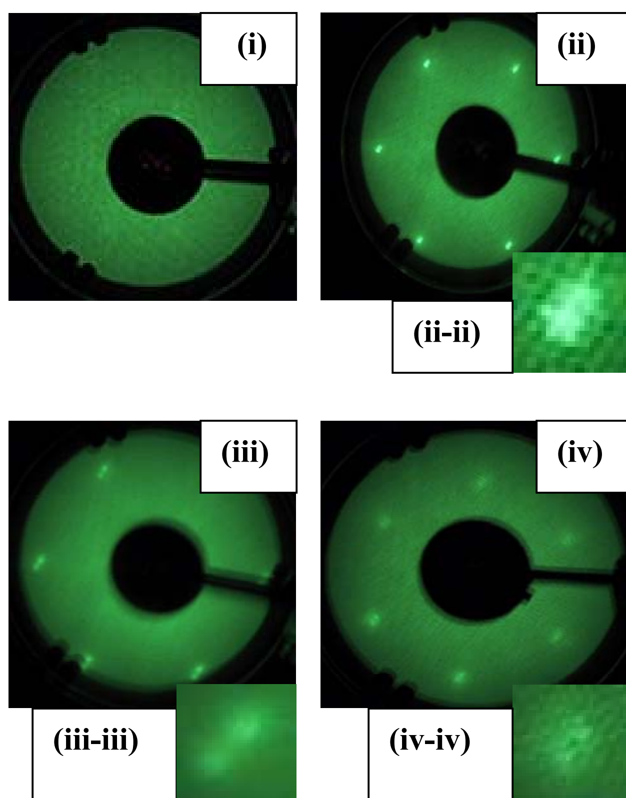

Figure 4.3. LEED images, and corresponding insets, taken of ZnO($000\bar{1}$) surface at primary beam energies of (i) 100 eV for samples in the as-received state (ii) 42 eV after remote plasma cleaning, (iii) 42 eV following oxygen adsorption and (iv) at 80 eV after 100 nm Au metallization, in succession.

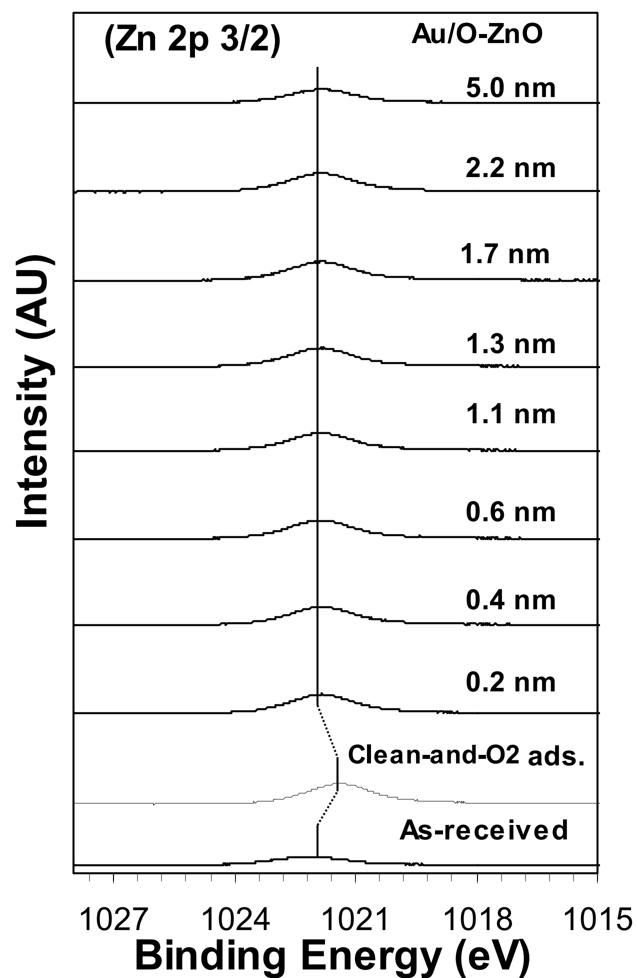

Figure 4.4. XPS Zn $2p_{3/2}$ core level spectra from the as-received ZnO($000\bar{1}$) surface and following remote plasma cleaning, O_2 adsorption, and sequential Au metallization. All spectra were acquired using Mg Kα (hν = 1253.6 eV) radiation.

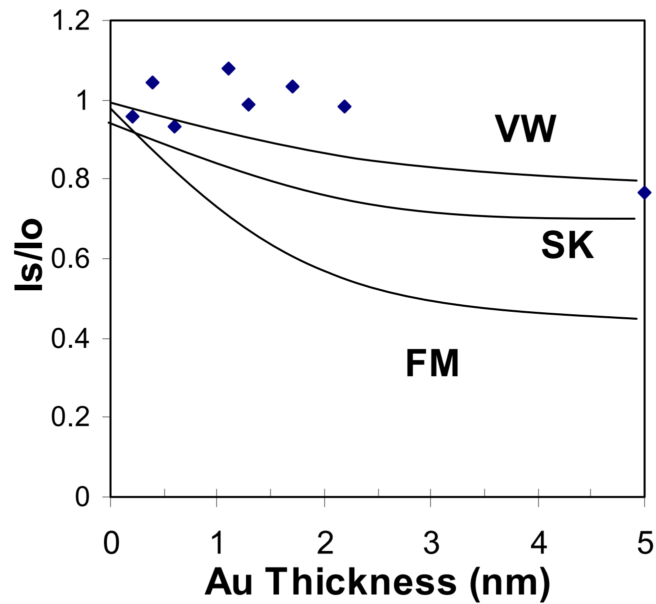

Figure 4.5. Attenuation of the Zn 2p core level photoelectron peak as a function of the overlying Au thickness. The experimental data is indicated by solid diamonds for comparison to Volmer-Weber (VW), Stranski-Krastanov (SK), and Frank-van der Merwe (FM) growth modes.

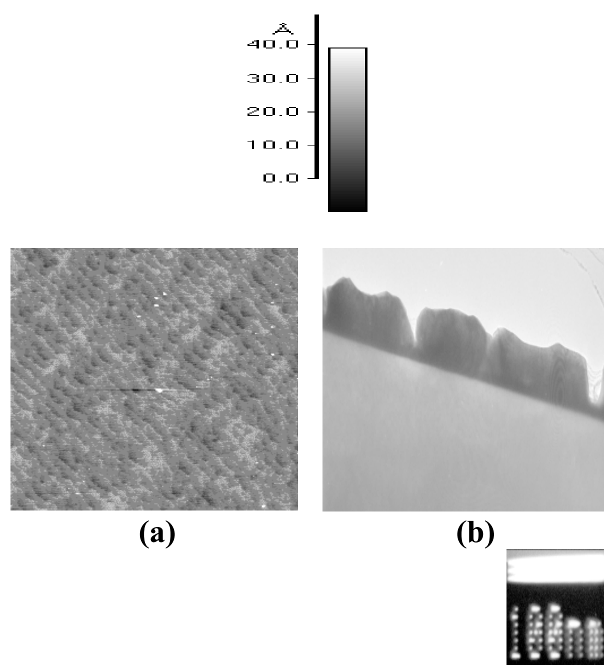

Figure 4.6. AFM image of ZnO$(000\bar{1})$ surface (a) remote plasma cleaned (5 x 5 μm scan size) showing an atomic step and terrace microstructure and (b) TEM image of Au islands in the coalescence phase after oxygen adsorption and 100 nm Au metallization.

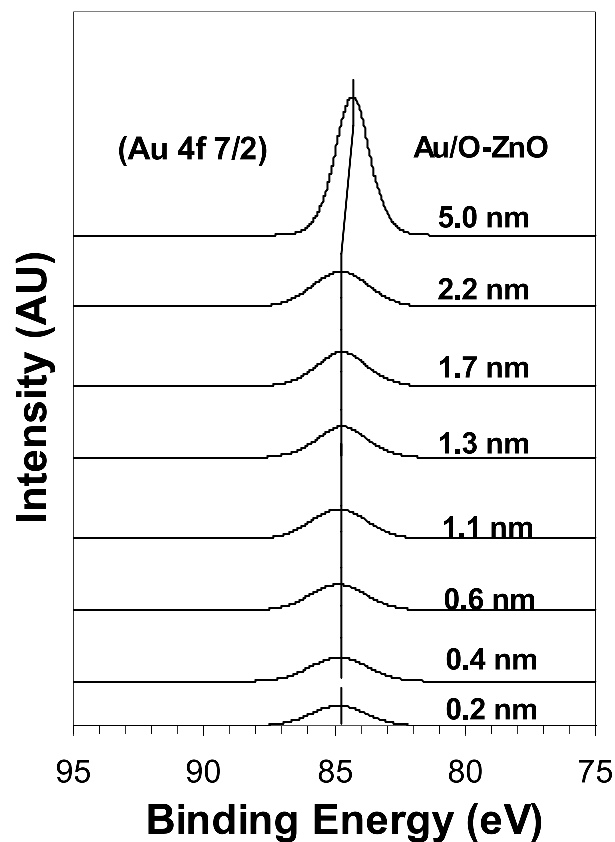

Figure 4.7. XPS Au $4f_{7/2}$ core level curve-fitted spectra as a function of Au deposition following remote plasma cleaning and O_2 adsorption. Shifts of 0.5 eV and 1.0 eV are depicted for the peak position and FWHM, respectively, over the course of sequential Au metallization. All spectra were acquired using Mg Kα (hν = 1253.6 eV) radiation.

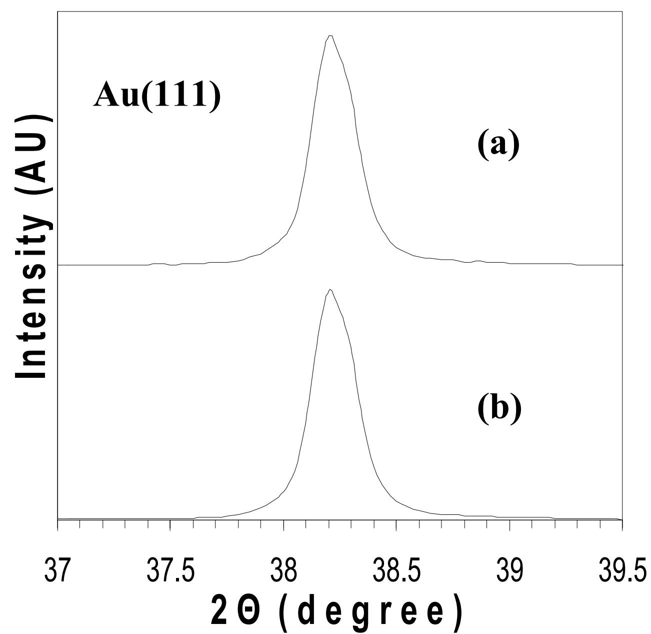

Figure 4.8. XRD 2θ plots for 100 nm Au contacts on a cleaned-and-oxygen adsorbed ZnO($000\bar{1}$) surface (a) as-deposited at room-temperature and (b) after post-deposition annealing in air at 175 °C for 15 min. The spectrum was acquired using Cu $K\alpha$ (λ = 0.1542 nm) radiation.

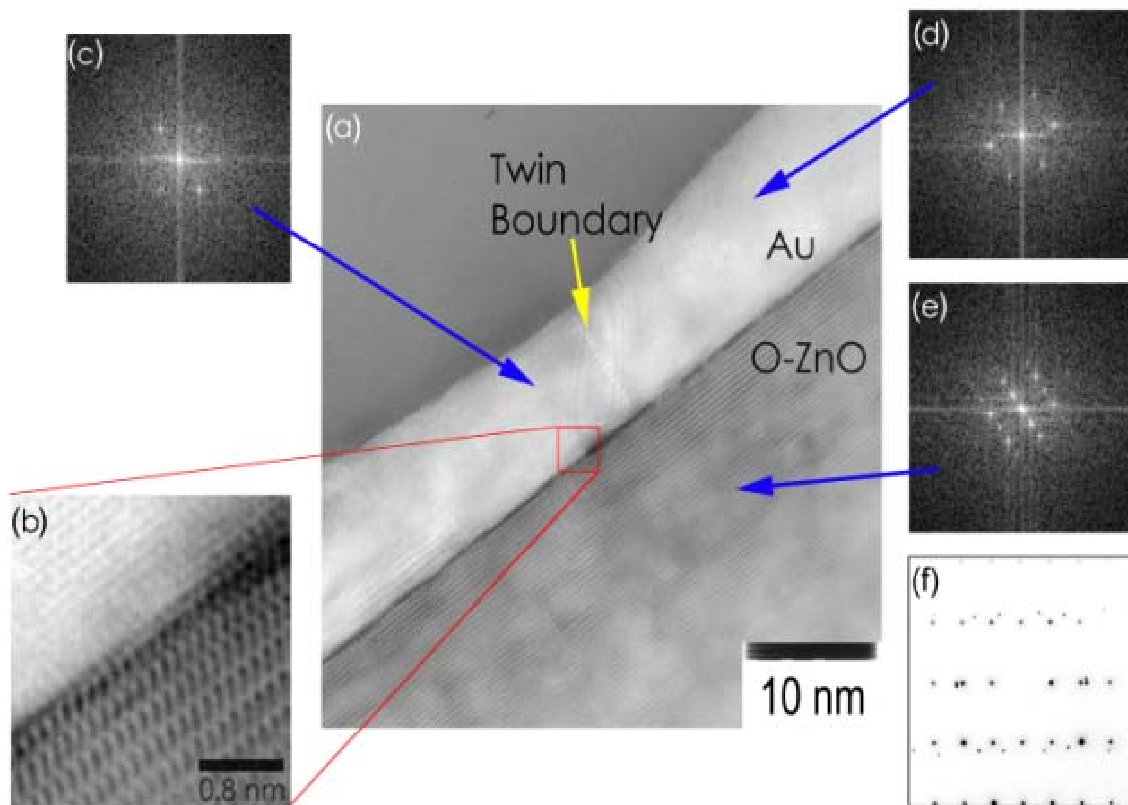

Figure 4.9. (a) Moderate and (b) high resolution TEM images of the cleaned-and-oxygen adsorbed (100nm)Au/ZnO($000\bar{1}$), (c) and (d) fast-fourier transform (FFT) of the twin boundary region of Au, and (e) FFT of ZnO, and (f) diffraction pattern of ZnO and Au.

5. STRUCTURAL, MICROSTRUCTURAL, CHEMICAL, AND ELECTRIAL PROPERTIES OF GOLD SCHOTTKY CONTACTS ON REMOTE PLASMA-CLEANED, n-TYPE ZnO(0001)

Submitted for consideration for publication

to

The Journal of Applied Physics

by

B. J. Coppa, C. C. Fulton and R. F. Davis*
Department of Materials Science and Engineering
North Carolina State University
Box 7907
Raleigh, NC 27695

and

C. Pandarinath, J. E. Burnette and R. J. Nemanich
Department of Physics
North Carolina State University
Box 8202
Raleigh, NC 27695

*Corresponding Author:
Tele: 919-515-3272
FAX: 919-515-7724
robert_davis@ncsu.edu

5.1 ABSTRACT

Current-voltage results of Au contacts deposited on as-received, n-type ZnO(0001) surfaces showed an ~0.01 A/cm^2 leakage current density to 4.6 V reverse bias and ideality factors >2 before sharp, permanent breakdown. These effects were related to the presence of ~2.0±0.1 ML of hydroxide, which leads to an increased surface conductivity and an electron accumulation layer. Remote plasma cleaning reduced the hydroxide layer to ~0.4±0.1 ML. Subsequent cooling in the plasma ambient resulted in the chemisorption of oxygen and the formation of a depletion layer of lower surface conductivity. These process steps produced smooth, highly-ordered, stoichiometric ZnO(0001) surfaces that possessed 0.3 eV of upward band bending. Sequentially deposited unpatterned Au and the most rectifying gold contacts initially grew on these surfaces via the formation of islands that subsequently coalesced. The coalesced film displayed a possessed a barrier height of 0.71±0.05 eV, a saturation current density of 4.04 µA/cm^2, a lower value of n = 1.17±0.05, a significantly lower leakage current density of ~0.1 mA/cm^2 to 8.5 V reverse bias, and a sharp, permanent breakdown at ~ –8.75 V. All measured barrier heights were lower than the predicted Schottky-Mott value of 1.0 eV, indicating that the interface structure and the associated interface states affect the Schottky barrier. However, the constancy in the FWHM of the core levels for Zn 2*p* (1.9±0.1 eV) and O 1*s* (1.5±0.1 eV), before and after sequential *in situ* Au depositions indicated an abrupt, unreacted Au/ZnO(0001) interface.

5.2 INTRODUCTION

Zinc oxide (ZnO) occurs most commonly in the hexagonal wurtzite crystal structure that possesses a direct band-gap of ~3.4 eV at room temperature (RT) and exhibits spontaneous polarization along the {0001} directions.[1] 'Single-crystal' boules and wafers of this material have recently been produced commercially.[2] High-purity crystals of ZnO are typically n-type; this characteristic has traditionally been attributed to native defects such as oxygen vacancies and zinc interstitials.[3] However, recent theoretical calculations by Kohan, *et al*.[4] have shown that none of the native defects exhibit characteristics consistent with a high-concentration shallow donor. Van de Walle[5] has noted that only vacancies have sufficiently low energies to form during growth of ZnO; however, Zn and O vacancies act as deep acceptors and deep donors, respectively. First-principals calculations by the last author have provided strong evidence that H behaves as a shallow donor in ZnO and can be incorporated in high concentrations in this oxide (and in the hydroxide that invariably forms of the surface of this oxide) via the formation of O-H bonds when exposed to the normal laboratory ambient. This is also likely the initial step in the incorporation of H into the ZnO crystal, as it is grown, which may be the principal reason for the n-type behavior of this wide band-gap material.

Several important ZnO-based devices can be fabricated that employ Schottky barrier diodes (SBDs). For example, Schottky-type, ZnO ultra-violet photodetectors have technical advantages in speed and lower noise than their photoconductive counterpart.[6] The former are expected to be particularly useful in space applications, as this material is very resistant to MeV proton irradiation relative to other semiconductors.[7] These types of diodes are also essential for probing defects in semiconductors by junction spectroscopic

characterization techniques such as deep-level transient spectroscopy (DLTS)[8] and admittance spectroscopy.[9] For example, Auret *et al.*,[7] employed Au as the rectifying contact on the ZnO($000\bar{1}$) surface for DLTS studies. They reported a 1 nA leakage current to an applied bias of –1 V and an ideality factor of 1.19. Metal-semiconductor-field-effect-transistors rely on SBD structures. However, the capability of ZnO in these devices is expected to be limited to low power applications, since Schottky contacts to this material have shown a low breakdown voltage (an assessment of material quality), as shown later. Furthermore, ZnO has a low decomposition temperature.[10]

The Schottky-Mott model[11] predicts that metals with high work functions are prime candidates for rectifying contacts on n-type semiconductors. In the case of ZnO, it has been shown[12] that these metals should also possess a low oxygen affinity; thus, the most ideal candidate materials are essentially limited to gold, palladium, and platinum. Kanai[9] found that for gold contacts on as-received Zn-terminated Zn(0001), electrons were possibly trapped at a surface state, which stretched out the capacitance-voltage (*C-V*) curve and decreased the capacitance at high frequencies.[9] As an explanation of these characteristics, this investigator has inferred qualitatively that the likelihood of forming rectifying contacts on the ZnO(0001) surface may be limited by the polar and ionic character of this material. This character could lead to surface states that are occupied by free electrons that need not form ionic bonds with O atoms. In contrast, free electrons are not common on the ZnO($000\bar{1}$) polar O-terminated face, reducing the likelihood of a surface state, which could lead to poor rectifying or ohmic behavior.

Only a few groups, at this writing, have reported investigations of Schottky contacts to ZnO, and none of these studies focused specifically on the ZnO(0001) surface.

Rabadanov, et al.[12] measured the same barrier height of 0.65±0.05 eV for Au, Pt, Pd, and Ag contacts deposited in vacuum at RT on ZnO monocrystals of an unspecified orientation and cleaved in vacuum. However, neither the ideality parameters nor the breakdown voltages were reported. Silver Schottky contacts with a Au cap have been fabricated on as-received ZnO($11\bar{2}0$) epilayers.[13,14] The values of the Schottky barrier height (Φ_B) determined via *I-V* and *C-V* measurements, were 0.89 eV and 0.92 eV, respectively. A leakage current of 0.1 nA at 1 V reverse bias[13,14] and an ideality factor of 1.33[14] were also reported. The high ideality factor was attributed to an interfacial layer and/or surface states. A prior determination of the Φ_B for Au on chemically prepared ZnO crystals with an unspecified orientation resulted in a value of 0.66 eV by *I-V*, *C-V*, photo-response, and thermal activation energy measurements; an ideality factor (*n*) of 1.05 was reported (but below the valid forward bias (V_F) range of $V_F > 0.075$ V) without specifying the reverse bias leakage current.[15] Fabricius, *et al*.[6] measured $n = 2.7$ for Au Schottky photodiodes fabricated on as-received polycrystalline ZnO, but neither Φ_B nor leakage currents were indicated. This high value of *n* was reportedly influenced by recombination processes.

Device-quality Schottky contacts typically require intimate metal-semiconductor interfaces free of surface contamination. A major deterrent to the development of low leakage Schottky contacts on ZnO with low ideality parameters, is the ~3 monolayer (ML) thick native contamination layer, which includes ~1 ML of adventitious carbon and ~2 ML of hydroxide.[16] It has been proposed that H atoms donate ~0.5 e^- to each surface oxygen ion on both the (0001) and ($000\bar{1}$) hydroxylated surfaces of ZnO.[17] This strong interaction, comparable to O-metal bonding in the bulk oxide lattice can result in the formation of a shallow electron donor state through the proposed reaction: ($H + O^{2-} \rightarrow OH^- + e^-$) and can

increase the carrier concentration in the space charge layer by several orders of magnitude.[17] As such, several groups[18-20] have reported that the hydroxide leads to the formation of an accumulation layer that results in a high surface conductivity on both polar faces of ZnO. This is very likely the reason for the reported high leakage currents above – 1 V[7-8,12-14] and relatively high ideality factors (>2)[6,16] for high work function metals (Au) deposited on these uncleaned surfaces.

The sensitivity of the surface conductivity of ZnO to hydrogen and oxygen has been utilized in sensor devices.[12] In contrast with H, adsorbed oxygen species on ZnO act as electron acceptors that generate a depletion layer, which lowers the surface conductivity by several orders of magnitude[21-22] and is advantageous for Schottky barrier formation. It has been proposed[23] that chemisorption of oxygen occurs preferentially at surface defect sites as O^{2-} or O^{-}.

In this study, an *in situ* remote plasma cleaning procedure and a subsequent oxidation step were developed in conjunction with investigations of the deposition and the temperature-dependent current-voltage (*I-V-T*) properties of Au Schottky contacts on polished ZnO(0001) surfaces. Photoemission of the electronic structure and the growth mode of the Au on the ZnO(0001) interface were also studied via X-ray photoelectron spectroscopy (XPS) and ultraviolet photoelectron spectroscopy (UPS). The structural and microstructural characteristics of all the materials used in this program were investigated using X-ray diffraction (XRD), low-energy electron diffraction (LEED) and atomic force microscopy (AFM).

5.3 EXPERIMENTAL PROCEDURES

Two millimeter-thick, nominally single-crystal ZnO(0001) 2-inch-diameter wafers, diced from boules produced by seeded chemical vapor transport by Eagle-Picher Technologies, Inc.[2] and chemo-mechanically polished on both sides, were employed in the present research. Each wafer contained highly textured domains with very low angle boundaries and with a collective range of full width half maxima in their rocking curves acquired about the [0001] direction. Thus the term "single-crystal" is used with this caveat. Grade I samples, free of internal microvoids, were utilized for the *I-V-T* studies, while Grade II wafers were used in all other experiments. Hall and C-V measurements, the latter at 1 x 10^4 Hz, taken from the (0001) surface of the as-received wafer, showed a bulk carrier concentration of 1±5 x $10^{17}/cm^3$ and a nominal effective donor concentration, (N_D-N_A), of 5±5 x $10^{16}/cm^3$, respectively. The wafers were then cleaved into smaller sections (> 1cm^2), rinsed *ex situ* in methanol for 5 sec and dried in flowing nitrogen. These samples are denoted herein by the term "as-received".

All *in situ* metal deposition, cleaning and surface characterization experiments described below were conducted within a unique ultrahigh vacuum (UHV) configuration, which integrates several independent cleaning, thin-film growth and analysis systems via a transfer line having a base pressure of <1 x 10^{-9} Torr[24]. A (40-100)-nm-thick Ti film was deposited by e-beam evaporation from a 99.999% pure metal source onto the entire $(000\bar{1})$ face of each ZnO section. This film served (1) to absorb radiation from the underlying Pt-Rh heater and to conduct heat into the wafer during the *in situ* cleaning of the (0001) face and (2) as an ohmic contact. ZnO(0001) surfaces and ZnO(0001)/Au interfaces, with hydrocarbons and essentially hydroxide below our detection limits, were achieved via

exposure of the former to a 20 W, 20% O_2/80% He (by volume) remote plasma at 550±20 °C and 0.050±0.001 Torr for 60 min. Each cleaned surface was then cooled to either 425 °C and subsequently in vacuum to RT or to approximately RT in the unignited plasma gas. The temperature of 425 °C was phased into this routine, since it was previously found that a smooth ZnO surface could be retained, as found by atomic force microscopy, after annealing in vacuum. Thus, 425 °C became the standard temperature for purging the chamber with helium and oxygen prior to generating a plasma. A detailed description of this cleaning procedure and the results of the associated structural, microstructural and photo-optical investigations have been reported.[25]

Gold was deposited *in situ* via e-beam evaporation from a 99.999% pure metal source onto the cleaned surfaces cooled in the plasma gas ambient either sequentially as very thin regions of increasing thickness or through a gold-coated molybdenum shadow mask as contacts having a thickness and diameter of ~150 nm and ~100 μm, respectively, and arranged in an 8 x 8 array. The nominal thickness of each Au layer was determined using a quartz crystal deposition rate monitor. The base and process pressures within the 3-kW Thermionics e-beam system, used to deposit both the Ti and the Au contacts were ~7 x 10^{-10} Torr and ~7 x 10^{-9} Torr, respectively. Deposition rates varied from 0.1-1 Å/sec, depending on the application, and were regulated with a Sycon Instruments STM-100 MF film thickness/rate monitor. The resulting Au/ZnO/Ti structure allowed current to pass through the bulk wafer and eliminated the need for complex isolation of the contacts.

Current-voltage results were acquired for all samples at either RT or an elevated temperature using 50-μm diameter tungsten fine-wire-tip probes and a Keithley 236 source unit having the capability of measuring currents in the 1 pA - 100 mA range. Selected

samples were heated on the sample stage to 80±5°C and 150±5°C for subsequent temperature-dependent analyses. A hand-held K-type thermocouple in contact with the Au surface provided digital temperature readout. *C-V* measurements were used for determining the series resistance of the wafers and were performed using a Hewlet-Packard LCR meter with the capability of measuring capacitances in the range (0.01 fF - 10 μF).

XRD 2θ scans were conducted *ex situ* on the unannealed and annealed thick Au contacts to determine their crystallographic orientation and its stability during heating. A Rigaku Geigerflex diffractometer was used with Cu *Kα* (λ = 0.1542 nm) radiation at a tube voltage and current of 27-kV and 20-mA, respectively. The X-ray beam was directed by 1° diffraction and scattering slits to the 43% resolution scintillator detector.

5.4 RESULTS AND DISCUSSION

5.4.1 *Analyses of the cleaned ZnO(0001) surface cooled in vacuum*

Low-energy electron diffraction of the as-received ZnO(0001) surface showed only a bright background, indicative of a disordered contamination layer.[16] Deconvolution of the O 1*s* core level peak obtained via XPS studies revealed that this surface contained ~2.0±0.1 ML (20±1 atomic percent of the measured volume) of OH^-, as determined by the peak at 532.9 0 eV. Approximately 1 ML of adventitious carbon was similarly detected. The Zn/O ratio was 0.5±0.1. It is interesting to note that atomic modeling studies of [0001]-oriented ZnO samples by E. Chen[26] have shown that step edges oriented in the $[\bar{1}010]$ direction have two dangling bonds and are more energetically favorable for adatoms than the $[\bar{1}100]$ oriented step edges with only one dangling bond.[26] Thus, we have proposed that surface contaminants from ambient lab conditions and/or the adsorbed

oxygen on the samples cooled in the plasma ambient (see below) would preferentially bond to the $[\bar{1}010]$ step edge.

The remote plasma cleaning process reduced the carbon species to below the detection limit. Examination of the XPS spectra of the plasma-cleaned (0001) surface cooled in vacuum revealed a shift in the lattice O 1s peak from 530.9 (FWHM = 1.6 eV) to 530.4 eV (FWHM = 1.4 eV), which is attributed to a change in band bending (see UPS results below). These results also showed a peak at 532.7 eV, which indicates ~0.4 ML of OH. A corresponding core level shift of 0.6 eV was deduced from the change in respective Zn $2p_{3/2}$ and Zn $2p_{1/2}$ peak positions from 1022.0 eV and 1045.1 eV (both FWHM = 2.3 eV) for the as-received samples to 1021.4 eV and 1044.5 eV (both FWHM = 2.1 eV) after plasma-cleaning, which is also attributed to a change in band bending. The positions of all the XPS peaks noted above had an uncertainty of ±0.1 eV. A sharp (1x1) hexagonal LEED pattern was observed at 50 eV from the cleaned (0001) surface, conveying a high degree of structural order.

The removal of the ~1.6 ML of the OH was critical for eliminating the proposed accumulation layer of high surface conductivity[18-20] and for generating a surface with a Zn/O stoichiometric ratio of 1.0. The change in band bending of 0.6 eV due to the cleaning process was confirmed from UPS spectra (±0.1 eV uncertainty). Figures 5.1(a) and (b) indicate that the surface Fermi level shifted from 0.6 eV above the conduction band minimum (CBM) for the as-received ZnO(0001) to 0.1 eV below the CBM after the plasma cleaning. The bulk Fermi level in ZnO is accepted to be 0.3 eV below the CBM, and this value was used in determining the band bending from the UPS spectra.[27] In addition, it is shown in Figs. 5.1(a) and (b) that the downward band bending is reduced

from 0.9 eV to 0.2 eV for the as-received and plasma-cleaned surfaces, respectively, as the accumulation layer is reduced. The electron affinity of 4.0±0.2 eV, derived from the UPS spectra, essentially remained constant after cleaning.

5.4.2 *Analyses of the cleaned ZnO(0001) surface cooled in the plasma ambient*

Cooling the cleaned ZnO in the unignited plasma gas from 550°C to approximately RT was employed, because we had previously determined[16] that exposure of the ZnO($000\bar{1}$) surface to an O_2-containing ambient improved the behavior of subsequently deposited contacts. The reported[28] submonolayer of chemisorbed oxygen was below the detection limit of our XPS, as expected. It neither varied the Zn or O core level positions nor altered the 1.0 value of the Zn/O ratio. However, UPS is more surface-sensitive than XPS, and a significant variation in the spectra of the former was observed, as shown in Fig. 5.2 and described below. It has been reported by Henrich and Cox[28] that changes in electron energy loss (EELS) and UPS spectra occur upon chemisorption of O_2 on ZnO. However, the actual coverage of the surface was determined to be $<2.5 \times 10^{-4}$ ML in the chemisorption temperature range (20 °C – 377 °C) with a sticking coefficient of 10^{-5}.[28] Typically, the chemisorbed O_2 resides on the surface as O_2^-, although it has been found as O^- as well.[21-22,28] Physisorption of O_2 primarily occurs below 20 °C without any detectable charge transfer.[28] However, O_2 that adsorbs to the surface has been shown to change the band bending by ~1 eV, consequently decreasing the surface conductivity by several orders of magnitude.[21-22]

The UPS results provided evidence for a change in band bending that is associated with O_2 adsorption, that was preferable for the formation of a Au Schottky barrier. Figures

5.1(b) and (c) show a 0.5 eV change in band bending due to the exposure of the cleaned surface to the unignited O_2-containing plasma gas on cooling. This corresponds to a shift of the Zn 3*d* feature from 10.9 eV to 10.4 eV for the plasma-cleaned surfaces cooled in vacuum and in the O_2/He ambient, respectively. Moreover, it is shown that the 0.2 eV of downward band bending for the clean surface is changed to 0.3 eV of upward band bending, after the exposure to the O_2/He ambient during cooling. Figures 5.1(b) and (c) indicate that the surface Fermi level shifted from 0.1 eV below the CBM for clean ZnO(0001) to 0.6 eV below the CBM after cooling in the O_2-containing gas. This shift away from the CBM corresponds to a reduction in n-type surface conductivity and may be attributed to the adsorption of oxygen species acting as electron acceptors for ZnO.[21-22] The electron affinity varied from 4.1-4.3±0.2 eV between the two processing steps. Surface states were neither observed after cooling–in vacuum nor the plasma ambient;[24] however, a shoulder was observed in the O 2*p* feature at 5.7 eV presented in Fig. 5.2, indicative of O_2 adsorption, after cooling in the plasma ambient. After the latter process, a sharp (1x1) hexagonal LEED pattern was observed at 60 eV, indicating that any adsorbed oxygen did not affect the high degree of structural order observed after plasma cleaning.

5.4.3 *AFM analyses of remote plasma-cleaned ZnO(0001)*

Prior and post-cleaning AFM analysis of the (0001) surface microstructure confirmed the absence of any observable damage associated with the annealing and/or plasma exposure. The RMS surface roughness of this surface was 1.2±0.2 nm before and 1.7±0.2 nm after cleaning.

5.4.4 *Growth mode of Au and characterization of the Au/ZnO(0001) interface*

The growth mode of Au deposited on the cleaned surface exposed to the plasma ambient on cooling was determined from the results shown in Figs. 5.3 and 5.4 using an approach employed by Sitar *et al.*[29] and Wolter *et al.*[30] The three possible growth modes considered in this study were (i) Frank-van der Merwe (two-dimensional, layer-by-layer growth), (ii) Volmer-Weber (three-dimensional growth of discrete islands), and (iii) Stranski-Krastanov (a combination of the two previous models wherein the initial film growth occurs via a layer-by-layer mechanism and is subsequently followed by the initiation of island growth). The substrate, film and interfacial surface energies, and strain determine the prevailing growth mode.

In XPS measurements, Frank-van der Merwe (FM) growth is expressed as

$$I_s/I_o = \exp(-t/\lambda_o), \qquad (1)$$

where I_s is the core level intensity for a given overlayer thickness (t), I_o is the baseline core level intensity acquired from the ZnO surface following the cleaning and subsequent O_2 exposure, and λ_o is the attenuation length of the particular core level electron. The Volmer-Weber (VW) mode of deposition would follow the expression

$$I_s/I_o = (1-\theta) + \theta * \exp(-t/\lambda_o), \qquad (2)$$

where θ is the surface coverage of the islands (value between 0 and 1). Stranski-Krastanov (SK) growth is represented by the expression

$$I_s/I_o = (1-\theta) * \exp(-q/\lambda_o) + \theta * \exp(-t/\lambda_o), \qquad (3)$$

where q is the deposited thickness before three-dimensional island growth or nucleation. These graphs of these three equations are shown in Fig. 5.5. The value of I_s for each Au

deposit was determined using a quartz crystal deposition rate monitor and, therefore, represents that thickness that would be present if the layer was uniform in thickness across the surface of the ZnO sample. The experimental values of I_s/I_o shown in Fig. 5.5 for the O 1*s* core level decreased from 1.00 before Au deposition to 0.83±0.03 at a nominal Au thickness of 5.0 nm. A close match to the theoretical curve for VW growth was determined, but there is significant scatter in the data. The values of I_s/I_o for the Zn $2p_{3/2}$ followed the same trend as those for the O 1*s*. These results correspond well with those obtained from prior experiments concerning the growth of Au on ZnO($000\bar{1}$).[31] Moreover, transmission electron microscopy (TEM) of this interface showed the coalescence of islands.

In contrast to the above results, AES spectra obtained by Roberts and Gorte[32] indicated that Pt initially grows in a layer-by-layer mode on a ZnO(0001) surface that has been cleaned via Ar^+ ion bombardment, annealed in vacuum at 527 °C for 30 min. and exposed to 1 x 10^{-8} Torr of O_2 at 427 °C for 30 min. Transmission electron microscopy of the (0001) surface revealed that the Pt(111) plane was parallel to this surface with a 30º rotation between the two lattices. Three-dimensional islands were observed after annealing this sample for an unspecified period at 300 °C in vacuum. Henrich and Cox[33] have also reported that Pt as well as Pd initially grows by a Frank-van de Merwe mechanism on UHV-cleaved ZnO(0001). Auger electron spectroscopy (AES) and UPS spectra acquired from polished (0001) surfaces subsequently annealed in UHV confirmed this layer-by-layer growth mode. The [111] directions of the polycrystalline grains of Pd were preferentially oriented parallel to the surface without azimuthal alignment.[33]

The Schottky barrier height (SBH) of the Au/ZnO interface produced in the present research was determined from both XPS and UPS spectra to compare with those values determined from *I-V* measurements. Figures 5.3 and 5.4 show the respective evolution of the O 1*s* and Zn 2*p* core level XPS spectra as a function of the thickness of the Au overlayer deposited on a cleaned ZnO(0001) surface exposed to the plasma ambient on cooling to ~RT. These spectra were acquired *in situ* over an ~30 hour period. The shifts in the Zn $2p_{3/2}$ and O 1*s* (lattice) core level positions and their FWHM after cleaning, exposure to the oxygen-containing plasma ambient on cooling and sequential Au depositions are given in Tables 5.1 and 5.2, respectively. Deposition of 0.2 nm of Au caused the O 1*s* lattice peak to shift 0.2 eV from 530.4 eV to 530.6 eV and the Zn 2*p* multiplet to shift 0.3 eV from 1021.4 eV and 1044.5 eV to 1021.7 and 1044.8 eV, respectively. Deposition of an additional 0.2 nm of Au caused the O 1*s* core level to shift 0.1 eV to 530.7 eV; the Zn 2*p* remained unchanged. The agreement in the shifts of the O 1*s* and the Zn 2*p* core levels indicates that these shifts were caused by changes in band bending rather than being chemically induced. Both core levels remained fixed at these values after subsequent Au depositions, as shown in Figs. 5.3 and 5.4, which indicates that the Schottky barrier is completely formed after the deposition of ~0.4 nm of Au. The lack of a discernible change in the FWHM of 1.5±0.1 eV and 1.9±0.1 eV for the O 1*s* and Zn 2*p* core levels after the formation of the Schottky barrier is indicative of an abrupt, unreacted interface. In related studies, UPS spectra acquired by Göpel, *et al.*[34] indicated that Schottky barrier formation occurred over the first 1.0 nm of metal coverage on ZnO($10\bar{1}0$) without an interface reaction.

The evolution of the Au $4f_{7/2}$ curve-fitted core level peak, during sequential Au depositions, depicted in Fig. 5.6 provided additional information regarding the formation of the Au Schottky barrier. Core level peaks for Zn $3p_{1/2}$ and Zn $3p_{3/2}$ at 91 eV and 89 eV, respectively, nearly overlap the Au $4f$ core level; thus, only the curve-fitted Au $4f_{7/2}$ spectra is presented. Gold island formation likely influenced the actual values of Au thickness. The results presented in Table 5.3 show that the binding energy of this peak decreased from an initial value of 85.3 eV at 0.2 nm to 84.0 eV for 100 nm of Au (Δ = 1.3 eV), while the FWHM of both peaks decreased from 2.5 eV to 1.2 eV (Δ = 1.3 eV), as a function of Au thickness. Also, the integrated area of the Au $4f$ peak is increased as a function Au thickness, as listed in this table. The 1.3 eV shift in the Au $4f_{7/2}$ peak is most likely due to islanding associated with the VW growth mode of this metal. However, this shift may be also be attributed to the deposition of Au into varying depths of the wafer through microvoids, constituting at least 20% of the surface. Ideally, the Au $4f_{7/2}$ core level position and FWHM should remain at a fixed value over the course of sequential depositions in order to use XPS for measuring the SBH. The following equation[35] was used to calculate the value of Φ_B from these results.

$$\Phi_B = E_g - E^m_{core} + (E^i_{core} - E^{c,ox.}_{VBM}), \qquad (4)$$

where E_g is the RT band-gap of ZnO (3.4 eV), E^m_{core} is the final position of the Zn (or O) core level after sequential Au depositions, E^i_{core} is the position of the Zn (or O) core level before metal deposition and $E^{c,ox.}_{VBM}$ is the Fermi level position relative to the VBM for the cleaned surface cooled in the plasma ambient. The value of $E^{c,ox.}_{VBM}$ was determined from UPS measurements to be 2.8 eV. The calculated value of the SBH is 0.3±0.1 eV for both the Zn $2p_{3/2}$ and the O $1s$ core levels is lower than the 0.71±0.05 eV value determined from

analyses of the *I-V* measurements. Current-voltage measurements are conducted with bulk metal contacts; thus, this technique is not as sensitive to effects that have influenced photoemission results (*ie.* islanding during initial stages of growth).

The UPS results presented in Fig. 5.2 show that the binding energy of the O 2*p* core level shifted from 4 eV for the cleaned surface cooled in the plasma ambient to 4.4 eV after the deposition of 0.2 nm of Au. A corresponding shift occurred in the Zn 3*d* peak from 10.4 eV to 10.7 eV, while the Au 5*d* feature began to emerge at 6.2 eV. The position of the O 2*p* peak remained unchanged following the next 0.2 nm of Au deposition (0.4 nm total thickness); however, the Zn 3*d* shifted slightly to 10.8 eV. The correlation of these peak shifts with those measured by XPS indicates that the observed shifts are caused by changes in band bending rather than chemical shifts or charging effects. As expected, the intensity of the Au 5*d* bulk feature intensified as a function of Au thickness. No apparent surface states were observed, as also reported in related studies by Göpel, *et al.*[34] The following equation[28] was used to calculate the value of Φ_B from these results

$$\Phi_B = E_g - (E_F - E^m_{VBM}), \qquad (5)$$

where E_g is the RT band gap of ZnO (3.4 eV), ($E_F - E^m_{VBM}$) (3.2 eV) is the difference between the VBM of ZnO for a 0.4 nm-Au-coated surface and the Fermi level position. The use of equation (5) generated a value of $\Phi_B = 0.2\pm0.1$ eV, which agrees with the XPS value of 0.3±0.2 eV.

Additional research involved the deposition and characterization of "thick" 75 nm Au contacts, having an ~11% lattice mismatch to ZnO. Strain due to this mismatch is likely relieved by twinning in the Au layers, which was observed in TEM of the Au/ZnO($000\bar{1}$) interface.[25] However, other defects at this interface are possible but were

not observed. The curve-fitted XRD spectra of the Au peak at 38.3±0.1º (FWHM = 0.2±0.1º (800”)) presented in Fig. 5.7 revealed that these contacts are oriented along [111] on (1) clean ZnO(0001) wafers exposed to the plasma ambient on cooling (Fig. 5.7 (a)), and (2) similarly treated wafers that were subsequently heated *ex situ* in air at 175 °C for 15 min. without a change in FWHM (Fig. 5.7 (b)). The (111) d-spacing of 0.0235±0.0001 nm, determined for both films and equivalent to that for single crystal Au, indicates that the films were not coherently strained to match the ZnO surface crystal structure. The ZnO(0002) and (0004) reflections (not shown) were acquired at 34.4±0.1º and 72.5±0.1º, respectively, for both samples. These results supplement those obtained in previous TEM investigations by Wassermann and Polacek[36] that indicated epitaxial growth of Au(111) on the polar surfaces of vacuum-cleaved ZnO.

A high degree of structural order was indicated by the well-defined (1x1) hexagonal LEED patterns with a dark background acquired from Au(75nm)/ZnO(0001) and Au(2.2nm)/ZnO(0001) samples using an incident energy of 60 eV; a sharper pattern was obtained for the thinner Au coverage.

5.4.5 *I-V-T characterization of Au/ZnO(0001)/Ti*

The *I-V* data obtained from the Au contacts deposited on Grade I wafers were analyzed using the following methodology. For thermionic emission and V greater than 3 kT/q, the general diode equation in forward bias is

$$J = J_o \exp(\frac{qV - IR}{nkT}), \tag{6}$$

where J is the current density, q is the charge of an electron, V is the voltage, I is the current, R is the series resistance, n is the ideality factor, k is Boltzman’s constant, and T is

the absolute temperature. The saturation current density J_0 is given by $J_0 = A^*T^2 \exp(-\Phi_B/kT)$ where A* is the Richardson constant. The of $A^* = 32$ A cm^{-2} K^{-2} was used in this study, since the experimental value was not determined. The ideality factors were obtained by fitting the forward bias ln(*J*)-V curve between 0.22 – 0.29 V for the unheated samples and between 0.08 – 0.23 V for the annealed samples over several decades of current and correcting for the substrate series resistance theoretical value[37] measured directly by *C-V*. Barrier height measurements could not be obtained using *C-V* measurements due to the high series resistance of the unintentionally doped, 2 mm thick wafers. Previous results indicated that top-side and bottom-side Ti contacts showed good ohmic behavior through the bulk ZnO wafer. The best Au rectifying contact characteristics are presented and discussed for all sample types.

The data obtained from RT (~20 °C) *I-V* measurements of the Au contacts on as-received ZnO(0001) wafers and shown in Fig. 5.8 reveal reverse bias leakage current densities below ~0.01 A/cm^2 (2.20 x 10^{-4} cm^2 contact area) to -4.6 V before sharp, permanent breakdown. The ideality factors were >2; thus making any derived value of the SBH or J_0 invalid. These effects were attributed to the presence of the hydroxide, which increased the surface conductivity. It was determined previously[16] that both (1) plasma-cleaning and (2) subsequent exposure of the O-terminated ZnO($000\bar{1}$) surface to the plasma ambient on cooling improved the rectifying properties of the contacts.

Significant improvements in the *J*-V characteristics were also obtained for the Au contacts on cleaned-and-oxygen adsorbed ZnO(0001) surfaces, as shown in Fig. 5.9. Cooling the cleaned surfaces in the unignited plasma gas to ~RT resulted in a barrier height of 0.71±0.05 eV, a saturation current density of 4.04 μA/cm^2 (2.20 x 10^{-4} cm^2

contact area), a lower value of n = 1.17±0.05, a significantly lower leakage current density of ~0.1 mA/cm^2 to 8.5 V reverse bias, and a sharp, permanent breakdown at ~ -8.75 V, as observed in curves (i) and (ii) in Fig. 5.9. Thirty-one percent of these contacts exhibited leakage current densities of the order of 4 μA/cm^2 range; the balance of the contacts were influenced by defects, including scratches on the ZnO(0001) surface.

The barrier height calculated from the *J-V* results of Au on our cleaned-and-oxygen adsorbed ZnO(0001) surface corresponds well with the value of 0.66±0.05 eV found via the same processing routine for ZnO(000) surface.[16] Furthermore, reports by Rabadanov *et al.*[12] and Neville and Mead[15] for annealed and UHV-cleaved surfaces of unspecified orientations, respectively, show values in agreement with our assessment. The markedly lower values of the barrier height obtained from our photoemission data relative to those obtained from the *J-V* data acquired on much thicker films appear to be due to Au island formation. The Schottky-Mott model predicts Φ_B = 1.0 eV for this interface; differences between the theoretical and measured barrier heights infer the presence of an interface dipole.

Slight degradation in the electrical properties was observed in the contacts heated to 80 °C and 150 °C and analyzed at the annealing temperature. The *I-V-T* performance at 80 °C resulted in a barrier height of 0.82±0.05 eV, a higher saturation current density of 9.05 μA/cm^2, n = 1.12±0.05, and a leakage current of ~2 mA/cm^2 to 6 V reverse bias. However, breakdown measurements were not taken for data displayed in curves (iii) and (iv) in Fig. 5.9. Further reduction in reverse bias performance was detected in the samples heated to 150 °C, as shown in curves (v) and (vi) in Fig. 5.9. A barrier height of 0.79±0.05 eV, a saturation current density of 4.34 mA/cm^2, a lower value of n = 1.09±0.05, a leakage

current of ~20 mA/cm^2 to 7 V reverse bias, and a soft, permanent breakdown at this voltage was calculated from these results. Thermal cycling of the contacts between the annealing temperature and RT had no measurable impact on the rectifying properties. An increase in thermally generated carriers is likely the mechanism causing the increased reverse bias leakage currents as the temperature is increased. A change in the interface structure and/or chemistry during the *I-V-T* measurement may explain the slight variance in n and Φ_B.

5.5 SUMMARY

Unpatterned and patterned Au contacts, deposited *in situ* on n-type ZnO(0001) wafers either (1) in the as-received state and/or (2) cleaned via a 20% O_2/80% He remote plasma at 550°C and cooled in the unignited plasma ambient, nucleated and initially grew via the Volmer-Weber (island) mode until coalescence. Cooling in the plasma ambient caused the chemisorption of oxygen and a 0.5 eV change in band bending which resulted in 0.3 eV of upward band bending, indicative of a depletion layer and lower surface conductivity. *J-V* results obtained from the contacts deposited on the as-received surfaces showed ~0.01 A/cm^2 to 4.6 V reverse bias and ideality factors >2, before sharp, permanent breakdown occurred. These results were ascribed to the presence of ~2.0 ML of hydroxide, which typically increases the surface conductivity and forms an accumulation layer. Plasma cleaning eliminated all detectable hydrocarbon contamination, reduced the amount of the hydroxide layer to ~0.4 ML and resulted in a 0.7 eV reduction in downward band bending and a lowering of the surface Fermi level. The surfaces of the cleaned wafers were also smooth, highly-ordered, and stoichiometric. Subsequent exposure to the

unignited plasma ambient likely resulted in the chemisorption of oxygen. This latter process step resulted in a 0.5 eV change in band bending, resulting in 0.3 eV of upward band bending, which is indicative of a depletion layer and lower surface conductivity. The best gold contacts were measured on these last surfaces and displayed a barrier height of 0.71±0.05 eV, a saturation current density of 4.04 μA/cm^2, a lower value of n = 1.17±0.05, a significantly lower leakage current density of ~0.1 mA/cm^2 to 8.5 V reverse bias, and a sharp, permanent breakdown at ~ -8.75 V. The lower values of the barrier height calculated from our photoemission data relative to those obtained from the *J-V* data acquired on much thicker films appear to be due to Au island formation. All measured barrier heights were lower than the predicted Schottky-Mott value of 1.0 eV. The Au/ZnO(0001) interface structure are likely the cause of this difference. However, the constancy of the FWHM of core levels for Zn 2*p* (1.9 eV) and O 1*s* (1.5 eV), before and after sequential Au depositions conducted *in situ* indicates an abrupt, unreacted Au/ZnO(0001) interface. Slight degradation in the electrical properties of these contacts occurred during annealing at 80±5 °C and 150±5 °C. The [111] crystallographic orientation of the contacts was unchanged during heating.

5.6 ACKNOWLEDGMENTS

This research was partially funded by both the Kenan Institute for Technology, Engineering and Science at North Carolina State University and by the Office of Naval Research under contract N00014-98-1-0654 (H. Dietrich, monitor). R. F. Davis was partially supported by a Kobe Steel Ltd. Professorship. The authors acknowledge their appreciation to Professor Gerry Lucovsky of NCSU for the use of *C-V* equipment.

5.7 REFERENCES

1. D. C. Look, Materials Science and Engineering B80, 383 (2001).
2. D. C. Look, D. C. Reynolds, J. R. Sizelove, R. L. Jones, C. W. Litton, G. Cantwell, and W. C. Harsch, Solid State Commun. 105, 399 (1998).
3. P. Bonasewicz, W. Hirschwald, and G. Neumann, Appl. Surf. Sci. 28, 135 (1987).
4. A. F. Kohan, G. Ceder, D. Morgan and C. G. Van de Walle, Phys. Rev. B 61, 15019 (2000).
5. C. G. Van de Walle, Phys. Rev. Lett. 85, 1012 (2000).
6. H. Fabricius, T. Skettrup, and Paul Bisgaard, Applied Optics 25, 2764 (1986).
7. F. D. Auret, S. A. Goodman, M. Hayes, M. J. Legodi, H. A. van Laarhoven, and D. C. Look, Appl. Phys. Lett. 79, 3074 (2001).
8. F. D. Auret, S. A. Goodman, M. Hayes, M. J. Legodi, W. E. Meyer, and D. C. Look, Appl. Phys. Lett. 80, 1340 (2002).
9. Y. Kanai, Jpn. J. Appl. Phys. 29, 1426 (1990).
10. D. Kohl, M. Henzler, and G. Heiland, Surf. Sci. 41, 403 (1974).
11. N. F. Mott, Proc. Cambr. Phil. Soc. 34, 568 (1938).
12. R. A. Rabadanov, M. K. Guseikhanov, I. Sh. Aliev, and S. A. Semiletov, Fizika 6, 72 (1981).
13. Y. Liu, C. R. Gorla, S. Liang, N. Emanetoglu, Y. Lu, H. Shen, and M. Wraback, Journal of Electronic Materials 29, 69 (2000).
14. H. Sheng, S. Muthukumar, N. W. Emanetoglu, and Y. Lu, Appl. Phys. Lett. 80, 2132 (2002).
15. R. C. Neville and C. A. Mead, J. Appl. Phys. 41, 3795 (1970).

16. B. J. Coppa, R. F. Davis, and R. J. Nemanich, Appl. Phys. Lett. 82, 400 (2003).
17. V. E. Henrich and P. A. Cox, *The Surface Science of Metal Oxides* (Cambridge Univ., Cambridge, 1994) p. 297.
18. H. Moormann, D. Kohl, and G. Heiland, Surf. Sci 100, 302 (1980).
19. G. Heiland and P. Kunstmann, Surf. Sci. 13, 72 (1969).
20. M. Nakagawa and H. Mitsudo, Surf. Sci. 175, 157 (1986).
21. E. Arijs, F. Cardon, and W. Maenhout-Van Der Vorst, Surf. Sci. 17, 387 (1969).
22. L. Lagowski, E. S. Sproles, Jr., and H. C. Gatos, J. Appl. Phys. 48, 3566 (1977).
23. V. E. Henrich and P. A. Cox, *The Surface Science of Metal Oxides* (Cambridge Univ., Cambridge, 1994) p. 288.
24. J. van der Weide, Ph.D. dissertation, N. C. State University, Raleigh, NC, 1994.
25. B. J. Coppa, C. C. Fulton, P. J. Hartlieb, R. F. Davis, B. J. Rodriguez, B. J. Shields and R. J. Nemanich, submitted to the J. Appl. Phys.
26. E. Y. Chen (private communications).
27. K. Jacobi, G. Zwicker, and A. Gutmann, Surf. Sci. 141, 109 (1984).
28. V. E. Henrich and P. A. Cox, *The Surface Science of Metal Oxides* (Cambridge Univ., Cambridge, 1994) p. 298.
29. S. D. Wolter, J. M. Delucca, S. E. Mohney, R. S. Kern, and C. P. Kuo, Thin Solid Films 371, 153 (2000).
30. Z. Sitar, L. L. Smith, and R. F. Davis, Journal of Crystal Growth 141, 11 (1994).
31. B. J. Coppa, C. C. Fulton, R. F. Davis, C. Pandarinath, J. E. Burnette, and R. J. Nemanich, submitted to J. Appl. Phys.
32. S. Roberts and R. J. Gorte, J. Chem. Phys. 93, 5337 (1990).

33. V. E. Henrich and P. A. Cox, *The Surface Science of Metal Oxides* (Cambridge Univ., Cambridge, 1994) p. 396-97.

34. W. Göpel, L. J. Brillson, and C. F. Brucker, J. Vac. Sci. Technol. 17, 894 (1980).

35. K. M. Tracy, Ph.D. dissertation, N. C. State University, Raleigh, NC (2000).

36. E. F. Wassermann and K. Polacek, Appl. Phys. Lett. 16, 259 (1970).

37. S. M. Sze, Physics of Semiconductors Devices (Wiley, New York, 1981) p. 849.

Zn $2p_{3/2}$ core level parameters (±0.1 eV)				
Experiment Step	**Center (eV)**	**Shift (eV)**	**FWHM (eV)**	**Shift (eV)**
As-received	1022.0	--	2.3	--
Plasma-cleaned	1021.4	0.6	2.1	0.2
O_2 adsorption	1021.4	0.0	1.9	0.2
0.2 nm Au	**1021.7**	**0.3**	**1.9**	**0.0**
0.4 nm Au	1021.7	0.0	2.0	0.1
0.6 nm Au	1021.7	0.0	2.0	0.0
1.1 nm Au	1021.7	0.0	1.9	0.1
1.3 nm Au	1021.7	0.0	2.0	0.1
1.7 nm Au	1021.7	0.0	1.9	0.0
2.2 nm Au	1021.7	0.0	1.9	0.0
5.0 nm Au	1021.8	0.1	2.0	0.1
Net Shift (eV)	**--**	0.2	--	0.3

Table 5.1. Zn $2p_{3/2}$ core level acquired from the as-received, cleaned in a 20%O_2/80% He remote plasma, cooled in the plasma ambient (O_2 adsorption) and as a function of Au overlayer thickness. The evolution of the Schottky barrier was observed up to a thickness of ~0.2 nm of Au.

O 1s core level parameters (±0.1 eV)				
Experiment Step	**Center (eV)**	**Shift (eV)**	**FWHM (eV)**	**Shift (eV)**
As-received	530.9	--	1.6	--
Cleaning	530.4	0.5	1.4	0.2
O_2 adsorption	530.4	0.0	1.5	0.1
0.2 nm Au	**530.6**	**0.2**	**1.6**	**0.1**
0.4 nm Au	**530.7**	**0.1**	**1.5**	**0.1**
0.6 nm Au	530.7	0.0	1.5	0.0
1.1 nm Au	530.7	0.0	1.5	0.0
1.3 nm Au	530.7	0.0	1.5	0.0
1.7 nm Au	530.7	0.0	1.5	0.0
2.2 nm Au	530.7	0.0	1.5	0.0
5.0 nm Au	530.8	0.1	1.5	0.0
Net Shift (eV)	**--**	0.1	--	0.1

Table 5.2. O 1s core level acquired from the ZnO(0001) surface in the as-received state, after cleaning in a 20%O_2/80% He remote plasma and cooling in either a vacuum or in the plasma ambient (O_2 adsorption) and as a function of the thickness of a Au overlayer deposited on the surface exposed to the last environment . The evolution of the Schottky barrier was monitored up to a thickness of ~0.4 nm of Au.

Gold $4f_{7/2}$ XPS Core Level Parameters (±0.1 eV)			
Experiment Step	**Integ. Area**	**Center (eV)**	**FWHM (eV)**
Clean/O_2 adsorbed ZnO(0001)	--	--	--
0.2 nm Au	361	85.3	2.5
0.4 nm Au	390	84.8	2.5
0.6 nm Au	421	84.6	2.5
1.1 nm Au	684	84.4	2.3
1.3 nm Au	697	84.3	2.2
1.7 nm Au	849	84.3	2.2
2.2 nm Au	1456	84.2	1.5
5.0 nm Au	1838	84.2	1.5
100 nm Au (bulk)	--	84.0	1.2
Net Shift (eV)	**--**	**1.3**	**1.3**

Table 5.3. Au $4f_{7/2}$ core level as a function of Au overlayer thickness on 20%O_2/80% He remote plasma-cleaned ZnO(0001) surface cooled in the plasma ambient to ~RT.

(a) As-received (b) Cleaned (c) O_2 adsorption

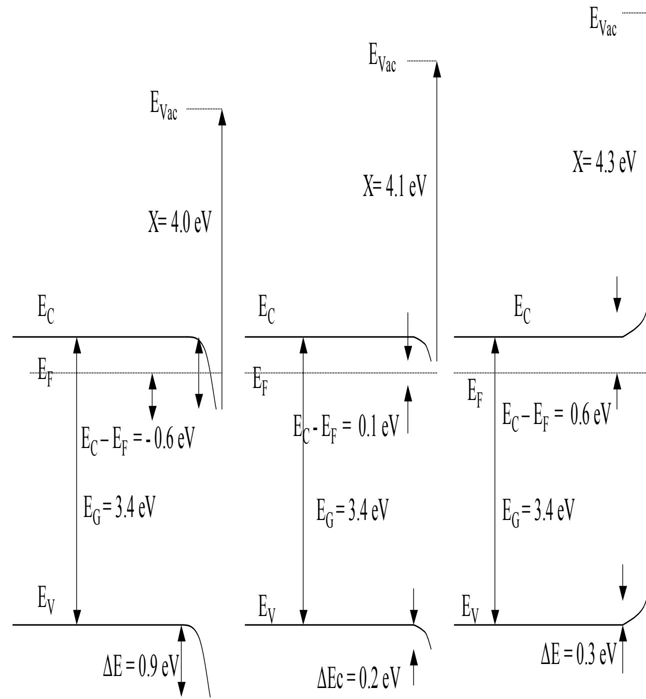

Figure 5.1. Electronic band structure derived from UPS spectra for ZnO(0001) surfaces (a) in the as-received state, (b) after exposure to a 20-W 20% O_2/ 80% He remote plasma for 60 min. at 550 °C and 0.050 Torr and cooling in vacuum from 425°C, and (c) after cooling under the same conditions to ~RT in the unignited plasma ambient (O_2 absorption).

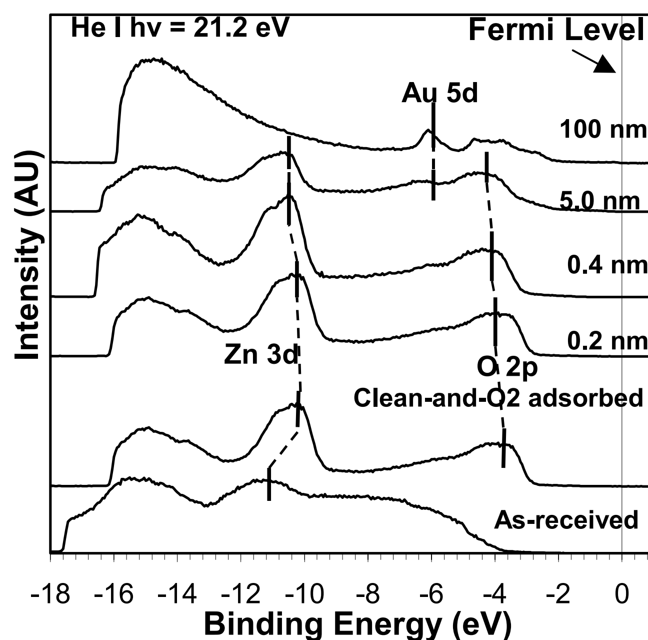

Figure 5.2. UPS valence band spectra from the as-received ZnO(0001) surface, after exposure to a 20-W 20% O_2/ 80% He remote plasma for 60 min. at 550 °C and 0.050 Torr and cooling in the unignited plasma ambient (O_2 adsorption), and after several sequential Au depositions of increasing thickness. Au-induced band bending is indicated by the movement of the Zn 3d and O 2p bulk features located at 10.4 eV and 4 eV, respectively. All spectra were acquired using the He I photon line (hν =21.2 eV). The binding energy is measured with respect to the Fermi level (E_F = 0 eV).

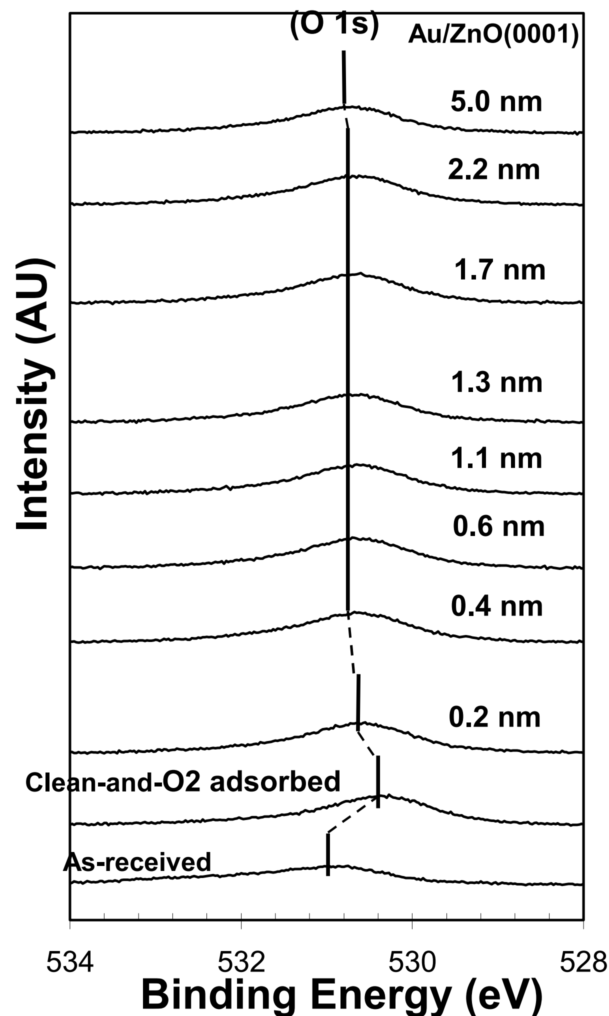

Figure 5.3. XPS O 1s core level spectra from the as-received ZnO(0001) surface, after remote plasma cleaning and cooling from 425°C in the plasma ambient to ~RT (O_2 adsorption), and sequential Au metallization. All spectra were acquired using Mg Kα (hν = 1253.6 eV) radiation.

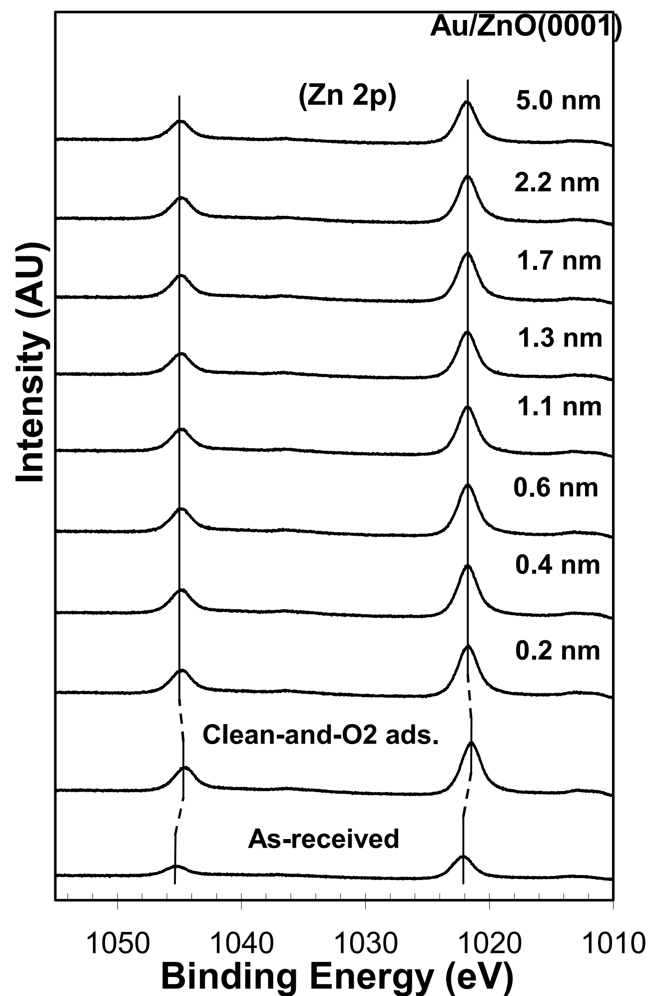

Figure 5.4. XPS Zn 2p core level spectra from the as-received ZnO(0001) surface after remote plasma cleaning and cooling from 425°C in the plasma ambient to ~RT (O_2 adsorption), and sequential Au metallization. All spectra were acquired using Mg Kα (hν = 1253.6 eV) radiation.

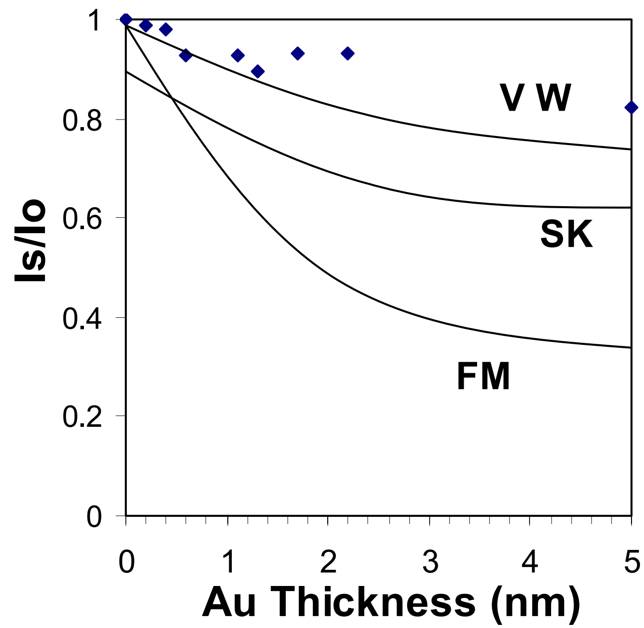

Figure 5.5. Attenuation of the O1s core level photoelectron peak as a function of the overlying Au thickness. The experimental data is indicated by solid diamonds for comparison with theoretical curves for Volmer-Weber (VW), Stranski-Krastanov (SK), and Frank-Van der Merwe (FM) growth modes.

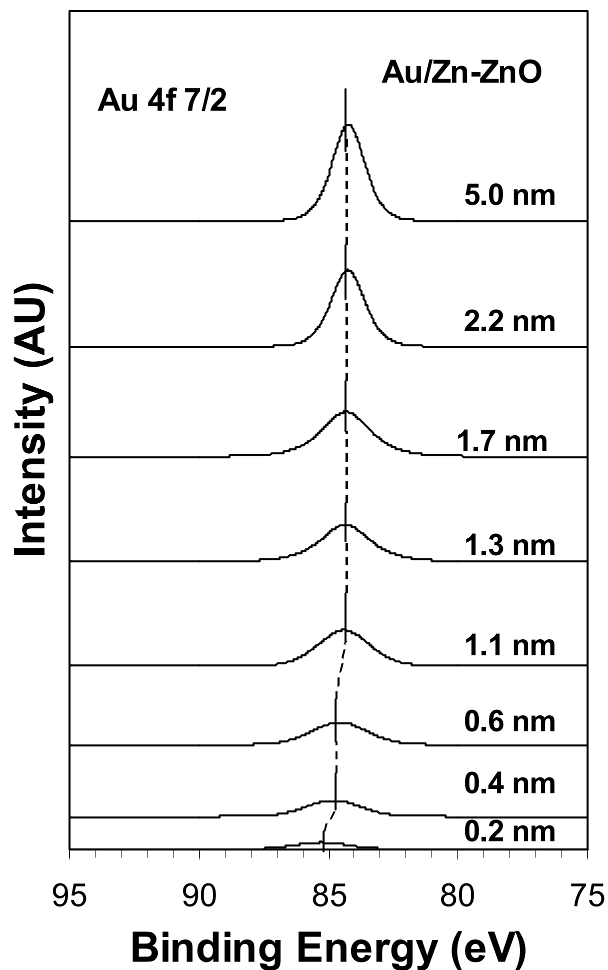

Figure 5.6. XPS Au $4f_{7/2}$ core level curve-fitted spectra as a function of Au deposition following remote plasma cleaning and O_2 adsorption. A shift of 1.1 eV and 1.0 eV is depicted for the peak position and FWHM, respectively, over the course of sequential Au metallization. All spectra were acquired using Mg Kα (hν = 1253.6 eV) radiation.

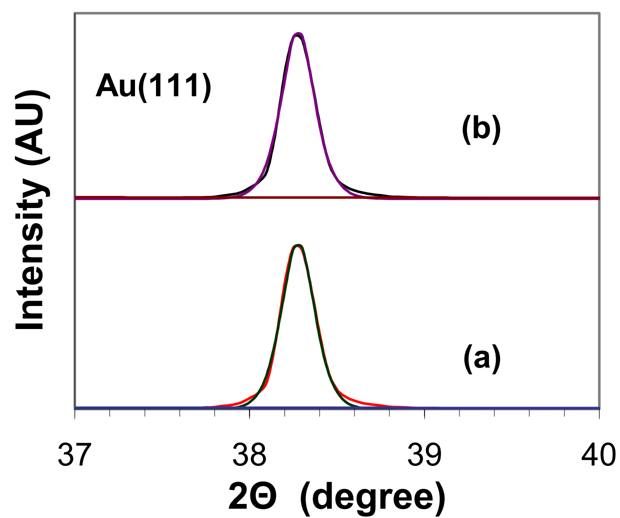

Figure 5.7. Curve-fitted XRD 2θ plots for 75 nm thick Au contacts deposited on a cleaned ZnO(0001) surface cooled in the plasma ambient. (a) as-deposited and (b) after post-deposition annealing in air at 175 °C for 15 min. The spectrum was acquired using Cu *Kα* (λ = 0.1542 nm) radiation.

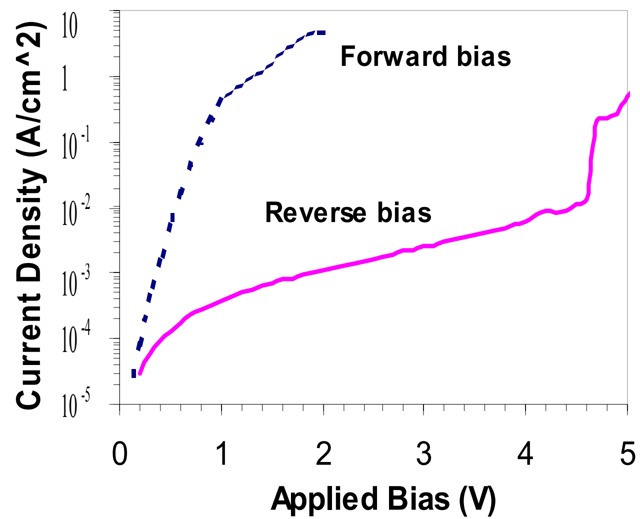

Figure 5.8. *J-V* characteristics for the best performing ~100-μm-diameter Au contact deposited on an as-received ZnO(0001) surface.

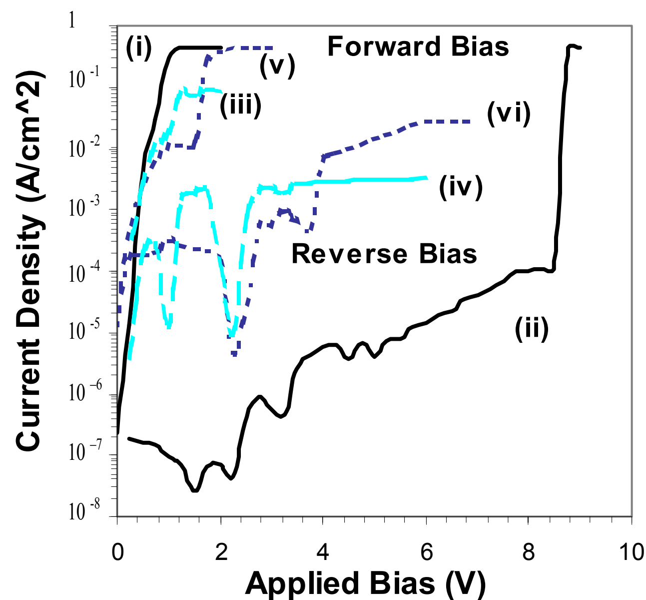

Figure 5.9. *J-V* characteristics for the best performing ~100-μm-diameter Au contact deposited on cleaned-and-oxygen adsorbed ZnO(0001) surface in (i) forward and (ii) reverse bias; at 80 °C in (iii) forward and (iv) reverse bias; at 150 °C in (v) forward and (vi) reverse bias.

6. SUMMARY

Several investigators have reported the results of various types of studies concerned with the effects of *ex situ* and *in situ* surface preparation methods on the chemical, electrical, and structural properties of Schottky contacts deposited on n-type ZnO{0001} surfaces. However, a clear understanding of the nature of the surface contamination, the mechanism through which it is removed, and the effects of its removal on the ZnO surface and metal contacts deposited on these surfaces did not emerge from a synthesis of these results and conclusions. The lack of an effective surface pre-treatment, which results in a clean, stoichiometric, and ordered ZnO surface is a major detriment to the development of device-quality Schottky contacts. One of the most common methods of cleaning ZnO is ion bombardment, which typically results in an atomically-clean surface, but this process may cause physical and chemical alteration of the surface and the underlying layers though mixing, roughening, formation of craters, and/or a change in oxidation state.

Schottky contacts require intimate metal-semiconductor contacts; thus, the initial phase of this investigation focused on the development of a smooth, clean, ordered, and stoichiometric ZnO surface. It was confirmed that annealing ZnO($000\bar{1}$) in pure oxygen is effective for desorbing the surface contaminants of adventitious carbon and hydroxide to concentrations below the detection limits of X-ray photoelectron spectroscopy (XPS) by annealing for 15 min. in pure O_2 at 700 °C. However, thermal decomposition degraded the surface microstructure. Thus, an alternative, non-destructive cleaning process was developed.

Smooth, highly-ordered, atomically-stepped and stoichiometric ZnO($000\bar{1}$) surfaces with nearly flat bands were developed by exposure to a 20-W remote plasma of

20% O_2/80% He for the optimized time, temperature, and pressure of 30 min, 525 °C, and 0.050 Torr. Only ~0.4 ML of hydroxide remained as the sole contaminant. A 0.5 eV change in band bending and a significant reduction in the conductivity of the OH surface layer were also achieved. The hydroxide appeared more tightly bound to the ZnO(0001) surface, which was attributed to the presence of unfilled dangling bonds associated with the polarity of ZnO. Consequently, increased temperature and time of the plasma cleaning process were required to obtain nearly identical results relative to the ZnO($000\bar{1}$) surface. The optimum cleaning procedure entailed a 60 min. 20% O_2/80% He remote plasma exposure at 550 °C.

Gold contacts were deposited *in situ* on n-type ZnO(0001) wafers that were either (1) in the as-received state or (2) cleaned via a 20% O_2/80% He remote plasma at 550 °C and cooled in the plasma ambient to ~ RT. The cooling in the oxygen-containing ambient was employed to chemisorb oxygen onto the cleaned surface. *J-V* results of the contacts on the as-received surfaces showed reverse bias current densities of ~0.01 A/cm^2 to 4.6 V and ideality factors >2, before sharp, permanent breakdown. These properties are related to the presence of ~2.0 ML of hydroxide, which typically increases the surface conductivity and forms an accumulation layer.

The aforementioned reduction in the hydroxide layer to ~0.4 ML also resulted in a 0.7 eV reduction in downward band bending and lowering of the surface Fermi level. Subsequent exposure to the plasma ambient during cooling generated a 0.5 eV change in band bending, resulting in 0.3 eV of upward band bending, which is indicative of a depletion layer and lower surface conductivity. The most rectifying gold contacts were measured on these surfaces and displayed a barrier height of 0.71±0.05 eV, a saturation

current density of 4.04 μA/cm^2, a lower value of n = 1.17±0.05, a significantly lower leakage current density of ~0.1 mA/cm^2 to 8.5 V reverse bias, and a sharp, permanent breakdown at ~ -8.75 V. The measured barrier heights differ from the predicted Schottky-Mott value of 1.0 eV, indicating that the interface structure significantly affects the Schottky barrier. However, the constancy in the FWHM of the core levels for Zn 2*p* (1.9 eV) and O 1*s* (1.5 eV) before and after sequential Au depositions conducted *in situ* indicates an abrupt, unreacted Au/ZnO(0001) interface. These Au(111)-oriented contacts, nucleated and grew via the Volmer-Weber (island) mode and exhibited good rectifying behavior and crystallographic stability to 175 °C.

Similarly, Au contacts were deposited *in situ* on n-type ZnO($000\bar{1}$) wafers that were either (1) in the as-received state (2) cleaned via a 20% O_2/80% He remote plasma at 525 °C for 30 min and cooled in vacuum beginning at 425 °C, and (3) cleaned via method (2) but cooled in the plasma ambient to ~RT for the chemisorption of oxygen. The surfaces of the wafers treated via the processes (2) and (3) were smooth, highly-ordered, stoichiometric and typically contained a step and terrace microstructure. *J-V* results of the contacts on the as-received surfaces showed reverse bias leakage current densities of ~0.02 A/cm^2 to 4 V and ideality factors >2, before soft breakdown at -4.5 V. These properties are related to the presence of ~1.6 ML of hydroxide, which typically increases the surface conductivity and results in an electron accumulation layer.

Plasma cleaning of this surface also reduced the amount of the hydroxide layer to ~0.4 ML, corresponding to a 0.7 eV reduction in downward band bending and lowering of the surface Fermi level. Subsequent exposure to the plasma ambient upon cooling again generated a 0.5 eV change in band bending, resulting in 0.3 eV of upward band bending,

which is indicative of a depletion layer and lower surface conductivity. The most rectifying gold contacts were measured on these oxygen-adsorbed surfaces in comparison to surfaces prepared using process routes (1) and (2). These contacts showed a barrier height of 0.60±0.05 eV, a saturation current density of 2.0±0.5 x 10^{-4} A/cm^2, a lower value of n = 1.03±0.05, a lower leakage current density of ~91 nA/cm^2 to 7 V reverse bias and soft breakdown at this voltage. These values are consistent with results obtained for similarly processed Au contacts on the ZnO(0001) face, which indicates a lack of polarity effects, since minor differences may be attributed to surface polishing. The measured barrier height differs from the predicted Schottky-Mott value of 1.0 eV, indicating, once again, that the interface structure significantly affects the Schottky barrier. Consequently, the lack of a discernible change in the FWHM of the core levels for Zn 2*p* (1.9 eV) and O 1*s* (1.6 eV), before and after sequential Au depositions indicates an abrupt, unreacted Au/ZnO($000\bar{1}$) interface. Transmission electron microscopy confirmed this result, while also showing an epitaxial, single-crystal Au film. These Au(111)-oriented contacts also grew via the Volmer-Weber (island) mode and exhibited crystallographic stability to 175 °C.

These studies highlight the critical nature of surface preparation, not only for achieving improved rectifying contact behavior, but also for the growth of light-emitting homoepitaxial ZnO device structures. The majority of ZnO researchers utilize ion bombardment and/or annealing, as the primary tools to clean ZnO. Serious considerations must be made concerning the possible incorporation of a remote oxygen plasma chamber into ZnO homoepitaxial growth and device processing.

7. RECOMMENDATIONS FOR FUTURE RESEARCH

Additional research in several areas would compliment this investigation and facilitate the fabrication of commercially viable ZnO devices. The optimized cleaning processes for ZnO{0001} described herein have implications for the growth of homoepitaxial ZnO p-n junction devices with significant light-emission. In addition, these processes may be utilized in the development of ZnO nanostructures. Schottky-type ultraviolet photodetectors and high-frequency transistors rely on low leakage, low ideality parameter Schottky diodes; thus, this investigation has a direct impact on this field. Future studies, described below, may assist in the transfer of remote plasma processing technology for ZnO to relevant device fabrication.

First and foremost, the growth of >1" ZnO wafers, with similar properties as those utilized in this study and free of internal microvoids, would allow for further electrical characterization, including temperature-dependent current-voltage (I-V-T) testing of Au, Pt, and Pd contacts on both polar surfaces of remote plasma-treated ZnO. At this writing, large-scale ZnO wafers of this quality are not commercially available; thus, it is more difficult to develop Schottky contacts. Internal microvoids in ZnO substrates lead to short-circuiting between the ohmic and the Schottky contacts. Guard rings may improve rectifying characteristics of Schottky contacts on ZnO; thus, the development of a photolithographic process would be beneficial. However, ZnO is highly sensitive to acids and bases and extreme caution would be necessary to avoid damaging the ZnO surface. In addition, the assessment of Au islands grown on cleaned-and-oxygen adsorbed ZnO{0001} surfaces would be strengthened by high resolution atomic force micrographs.

The correlation of X-ray diffraction, I-V-T, and cross-sectional high-resolution transmission electron microscopy (HRTEM) would develop a clearer understanding of the Au/ZnO interface. Transmission electron microscopy of Au on remote O_2/He plasma-treated ZnO($000\bar{1}$) has indicated that the Au is epitaxial, single-crystal, and partially twinned, forming an abrupt, unreacted interface. The latter result corresponds well with X-ray photoelectron spectroscopy results after sequential Au depositions on a cleaned-and-oxygen adsorbed ZnO($000\bar{1}$) surface. However, HRTEM of a sample annealed under the same conditions as I-V-T measurements would provide insight into any changes in the interface associated with the degradation in rectifying properties. This same analysis would be advantageous for the Au/ZnO(0001) interface as well. However, the lack of HRTEM of Au contacts on cleaned-and-oxygen adsorbed ZnO(0001) generates the need for at least (2θ-ω) X-ray diffraction of these contacts to be certain of the crystallinity of the Au.

A complete investigation, including the future work listed above, for Pt and Pd contacts on cleaned-and-oxygen adsorbed ZnO{0001} would complement the Au studies, since these metals have comparable high work functions. Moreover, it is less likely that Pt and Pd will grow by the Volmer-Weber mechanism characteristic for Au; thus, photoemission spectroscopy analysis of the Schottky barrier height is feasible.

Although this thesis has documented significant improvements in the development and understanding of Schottky contacts to ZnO, there is still a significant amount of work to be accomplished before the implementation of device structures. The incorporation of polarity effects into these device structures may be explored, as ZnO is further developed.

APPENDIX A. (published in Applied Physics Letters: 1/20/03)

Gold Schottky contacts on oxygen plasma-treated, n-type ZnO($000\bar{1}$) [1]

B. J. Coppa[*], R. F. Davis[*,a],
[*]*Department of Materials Science and Engineering, Campus Box 7907, North Carolina State University, Raleigh, NC 27695*

and R. J. Nemanich[**]
[**]*Department of Physics, Campus Box 8202, North Carolina State University, Raleigh, NC 27695*

Reverse bias current-voltage measurements of ~100 µm diameter gold Schottky contacts deposited on as-received, n-type ZnO($000\bar{1}$) wafers and those exposed for 30 minutes to a remote 20% O_2/80% He plasma at 525±20°C and cooled either in vacuum from 425°C or the unignited plasma gas have been determined. Plasma cleaning resulted in highly ordered, stoichiometric and smooth surfaces. Contacts on as-received material showed µA leakage currents and ideality factors >2. Contacts on plasma-cleaned wafers cooled in vacuum showed ~36±1 nA leakage current to –4 V, a barrier height of 0.67±0.05 eV, and an ideality factor of 1.86±0.05. Cooling in the unignited plasma gas coupled with a 30 sec. exposure to the plasma at room temperature resulted in decreases in these parameters to ~20 pA to -7 V, 0.60±0.05 eV, and 1.03±0.05, respectively. Differences in the measured and theoretical barrier heights indicate interface states.

[1] (0001) and ($000\bar{1}$) are used in this paper to designate the polar zinc- and oxygen-terminated surfaces, respectively.

[a] Corresponding author.
Email address: robert_davis@ncsu.edu

Zinc oxide (ZnO) more commonly occurs in the hexagonal wurtzite crystal structure and possesses the direct band gap energy of ~3.4 eV at room temperature.[1] Applications commonly associated with powdered and bulk polycrystalline ZnO include paints, phosphors, surface acoustic wave devices, gas sensors, piezoelectric transducers, varistors, and transparent conducting films for the photovoltaic industry.[2] Recent research has focused on the electrical and optical properties of this material and the associated device applications, e.g., ultraviolet (UV) photodetectors.[3-5] Large-area substrates are also commercially available for growth of ZnO-based films. This material is typically n-type due to oxygen vacancies and/or zinc interstitials.[6] Several groups have reported the achievement of p-type ZnO[7-8] via several process routes. However, at this writing, no approach has been successfully duplicated in separate laboratories by different investigators. A review of the recent advances in ZnO materials and devices has recently been published.[1]

A prior determination of the Au Schottky barrier height (Φ_B) on chemically prepared ZnO crystals with an unspecified orientation resulted in a value of 0.66 eV by current-voltage (I-V), capacitance-voltage (C-V), photoresponse and thermal activation energy measurements; an ideality factor (n) of 1.05 was reported without specifying the reverse bias leakage current.[9] Fabricius, *et al*.[3] measured n = 2.7 for Au Schottky photodiodes fabricated on as-received polycrystalline ZnO but did not indicate Φ_B nor leakage currents. This high value of n was reportedly influenced by recombination. Silver Schottky contacts with a Au cap have been fabricated on as-received ZnO($11\bar{2}0$) epilayers.[4,10] The values of Φ_B determined via I-V and C-V measurements were 0.89 eV and 0.92 eV, respectively. A leakage current of 0.1 nA at 1 V reverse bias, and an ideality

factor of 1.33 were also reported. The high ideality factor was attributed to an interfacial layer and/or surface states.

Investigations concerned with the properties of rectifying contacts deposited on as-received and cleaned surfaces of Si and GaAs have shown[11-13] that the ideality factors and the reverse bias leakage currents are both decreased in the contacts on the cleaned materials. In this regard, x-ray photoelectron spectroscopy (XPS) studies by Mintas and Filby[14] of the surfaces of as-received, sintered ZnO tablets revealed hydrocarbons and an hydroxide (OH) component in the O 1*s* core level located 1.5-2 eV higher in binding energy than lattice oxygen. The complete removal of these contaminants was achieved via Ar^+ bombardment for 20 min. at a potential and beam current of 6 kV ions and 40 μA, respectively. However, this process normally results in the chemical and physical alteration of the surface and the underlying layers via atomic mixing, vacancy formation, changes in oxidation state and surface roughening, and thus disallows the achievement of rectifying contacts with optimum properties. Liang *et al*.[5] employed an oxygen plasma to clean ZnO$(11\bar{2}0)$ films before depositing Ag contacts, but neither the conditions of use nor the evidence of its effectiveness were reported.

Two millimeter-thick, single-crystal ZnO$(000\bar{1})$ wafers, diced from boules produced by seeded chemical vapor transport by Eagle-Picher Technologies, Incorporated,[15] and chemo-mechanically polished on both sides were employed in the present research. Grade I wafers were used, as they were essentially free of internal microvoids, which we determined to produce highly ohmic behavior. Hall and C-V measurements, the latter at 1×10^4 Hz, taken from the $(000\bar{1})$ surface showed a bulk carrier concentration of $1 \times 10^{17}/cm^3$ and a nominal effective donor concentration,

(N_D-N_A), of 5 x 10^{16}/cm^3, respectively, for the as-received samples. The wafers were then cleaved into smaller pieces, rinsed *ex situ* in methanol for 5 sec. and dried in flowing nitrogen. A 40 nm thick Ti film was subsequently deposited by electron beam evaporation on the entire (0001) face of each ZnO piece. This film served (1) to absorb radiation from the underlying Pt-Rh heater and conduct heat into the wafer during the cleaning of the $(000\bar{1})$ face and (2) as an ohmic contact.

Low-energy electron diffraction (LEED) of the *ex situ* cleaned ZnO$(000\bar{1})$ surface showed only a bright background, indicative of an amorphous contamination layer. Deconvolution of the O 1*s* core level peak shown in Fig. 1a obtained via XPS studies (±0.1 eV uncertainty) revealed that this surface contained 16 atomic (at.) % (~1.6 ML) of OH^-, as determined by a peak at 532.3 eV, as well as weakly bound oxygen having a peak at 533.3 eV. One atomic percent of hydroxide is approximately equal to 0.1 ML. The resulting Zn/O atomic ratio was 0.7±0.1. Reverse bias I-V measurements of the Au contacts on as-received ZnO$(000\bar{1})$ showed μA leakage currents and ideality factors >2, primarily due to the presence of the hydroxide, which increased the surface conductivity.

For all subsequent research, each ZnO$(000\bar{1})$ wafer was placed in an ultra-high vacuum chamber having a base pressure of 5 x 10^{-9} torr, exposed to a 20 W remote plasma of 20% O_2/80% He for the optimized times, temperatures and pressures of 30 min., 525±20ºC and 0.050±0.001 torr, respectively. In the initial experiments, each wafer was then cooled to 425°C in the unignited plasma gas and further cooled to room temperature in vacuum. LEED studies revealed a sharp (1x1) hexagonal pattern, while the XPS C 1*s* core level indicated the complete removal of all detectable carbon. A comparison of Figs. 1a and 1b reveals a shift in the lattice O core level peak from 530.7 eV to 530.3 eV due to

band bending, which corresponds to a reduction in the OH^- concentration and an associated reduction in surface conductivity.[16-17] The XPS results in Fig. 1b also show the complete removal of all detectable weakly bound oxygen; 4±1 at.% (~0.4 ML) of the OH^- remained as the sole contaminant with a peak at 532.4 eV. This significant removal of ~1.2 ML of the OH^- was critical for eliminating the proposed accumulation layer[16-17] and for generating a Zn/O atomic ratio of 1.0±0.1. Atomic force microscopy (AFM) studies revealed a root-mean-square surface roughness of 0.2±0.2 nm before and after the plasma clean.

Adsorbed oxygen species on ZnO act as electron acceptors, which lower the surface conductivity.[18-19] This is advantageous for subsequent Schottky barrier formation.[18-19] As such, the initial cooling procedure was altered such that each cleaned sample was cooled in the unignited plasma gas to ~25°C over 50 min. and again exposed to the 20 W O_2/He plasma for 30 sec.

Gold contacts having a thickness and diameter of ~150 nm and ~100 µm, respectively, and arranged in an 8 x 8 array were subsequently deposited *in situ* via electron beam evaporation through a gold-coated molybdenum shadow mask. The resulting Au/ZnO/Ti structure allowed current to pass through the bulk wafer and reduced the need for complex isolation of the contacts. After removing from UHV, I-V measurements were obtained for as-received, cleaned, and cleaned and oxygen exposed samples.

For thermionic emission and V greater than 3kT/q, the general diode equation in forward bias is

$$J = J_o \exp\left(\frac{qV - IR}{nkT}\right) \qquad (1)$$

where J is the current density, q is the charge of an electron, V is the voltage, I is the current, R is the series resistance, k is Boltzman's constant, and T is the absolute temperature. The saturation current density J_0 is given by $J_0 = A^*T^2 \exp(-\Phi_B/kT)$ where A^* is the Richardson constant. The theoretical value of $A^* = 32$ A cm^{-2} K^{-2} was used in this study.[20] The ideality factors were obtained by fitting the forward bias ln(J)-V curve between 0.1 and 0.2 V over several decades of current and correcting for the substrate series resistance measured directly by C-V. Soft breakdown was observed for all contacts presented, as evidenced by non-repeatable low leakage current behavior after biasing to the breakdown voltage. The best results are presented and discussed for all sample types.

Room temperature (~293 K) I-V measurements of the Au contacts on as-received ZnO($000\bar{1}$) wafers revealed reverse bias leakage currents below ~4.6 μA to 4 V reverse bias, as shown in Fig. 2. The ideality factors were >2. These effects were primarily due to the presence of the hydroxide, which increased the surface conductivity. Soft breakdown occurred at -4.0 V. Significant improvements in the I-V characteristics were obtained for the Au contacts on a plasma-cleaned ZnO($000\bar{1}$) surface, as shown in Fig. 3. A barrier height of 0.67±0.05 eV was calculated based on $J_0 = 6.40 \times 10^{-5}$ A/cm^2 (2.40×10^{-4} cm^2 contact area). A 36±1 nA leakage current was measured to 4 V reverse bias with soft breakdown at -4.5 V. The value of the ideality factor was 1.86±0.05.

Cooling the cleaned surface in the unignited plasma gas coupled with the 30 sec. exposure to the plasma at room temperature resulted in a slightly smaller barrier height of 0.60±0.05 eV, a higher saturation current density of 2.27×10^{-4} A/cm^2 (2.20×10^{-4} cm^2 contact area), lower values of n = 1.03±0.05, a leakage current of ~20 pA to 7 V reverse bias and soft breakdown at this voltage, as observed in Fig 3. The values of the barrier

height correspond well with earlier results of 0.66 eV reported by Neville and Mead.[9] Thirty-three percent of these contacts exhibited leakage currents in the 10 nA range compared to 11% of the contacts that were cooled in vacuum from 425°C.

Ultraviolet photoelectron spectroscopy (UPS) measurements in the present research have shown that the electron affinity of a clean ZnO($000\bar{1}$) surface is 4.1 eV.[21] Calculations of Φ_B for the metals (work functions) of Pt (5.7 eV), Au (5.3 eV), and Ag (4.4 eV)[22] from the Schottky-Mott model predict values of 1.7 eV, 1.2 eV, and 0.4 eV, respectively. A review of the values of this parameter obtained in this and prior research shows them to be markedly different from the theoretical values and therefore indicative of interface states.

In summary, clean, stoichiometric, highly ordered, and smooth ZnO($000\bar{1}$) surfaces have been achieved via exposure to a remote O_2/He plasma. As a consequence, significant improvement in the I-V characteristics of as-deposited Au rectifying contacts was observed relative to those characteristics measured for similar contacts deposited on the same surfaces of as-received wafers. The best contact behavior was found for plasma-cleaned surfaces that were subsequently cooled to room temperature in the unignited plasma gas and subsequently exposed to the plasma for 30 sec.

This research was partially funded by both the Kenan Institute for Technology, Engineering and Science at NCSU and by the Office of Naval Research under contract N00014-98-1-0654 (H. Dietrich, monitor). The authors express their appreciation to G. Cantwell and D. Eason of the Eagle-Picher Corporation for helpful discussions.

REFERENCES

1. D. C. Look, Materials Science and Engineering B80, 383 (2001).
2. F. D. Auret, S. A. Goodman, M. Hayes, M. J. Legodi, H. A. van Laarhoven, and D. C. Look, J. Phys.: Condens. Matter 13, 1 (2001).
3. H. Fabricius, T. Skettrup, and Paul Bisgaard, Applied Optics 25, 2764 (1986).
4. Y. Liu, C.R. Gorla, S. Liang, N. Emanetoglu, Y. Lu, H. Shen, and M. Wraback, Journal of Electronic Materials 29, 69 (2000).
5. S. Liang, H. Sheng, Y. Liu, Z. Huo, Y. Lu, and H. Shen, Journal of Crystal Growth 225, 110 (2001).
6. W. Göpel, L. J. Brillson and C. F. Brucker, J. Vac. Sci. Technol. 17, 894 (1980).
7. T. Yamamoto and K. Yoshida, Jpn. J. Appl. Phys. 38, L166 (1999).
8. M. Joseph, H. Tabata, and T. Kawai, Jpn. J. Appl. Phys. 38, L1205 (1999).
9. R. C. Neville and C. A. Mead, J. Appl. Phys. 41, 3795 (1970).
10. H. Sheng, S. Muthukumar, N. W. Emanetoglu, and Y. Lu, Appl. Phys. Lett. 80, 2132 (2002).
11. R. P. Vasquez. B. F. Lewis, and F.J. Grunthaner, Appl. Phys. Lett. 42, 293 (1983).
12. M. Yamada and Y. Ide, Jpn. J. Appl. Phys. 33, L671 (1994).
13. C. M. Rouleau and R. M. Park, J. Appl. Phys. 73, 4610 (1993).
14. M. Mintas and G.W. Filby, Zeitschrift fur Naturforschung 36a, 140 (1981).
15. D. C. Look, D. C. Reynolds, J. R. Sizelove, R. L. Jones, C. W. Litton, G. Cantwell, and W. C. Harsch, Solid State Commun. 105, 399 (1998).
16. G. Heiland and P. Kunstmann, Surf. Sci. 13, 72 (1969).
17. M. Nakagawa and H. Mitsudo, Surf. Sci. 175, 157 (1986).

18. E. Arijs, F. Cardon, and W. Maenhout-Van Der Vorst, Surf. Sci. 17, 387 (1969).

19. L. Lagowski, E. S. Sproles, Jr., and H. C. Gatos, J. Appl. Phys. 48, 3566 (1977).

20. S. M. Sze, Physics of Semiconductors Devices (Wiley, New York, 1981) p. 849.

21. B. J. Coppa, to be published.

22. K. M. Tracy, Ph.D. dissertation, N. C. State University, Raleigh, NC (2000).

Figure Captions

Figure 1. XPS O 1*s* core level spectra acquired from ZnO($000\bar{1}$) surfaces (a) in the as-received state and (b) after exposure to a 20 W remote 20% O_2/ 80% He plasma for 30 min. at 525ºC and 0.050 torr.

Figure 2. I-V characteristics for an ~100 μm diameter Au contact on as-received ZnO($000\bar{1}$).

Figure 3. I-V characteristics for an ~100 μm diameter Au contact on plasma-cleaned ZnO($000\bar{1}$) in (a) forward and (b) reverse bias and for a similar contact on a plasma-cleaned and oxygen exposed ZnO($000\bar{1}$) in (c) forward and (d) reverse bias.

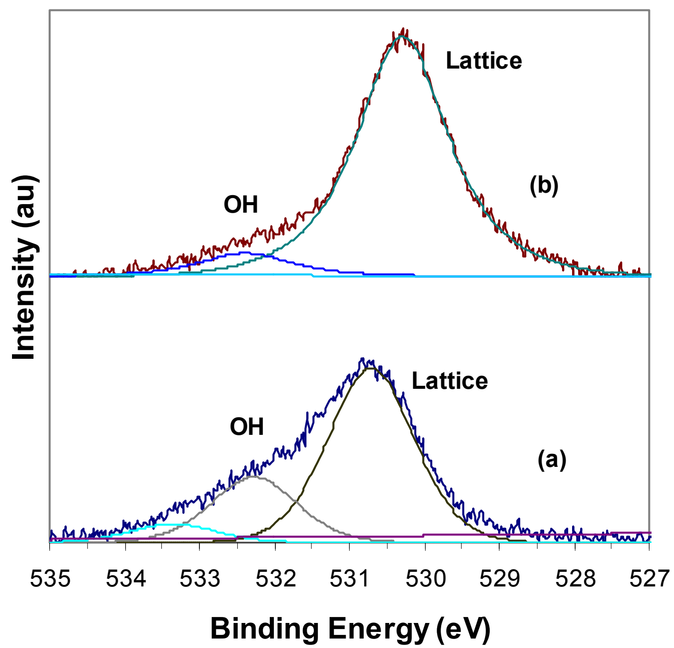

Figure 1. Brian Coppa APL

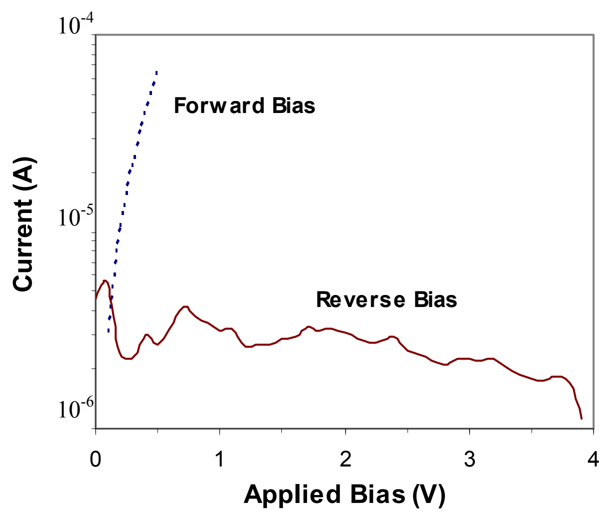

Figure 2. Brian Coppa APL

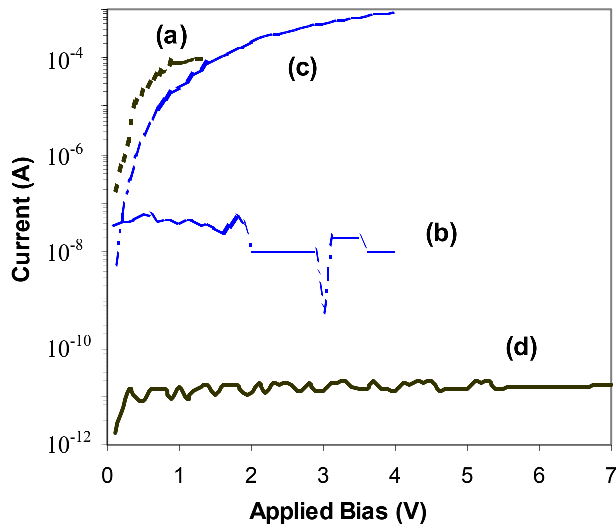

Figure 3. Brian Coppa APL